UNIVERSITAT DE BARCELONA

Mechanobiology of single cell migration on patterned fibronectin gradients

Isabela Corina Santos Fortunato

UNIVERSITAT DE BARCELONA

IBEC
Institute for Bioengineering of Catalonia

Mechanobiology of single cell migration on patterned fibronectin gradients

Memòria per optar al grau de Doctora
per la Universitat de Barcelona

Presentada per:

Isabela Corina Fortunato

Dirigida per:

Dr. Xavier Trepat

Dr. Raimon Sunyer

“To understand is to perceive patterns.”

(Isaiah Berlin)

Acknowledgements

This PhD would not have been possible without the support and encouragement of the following amazing people. They have been the driving force behind this journey.

Many, many, many thanks:

To my supervisors, Dr. Xavier Trepat and Dr. Raimon Sunyer:

Thank you for accepting me into the laboratory and allowing me to work on this challenging project. Your guidance and support over the past five years have been invaluable. It has been a pleasure to learn from your expertise on a daily basis.

To all my family:

Mom, dad, and sister – you believed in me and made this journey worth fighting for. Thank you for fighting alongside me. Everything I am and do is because of you. Desculpem por não estar tão presente como devia e obrigada por entenderem e apoiarem o meu sonho. Esta tese é dedicada a vocês. Não podia deixar de dar um beijinho especial ao resto da família: avós, tios, tias, primos e primas.

To my partner:

Daniel Peláez – Només nosaltres sabem com de durs han estat aquests anys de lluita constant, tant en l'àmbit professional com personal. Gràcies

per no deixar-me enfonsar i per donar-me les forces per seguir endavant. No podia deixar de referir-me als teus pares, que em van acollir a Menorca com a part de la vostra família i em van fer sentir com a part d'ella. Muchas gracias, Trudi y Kiko. Sois maravillosos.

To my friends:

All who stayed close (remotely) – Daniel Matias, João Macau, Francisco Alves, Pedro Nogueira, João Marques, João Matos, Ana Lourenço, Miguel Fernandes, Catarina Lourenço, Margarida Ferreira, Mafalda Gomes, Tatiana Saraiva, Andreia Pena, Dalila Silva, Regina Manuelito, and Filipe Correia – obrigada por fazerem a minha vida valer a pena de ser vivida, por todas as lágrimas, risos, abraços, beijinhos e todos os momentos partilhados. Há um lugar no meu coração para cada um de vocês.

To <u>all</u> my lab colleagues, past and present:

Especially Gerardo, Juanfra, Susana, Anghara, Nimesh, Sri, Eleni, Marija, Pau, Alice, Miguel, Laura, Leone, Macià, Irina, Sefora, Ona, Steffen, Rohit, Amy, Miquel, Ignasi, Aina, Özge, Zarina, Jenny, Tom, Marc, Ariadna, Clement, Thomas, Manu, Ibrahim, Jorge, Valeria, Yudish, Margherita, Guillermo, Emmanuel, Anabel-Lise, Gotthold and PCB colleague Carlota – all of you have been essential at every step of this project. You have been the brain, heart, inspiration, motivation, and guides. Each of you is special and unique in your own way, and it is undeniable that you will achieve anything you set your minds to. Thank you. Obrigada. Gracias. Grazas.

Gràcies. Merci. Grazie. Todah. Danke. Hvala. Efcharistó. Dhanyavaad. Teşekkürler. Rakhmet. Xièxiè.

No words can ever truly express my gratitude for everything you have done for me. I am here for you. regardless of mood, availability, or distance.

You can always count on me.

Thanks,

Isabela ♡

"Talvez mais do que esteticamente sensíveis ou politicamente correctos,
O que nós deveriamos mesmo ser era activamente bons." (José Saramago)

Resum

La migració cel·lular dirigida al llarg dels gradients de densitat de la matriu extracel·lular (ECM) – un procés anomenat haptotaxi – té un paper central en la morfogènesi, la resposta immune i la invasió del càncer. Se suposa habitualment que les cèl·lules responen a aquests gradients migrant direccionalment cap a les regions de major densitat de lligands. En contrast amb aquesta visió, aquí mostrem que la integració de la detecció del gradient ECM i la dinàmica de polaritat persistent pot donar lloc a trajectòries de migració no trivials, inclosa la migració contra el gradient i els cercles persistents. Hem generat patrons simètrics de densitat de fibronectina confinats a àrees rectangulars de diferent amplada. Com era d'esperar, en adherir-se a aquests patrons, les cèl·lules es van polaritzar i van migrar amb força cap a la direcció de la densitat de proteïnes més alta. Tanmateix, després d'assolir la densitat màxima, les cèl·lules van mostrar diferents patrons de migració en funció de l'amplada del gradient. En gradients 1D confinats, les cèl·lules no es van repolaritzar i van continuar migrant de manera persistent contra el gradient de fibronectina. En canvi, en gradients amplis, van fer un gir de 90º i van migrar per la carena definida per la densitat màxima de fibronectina. Per a amplades intermèdies, van sorgir trajectòries no trivials com els cercles. En general, el nostre estudi revela que el confinament modula la capacitat de les cèl·lules per detectar i respondre a senyals haptotàctiques i proporciona un marc per entendre com les cèl·lules naveguen per entorns complexos i dinàmics.

Abstract

Directed cell migration along gradients of extracellular matrix (ECM) density – a process called haptotaxis – plays a central role in morphogenesis, the immune response, and cancer invasion. It is commonly assumed that cells respond to these gradients by migrating directionally towards the regions of highest ligand density. In contrast with this view, here we show that the integration of ECM gradient sensing and persistent polarity dynamics can give rise to non-trivial migration trajectories, including migration against the gradient and persistent circles. We generated symmetric patterns of fibronectin density confined to rectangular areas of different width. As expected, upon adhering to these patterns, cells polarized and migrated robustly towards the direction of the highest protein density. However, after reaching the maximal density, cells exhibited different migration patterns depending on the gradient width. On confined 1D gradients, cells failed to repolarize and continued to migrate persistently against the fibronectin gradient. By contrast, on wide gradients, they made a 90º turn and migrated along the ridge defined by the maximal fibronectin density. For intermediate widths, non-trivial trajectories such as circles emerged. Overall, our study reveals that confinement modulates the ability of cells to sense and respond to haptotactic cues and provides a framework to understand how cells navigate complex and dynamic environments.

Table of Contents

Chapter 1 – Introduction

1. Directed cell migration

Coordinated movements are common among different organisms. For instance, migratory birds use organized patterns to optimize energy and improve locomotor performance (Weimerskirch et al., 2001). Similarly, cells in the body coordinate their movements to perform important physiological functions. Central to this self-organization is the ability of cells to perform directed migration (Fortunato & Sunyer, 2022).

Cell migration is a process by which cells move from one location to another within an organism. Although cells possess the ability to move both randomly and directly, the effectiveness of migration is improved when cells exhibit clear directionality (Roussos et al., 2011b). Therefore, directed cell migration plays a crucial role in several biological processes. During development, endothelial cells undergo proliferation and migration, contributing to the expansion of pre-existing vasculature, a phenomenon known as sprouting angiogenesis (Lamalice et al., 2007) (Figure 1A). The resulting vascular network serves as a vital source of oxygen and nutrients for the surrounding tissues and organs. Another illustrative example is the migration of intestinal epithelial cells from the bottom of the crypt to the tip of the villus, allowing constant renovation of the epithelium and maintenance of intestinal homeostasis (Krndija et al., 2019) (Figure 1B). Directed cell migration is also relevant to tissue repair mechanisms. Epidermal skin cells proximal to a wound exhibit migratory behavior, moving towards the site of injury and initiating the

healing process by re-establishing the epithelial layer (Krawczyk, 1971) (Figure 1C).

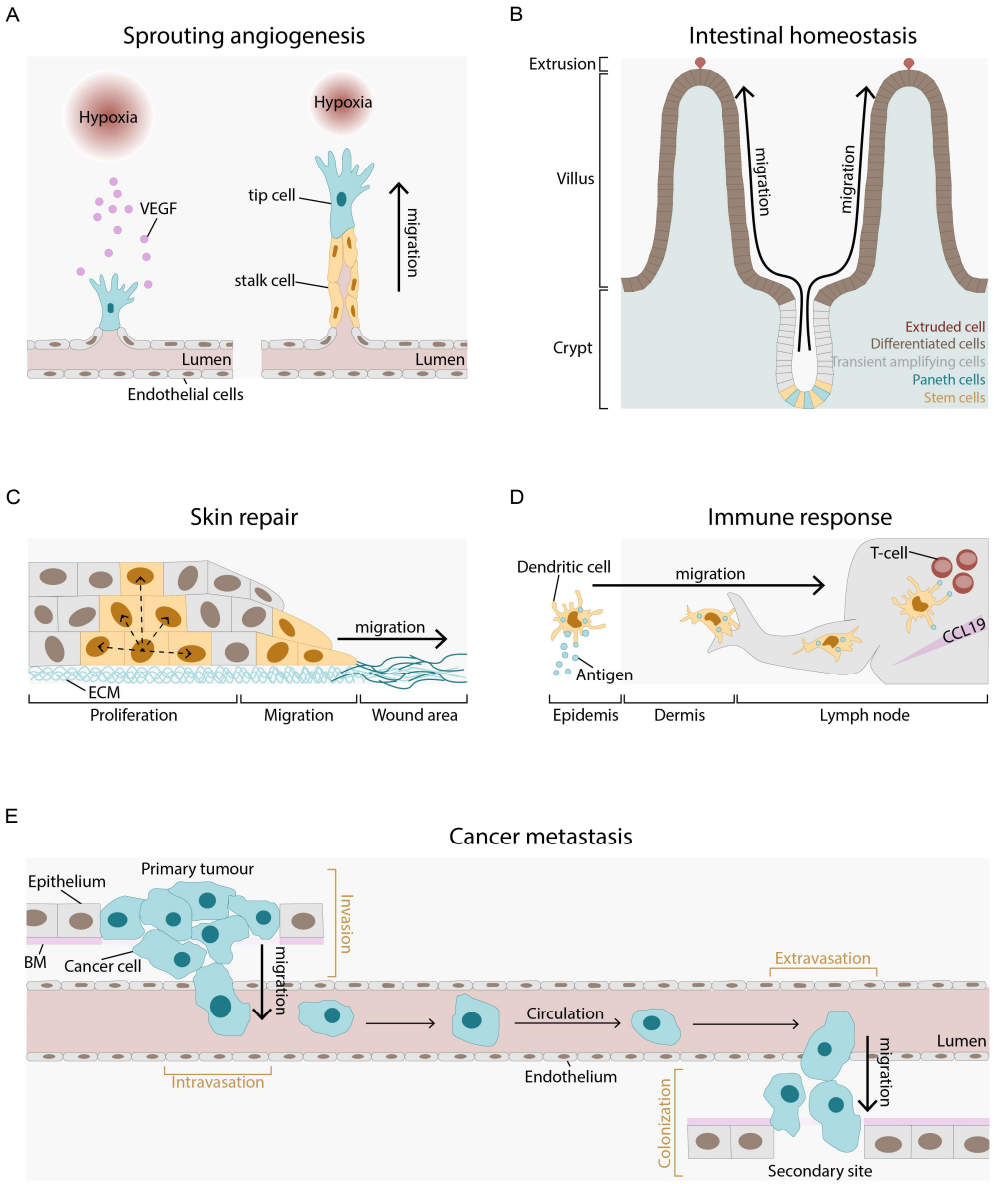

Figure 1 – Examples of directed cell migration. A: Endothelial cells migrate along a gradient of vascular endothelial growth factor (VEGF) during sprouting

angiogenesis. B: Intestinal epithelial cells migrate from the crypt to the tip of the villus for homeostasis. Once at the villus tip, they are further extruded. C: In response to a wound, keratinocytes migrate to repair and re-epithelize the damaged epithelium. D: Dendritic cells migrate from the site of antigen exposure towards the lymph node to present these antigens to T-cells. Upon reaching the lymph node, dendritic cells follow a chemokine gradient of CCL19 to locate T-cells. E: Upon disruption of the basement membrane (BM), cancer cells migrate into nearby blood vessels, where they intravasate and begin circulating in the bloodstream. Through extravasation from blood vessels and manipulation of the local microenvironment at the new site, cancer cells colonize distant organs. (Figure inspired and adapted from: panel A – Lee et al., 2022; panel B – Corominas-Murtra & Hannezo, 2023; panel C – DiPersio, 2007; panel D – Worbs et al., 2017; panel E – Schroeder et al., 2012)

Moreover, during the early stages of an immune response, dendritic cells migrate towards lymphatic vessels to present antigens collected to T cells (Weber at al., 2013) (Figure 1D). This organized movement plays a crucial role in effective communication and coordination of immune responses.

In these directed cell migration examples, precision and tight coordination characterize movement. Failure of this coordination can have serious implications and contribute to the development of diseases. One significant example is the formation of birth defects. Specifically, inadequate guidance of neural crest cells during early development has been identified as a contributing factor in neurocristopathies, which are a range of disorders involving various congenital abnormalities (Watt & Trainor, 2014). Conversely, excessive coordination among cells can also

lead to disease, as observed in the context of cancer. During cancer development, carcinoma cells migrate from the primary tumor site to intravasate blood vessels (Hapach et al., 2019; Roussos et al., 2011b). Afterwards, they extravasate into the bloodstream to establish colonies in distant organs, a process known as metastasis (Figure 1E). Thus, enhanced cell migration in cancer is often associated with poor prognosis.

Directed cell migration has been widely observed across different cell types and functions. Therefore, cells exhibit a spectrum of migration modes. This includes single cell migration, which can manifest in both amoeboid and mesenchymal forms, and multicellular migration, which may occur collectively or through streaming. However, cells exhibit a dynamic capability to transition between modes of single cell migration, and between single cell and multicellular migration. This adaptability depends on various factors, such as tissue topology, extracellular matrix (ECM) composition, degree of adhesion to the ECM, and the presence of biochemical cues (Liu et al., 2015; Ruprecht et al., 2015). For instance, under conditions of physical confinement and low adhesion, fibroblasts and epithelial cells can shift to a faster migration mode, favoring the development of large and stable blebs due to increased cell contractility (Ruprecht et al., 2015). Another illustrative example is hypoxia prevalent in solid tumors, which triggers the transition of collectively invading cancer cells into individually moving amoeboid cells, thereby increasing cancer dissemination (Lehmann et al., 2017). This extreme plasticity underscores the complexity inherent in the mechanisms that regulate directed cell migration.

1.1 Single cell migration

Single cell migration describes the motility of cells as an independent individual entity. Directed migration of single cells can be divided into two morphological variants: amoeboid migration and mesenchymal migration. These variants depend on the cell type, cell-matrix interactions, structure of the actin cytoskeleton, and protease production (Friedl & Wolf, 2003).

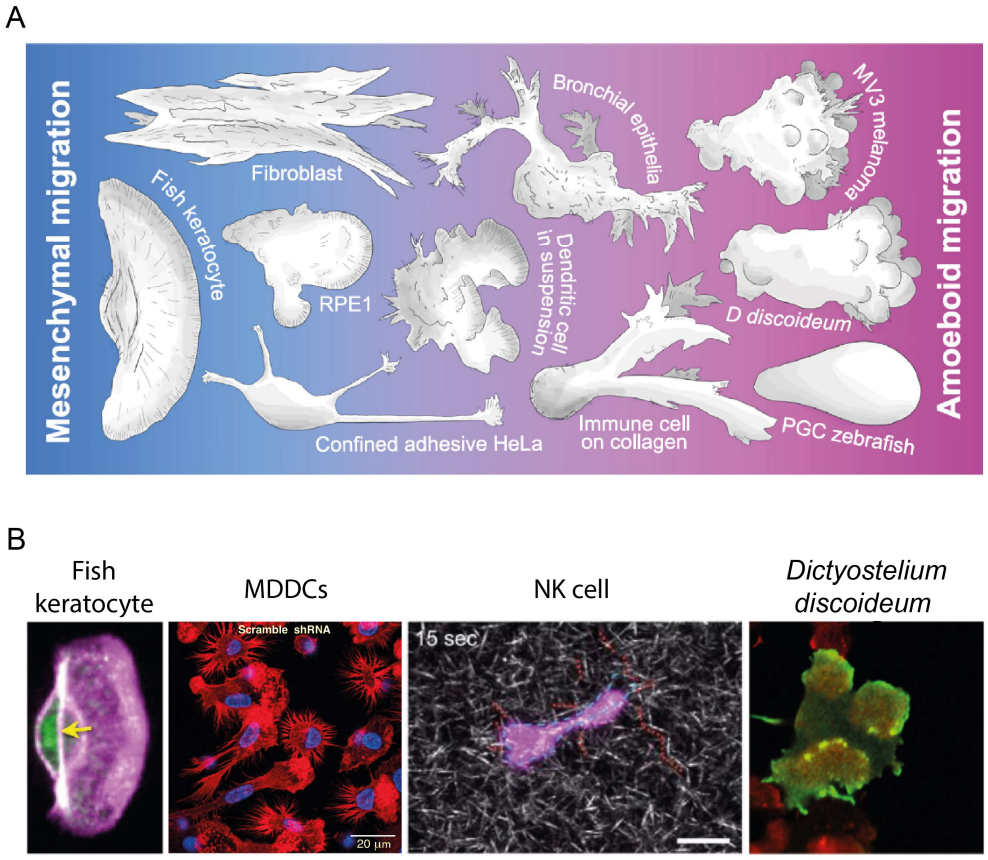

Figure 2 – Morphologies of mesenchymal and amoeboid migrating cells. A: From left to right, the cells are arranged to illustrate morphological shapes

corresponding to their migratory modes. On the far left, mesenchymal migration is characterized by protrusions rich in actin polymerization, such as lamellipodia and filopodia. On the far right, amoeboid migration is primarily driven by pressure-induced protrusions like blebs. B: Microscopic images from different migratory modes. From left to right: fish keratocyte labelled with actin (magenta) and myosin (green); human primary monocyte-derived dendritic cells (MDDCs) labelled with actin (red) and nuclei (blue) four days after scrambled shRNA transduction; natural killer (NK) cell labelled with calcein (pink). Scale bar: 10μm; *Dictyostelium discoideum* cell labelled with actin (red) and myosin (green). (Figure adapted from: panel A – García-Arcos et al., 2024; panel B – Okimura et al., 2018; Ménager & Littman, 2016; Czerwinski et al., 2023; Brzeska et al., 2014)

1.1.1 Mesenchymal migration

Mesenchymal migration (Figure 2) is a prominent mode of migration observed in various cell types, including fish keratocytes (Figure 2B), fibroblasts, neural crest cells, and tumor cells (Roussos et al., 2011b). Mesenchymal migratory cells typically have an elongated shape and exhibit actin-based protrusions, such as lamellipodia and filopodia, at their leading edge (Bear & Haugh, 2014). The migration velocity in this mode is relatively slow owing to a strong dependence on cell-matrix interactions (Friedl et al., 1998). Structurally, these cells exhibit a combination of a cortical and stress fiber-based actin cytoskeleton (Friedl & Wolf, 2003). This contributes to a higher adhesion force generation, which is characterized by fiber pulling and bundling. Therefore, this cellular migration mechanism is traction-dependent, implying that it relies on the forces exerted by the cell on the substrate through

contractile actin networks (Bear & Haugh, 2014). Moreover, a notable feature is the presence of proteolytic ECM remodeling (Wolf et al., 2003). This mechanism helps overcome ECM barriers by generating ECM defects and migratory pathways.

1.1.2 Amoeboid migration

Amoeboid migration (Figure 2) can be observed in the unicellular amoebae *Dictyostelium discoideum* (Figure 2B) (Condeelis et al., 1992) and cell types such as leukocytes (Figure 2B) or tumor cells (Devreotes & Zigmond, 1988). Unlike mesenchymal migration, amoeboid movements are fast because of either weak or no adhesion to the microenvironment (Yumura et al., 1984; Friedl et al., 1998; García-Arcos et al., 2024). Amoeboid protrusions are mainly blebs, which are actin-free membrane "bubbles" that rely on cell contraction and pressure-driven flow inside the cell (Charras & Paluch, 2008; Lämmermann & Sixt, 2009; García-Arcos et al., 2024). Structurally, cells exhibit cortical organization of the actin cytoskeleton, resulting in low adhesion force generation. Additionally, amoeboid migratory cells refrain from matrix metalloproteases (MMPs) activity, which enables them to navigate ECM barriers without active degradation (Wolf et al., 2003; Wyckoff et al., 2006).

1.2 Multicellular migration

Multicellular migration unfolds when cells move into groups or clusters. Multicellular migration can be categorized as collective or streaming migration. This classification depends on several factors,

including the cells' interaction capabilities, ability to degrade the ECM, necessity of cell-cell junctions, and morphological characteristics of the participating cells.

Collective migration describes the coordinated movement and behavior of a group of cells. This migration mode is fundamental during development, morphogenesis, vascular sprouting, tissue repair, and cancer invasion. Although a group of cells may exhibit a lower instantaneous velocity, their movement is notably more persistent (Mayor & Etienne-Manneville, 2016). This persistence allows them to efficiently cover longer distances compared to isolated cells. The key to collective migration is cell-cell interactions, serving not only for physical connections but also for facilitating essential communication among cells. This intercellular communication regulates individual cell motility and protrusion behavior within a group (Mayor & Etienne-Manneville, 2016).

Streaming migration plays a crucial role in development and cancer invasion (Roussos et al., 2011b). This migratory mode is characterized by the directed movement of individual cells situated close to each other, forming a dynamic cell cluster. While streaming, individual cells navigate the same tracks, maintaining alignment without the need for direct or intact cell-cell adhesion. Nevertheless, similar to collective migration, streaming migration frequently involves degradation of the ECM to carve out migratory paths (Roussos et al., 2011a). Therefore, comigrating cells can accurately navigate through these tracks, thereby facilitating their migration and directionality.

2. Cues that trigger directed cell migration

Directed cell migration is typically driven by spatial gradients within the cellular microenvironment. The nature and location of these gradients dictate the specific type of directed cell migration (Figure 3). Migration toward gradients of soluble chemical factors is termed chemotaxis, whereas migration aligned with variations in substrate topology is known as contact guidance. If migration is influenced by gradients in ECM stiffness this is referred to as durotaxis. Alternatively, migration toward variations in substrate-bound proteins is called haptotaxis.

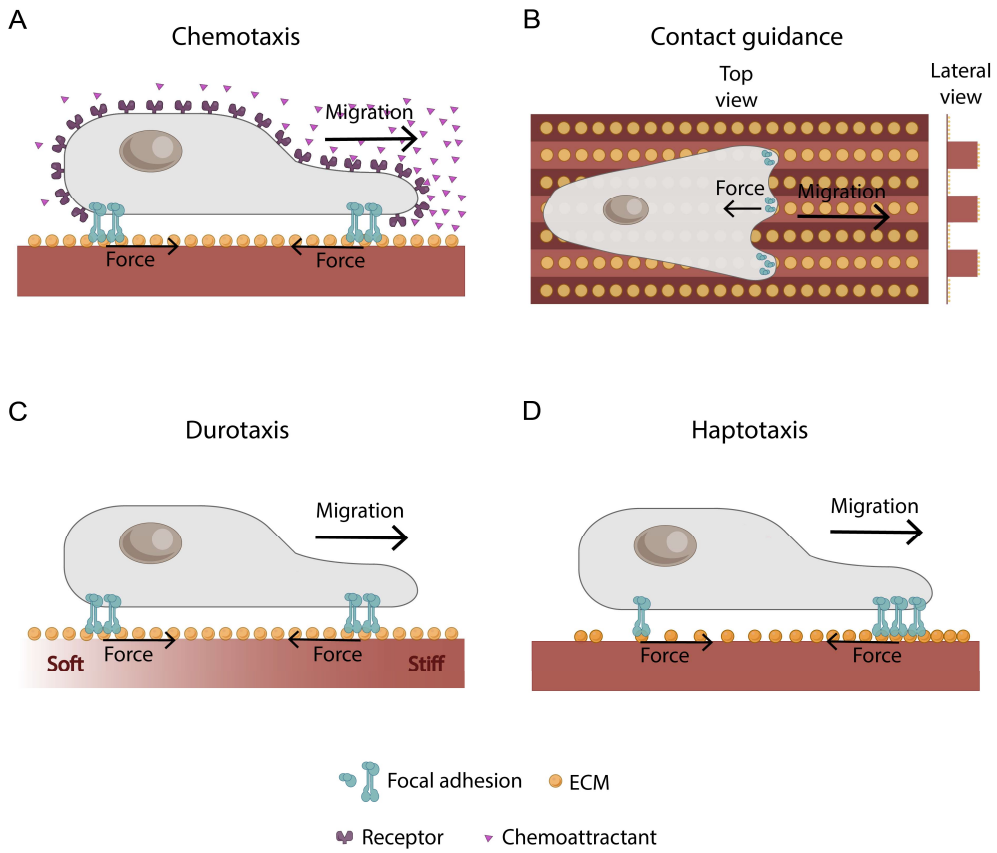

Figure 3 – Types of directed cell migration. A: Chemotaxis: cells navigate gradients of soluble chemical factors. B: Contact guidance: cells orient themselves with topological patterns. C: Durotaxis: cells respond to gradients in the stiffness of the ECM. D: Haptotaxis: cells follow gradients of substrate-bound proteins. (Figure adapted from: Fortunato & Sunyer, 2022)

Additional types of directed cell migration have been observed, including electrotaxis (migration in response to electric field gradients) (Shim et al., 2024; Leal et al., 2023), curvotaxis (migration affected by curvature variations) (Pieuchot et al., 2018; Sadhu et al., 2024), frictiotaxis (migration responsive to friction gradients) (Shellard et al., 2023), and barotaxis (migration influenced by pressure variations) (Lennon-Duménil & Moreau, 2021). However, this section will exclusively introduce the types represented in Figure 3, delving into the nature of these gradients, where they can be observed, and shed light on the current understanding of their underlying biochemical and mechanical mechanisms.

2.1 Chemotaxis

Chemotaxis was first discovered in the late 1800s and was described as the directed movement of cells in response to soluble chemicals (Figure 3A; Figure 4A) (Engelmann, 1881; Pfeffer, 1881; Jennings, 1931; Adler, 1966). Since its initial observation, chemotaxis has been extensively studied across various biological contexts, including *Escherichia coli* migration towards food sources (Adler, 1966; Rashid et al., 2019), *Dictyostelium discoideum* migration towards secreted cAMP

gradients (Gerisch et al., 1975; Huang & Iglesias, 2014), and leukocyte migration towards chemokines released during inflammation and infection (Schall et al., 1990; Wong et al., 2010). Most cells respond passively to chemical cues generated by neighboring cells or tissues. However, some cells, such as dendritic cells, possess the ability to autonomously generate their own gradients (Alanko et al., 2023). This capability enables them to migrate more effectively in complex environments (Alanko et al., 2023).

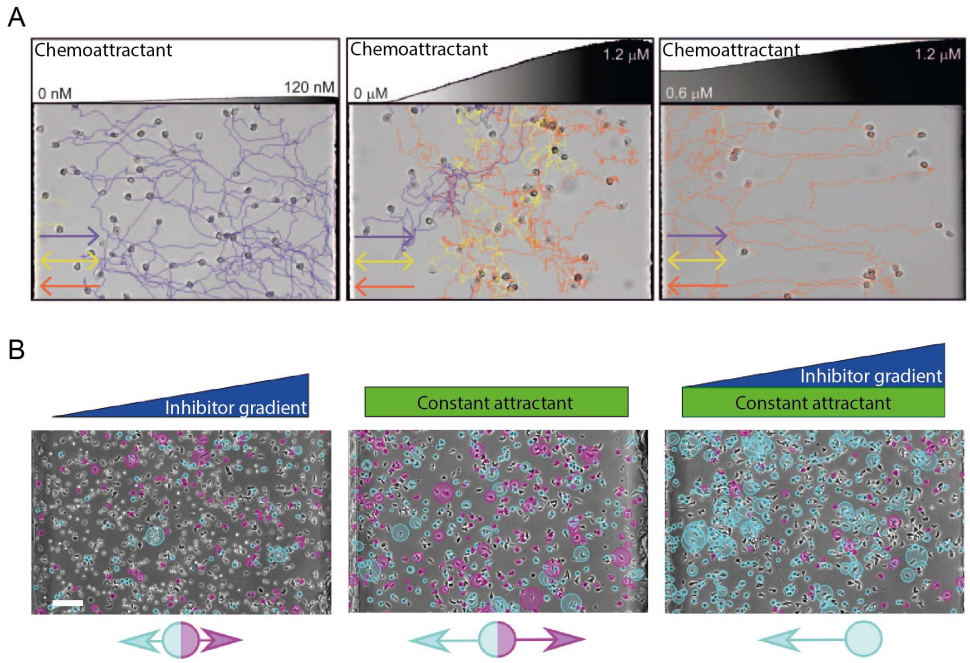

Figure 4 – Chemotaxis forms. A: Gradients of chemoattractant proteins depend on concentration to drive a chemotactic response towards the ligand. Above a defined threshold, this chemoattraction is transformed into chemorepulsion, revealing a chemotactic response driven not only by local ligand density but also by ligand slope. B: Some chemorepellents alone cannot drive any migration

response, and a homogeneous attractant leads to random directionality. However, when both are combined, the competition between the chemokines drives a response to the gradient ligand, resulting in chemorepulsion. (Figure adapted from: panel A – Tharp et al., 2006; panel B – Dowdell et al., 2023)

Chemotactic gradients are detected through the binding of soluble chemicals, commonly referred to as chemoattractants, to specific receptors, such as tyrosine kinase receptors (DesMarais et al., 2009) or G-protein-coupled receptors (Bagorda & Parent, 2008). Upon receptor binding, a chemotactic response is initiated, usually involving the production and degradation of phosphatidylinositol-3,4,5-trisphosphate (PI(3,4,5)P3) in the plasma membrane (Heit et al., 2002; Chung et al., 2001). PI(3,4,5)P3 levels are regulated by PI 3-kinases (PI3Ks) and the PI 3-phosphatase PTEN (Funamoto et al., 2002). When exposed to a chemoattractant gradient, PI3Ks and PTEN dynamically localize to the membrane at the leading and trailing edges of the cell, respectively, and induce cell polarity (Janetopoulos & Firtel, 2008). This localization leads to the selective accumulation of PI(3,4,5)P3 at the leading edge, promoting the extension of actin-enriched membrane protrusions and directed migration (Chen et al., 2007).

Studies have revealed additional complexities in chemotaxis. For example, negative chemotaxis (or chemorepulsion), where cells move away from the chemical source, has been identified during neutrophil migration (Figure 4) (Tharp et al., 2006). Additionally, in bacteria, certain soluble chemicals have been found to induce both positive and negative chemotaxis depending on the chemical concentration (Figure 4A) (Tharp

et al., 2006; Toews et al., 1979). In addition, an indirect negative chemotaxis has been demonstrated in eukaryotic cells, as cells do not directly respond to the chemorepellent but instead exhibit negative chemotaxis when competing for receptor binding with a homogeneous chemoattractant (Figure 4B) (Dowdell et al., 2023).

2.2 Contact guidance

After the discovery of chemotaxis, contact guidance was introduced as a form of directed cell migration in response to substrate topography, such as grooves, arrays, or pillars (Figure 3B) (Harrison, 1912; Weiss, 1934). Since then, contact guidance has been observed in various cell types using structured substrates that either mimic natural topographies or create artificial conditions to uncover hidden cellular properties (Tomba & Villard, 2015).

These studies have revealed that cell response to topographical cues depends on the mode of migration. For example, breast carcinoma cells with mesenchymal migration respond more strongly to aligned collagen fibrils than those with amoeboid migration (Wang et al., 2014). This strong contact guidance response is driven by actin-rich structures and cell-matrix adhesions aligned along the cue direction (Fujita et al., 2009; Albuschies & Vogel, 2013). When substrates present ECM with specific waveforms, cell polarization and directional migration can be delayed above the threshold amplitude. However, at lower amplitudes, the orientation of actin-rich structures and cell-matrix adhesions along the wave axis is facilitated, thereby promoting directed migration (Fischer et al., 2021). These findings reinforce that ECM fibril waveforms

may act as barriers to cell polarization due to subcellular disorientation and potentially affect tumor cell migration.

Although there is still much to understand, contact guidance is described as contractility-independent, as cells can polarize upon inhibition of the main contractile protein in the cells, myosin II (Kubow et al., 2017). Alternatively, Arp2/3, an actin-related protein complex, is seen to enhances topographical detection. This is likely due to a reduction in the membrane protrusion area, leading to an improvement of protrusions alignment along the lines (Ramirez-San Juan et al., 2017). Recent studies have demonstrated that substrate stiffness modulates cellular responses to contact guidance (Comelles et al., 2023). In this study, fibroblasts exhibited stiffness-independent responses in cell-matrix adhesion and actin dynamics. Conversely, both clusters and single breast carcinoma epithelial cells showed stiffness-dependent contact guidance, with increased substrate stiffness promoting more directional and efficient migration.

2.3 Durotaxis

Durotaxis is a phenomenon in which cells migrate directionally in response to stiffness gradients in their microenvironment (Figure 3C; Figure 5) (Lo et al., 2000). This response is usually from soft to stiff and is known as positive durotaxis (Figure 5). *In vivo* and *in vitro* observations of durotaxis include migration of neural crest clusters during *Xenopus laevis* development (Shellard & Mayor, 2021), pancreatic stellate cell activation (Lachowski et al., 2017), and cancer invasion (DuChez et al., 2019; McKenzie et al., 2018). Moreover, collective cell migration exhibits

a more efficient response to durotaxis when compared to single cell. This efficiency comes from long-range force transmission across cells through cell-cell contacts, facilitating their response to these gradients (Sunyer et al., 2016).

Positive durotaxis is driven by the exertion of higher tractions and increasing areas on stiffer surfaces (Espina et al., 2022). Thus, gradient detection requires the activity of proteins that mediate force transmission within cell-ECM adhesions. These pivotal proteins include integrins, two isoforms of myosin II (Raab et al., 2012), focal adhesion kinase (FAK) (Wang et al., 2001), and actin (Vincent et al., 2013). Variations in these proteins and intracellular contractility have been proposed to explain why some cells are more prone to durotaxis than others (Yeoman et al., 2021). However, the role of the Arp2/3 complex in durotaxis remains unclear. While Arp2/3 inhibition impedes single cell durotaxis in cancer cells (DuChez, 2017), contradictory findings indicate that durotaxis is unaffected in human retinal pigment epithelial cells (Rong et al., 2021). Recent studies have highlighted that durotaxis is also regulated by zyxin, a protein specifically found in mature cell-ECM adhesions (Beningo et al., 2001; Hakeem et al., 2022; Yip et al., 2021).

While durotactic responses typically occur due to ECM proteins, 3D epithelial clusters exhibit optimal stiffness when exposed to gradients coated with cell-cell adhesion proteins, such as E-cadherin (Pallarès et al., 2023). Thus, both cell-ECM and cell-cell adhesion can facilitate collective durotaxis. This phenomenon was explained using a continuum model that focused on the interplay between cellular traction, contractility, and surface tension.

In addition to positive durotaxis, also negative durotaxis have been described in recent years (Figure 5). Negative durotaxis, wherein

cells migrate towards softer areas, has been observed in single U-251MG glioma cells (Isomursu et al., 2022) and is thought to contribute to the metastasis of acral melanoma (Huang et al., 2022). This behavior is explained by migration towards cell-intrinsic optimal stiffness, where a cell's contractile and cell-ECM adhesion machinery determines the generation of maximal traction.

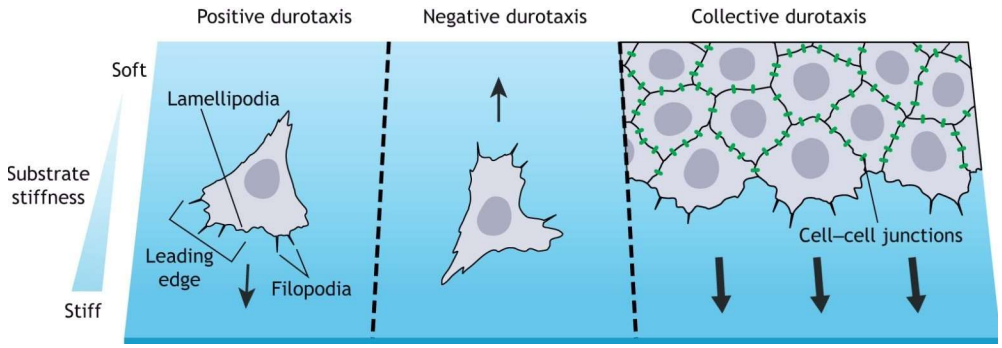

Figure 5 – Durotaxis forms. The most common form of durotaxis is positive durotaxis, where cells move from soft to stiff substrates. However, negative durotaxis, where cells move from stiff to soft substrates, also has been observed. In contrast to single cell, collective durotaxis is highly efficient and has only been observed in the form of positive durotaxis. (Figure adapted from: Mathieu et al., 2024)

2.4 Haptotaxis

Haptotaxis was first identified by Carter in 1965, who observed that fibroblasts migrated along adhesion gradients (Carter, 1965, 1967). Since then, haptotaxis has been defined as directed cell migration guided

by substrate-bound protein gradients (Figure 3D). Therefore, these gradients are typically associated with the ECM proteins.

In vivo observations have revealed the significance of haptotaxis in physiological processes. For example, during an immune response, gradients of the chemokine CCL21 fixed with an ECM component, heparan sulfates, have been identified within the mouse skin. These gradients guide dendritic cells towards the lymphatic vessels (Weber et al., 2013) to perform their immune function. Similarly, fibronectin gradients present in the perivascular space and periphery of breast tumor tissue promote changes in cell morphology and directional movement. These observations were made both *in vitro* and *in vivo*, highlighting the role of haptotaxis in cancer progression and invasion (Oudin et al., 2016; Lu et al., 2014; Santiago-Medina & Yang, 2016). Despite its relevance in physiology and pathology, haptotaxis remains one of the least studied types of taxis. In the following paragraphs, we will summarize what is currently known about haptotaxis.

Previous studies have presented conflicting evidence regarding the key mechanisms of haptotaxis. In 2016, it was demonstrated that myosin contractility and microtubule dynamics play crucial roles in 2D haptotatic gradient sensing (Autenrieth et al., 2016). Additionally, it has been shown that the Golgi apparatus reorients to a posterior position between the nucleus and trailing edge during haptotaxis (Figure 6A) (Autenrieth et al., 2016). In agreement with this work, myosin has also been highlighted as an important factor in haptotatic responses of fibroblasts in 3D environments (Figure 6B) (Moreno-Arotzena et al., 2015). However, in 2016, another study claimed that dynamics of actin-rich membrane protrusions, specifically lamellipodia, were the key determinant of haptotatic migration in fibroblasts and vascular smooth

muscle cells (King et al., 2016). Differences in lamellipodial dynamics were shown to bias cell migration towards higher protein concentrations (Figure 6C). This study also identified a specific subset of lamellipodia regulators crucial for haptotaxis by systematically dissecting the specific pathway upstream of the Arp2/3 complex (Figure 6D), further linking the components of this pathway to cancer metastasis (King et al., 2016). They also demonstrated that haptotaxis operates through this pathway, not only in 2D but also in 3D environments (King et al., 2016). Interestingly, this study rejects the idea that myosin contractility is necessary for gradient recognition during haptotatic migration of fibroblasts. Therefore, the role of contractility in haptotaxis and its key mechanisms remains unclear.

Although fibroblasts have been extensively studied in the context of haptotaxis, other cell types exhibit distinct behaviors in response to substrate-bound protein gradients (Autenrieth et al., 2016; Moreno-Arotzena et al., 2015; King et al., 2016; DeLong et al., 2005). Mesenchymal stem cells (MSCs) and fibroblasts encounter haptotactic gradients at the interface between healthy and fibrotic tissues as they migrate towards an injury site (Wen et al., 2015). However, in contrast to fibroblasts, which display robust haptotactic responses, MSCs require modulation of cell-matrix adhesions to exhibit similar behaviors (Wen et al., 2015). To understand how adhesion dynamics dictate haptotaxis, they developed RGD and collagen gradients in polyacrylamide hydrogels with physiologically relevant stiffnesses. These experiments indicated that haptotactic behaviors are limited by adhesion (Wen et al., 2015). Fibroblasts exhibited robust haptotaxis regardless of ligand composition and fiber deformation, whereas MSCs displayed haptotaxis only when cell-matrix adhesion was indirectly reduced by the addition of free

soluble matrix ligand mimetic peptides (Wen et al., 2015). This study highlights the importance of substrate adhesion dynamics in the regulation of haptotactic response. Additionally, it also provides insights into the distinct migratory behaviors of different cell types in response to substrate gradients. In addition to MSCs, protein gradients on surfaces have also been shown to modulate neuronal development. Using gradients of pure laminin to pure BSA, rat hippocampal neurons revealed that axons tend to grow in the direction of increasing laminin density (Figure 6E) (Dertinger et al., 2002). Specifically, linear gradients with a certain laminin concentration slope resulted in directed axon growth, whereas gradients with lower slopes had no detectable effect (Dertinger et al., 2002). Substrate-bound netrin-1 gradients have also been described to promote growth cone attachment and axon guidance in neurons (Dominici et al., 2017; Qiu et al., 2024).

Like other types of directed cell migration, haptotaxis also exhibits unconventional mechanisms. For instance, amoeboid human T lymphocytes move through haptotaxis mediated by integrin α4β1 found on endothelial venules (Figure 6F) (Luo et al., 2020). However, these lymphocytes are attracted to areas with decreased adhesion mediated by integrin αLβ4 (Figure 6F). This behavior was termed reverse haptotaxis and was not observed in the mesenchymal cells. Moreover, the described mechanisms of mesenchymal haptotaxis favor orientation towards increasing adhesion and cannot fully explain reverse haptotaxis (Luo et al., 2020). Nevertheless, multidirectional integrin-mediated haptotaxis might operate around transmigration ports on endothelia, stromal cells in lymph nodes, and inflamed tissues where integrin ligands are spatially modulated (Luo et al., 2020).

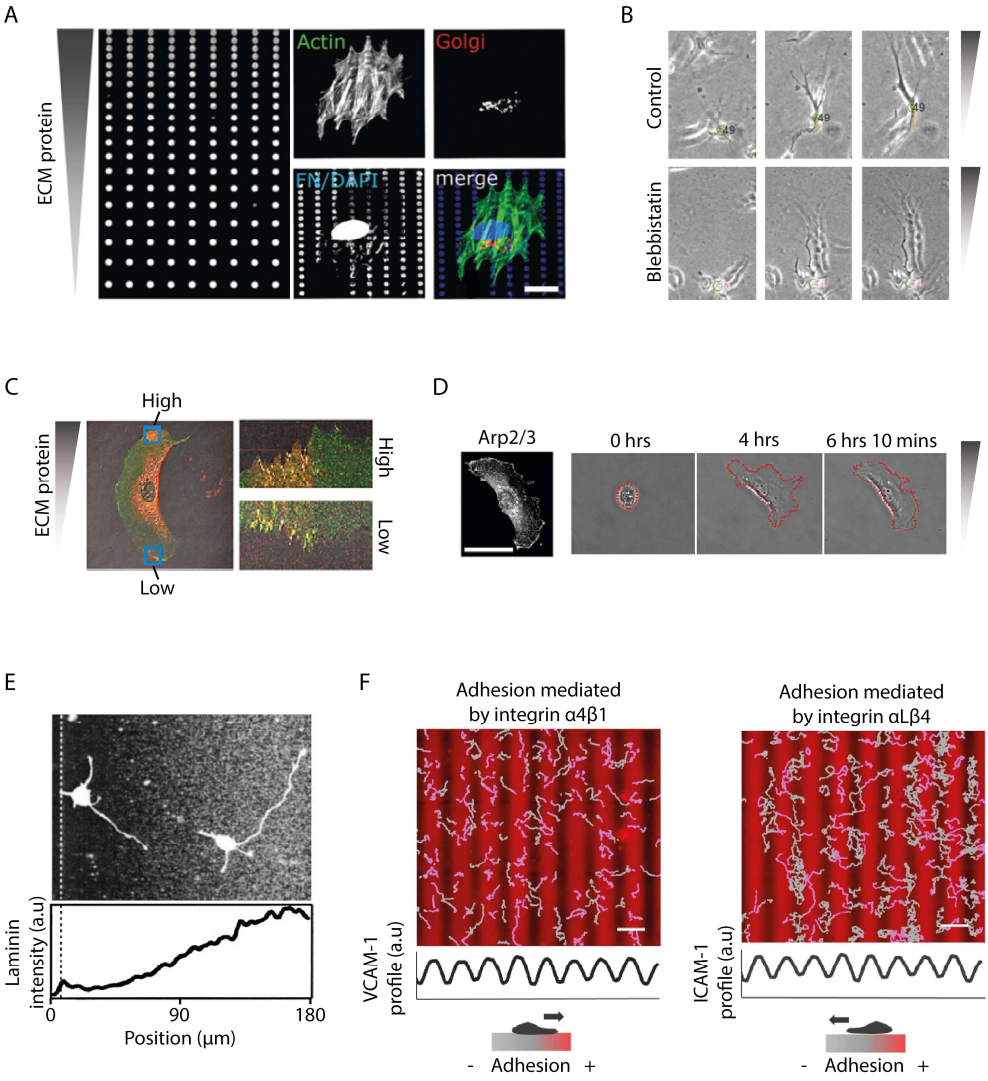

Figure 6 – Described mechanisms of haptotaxis. A: Chick embryonic fibroblasts migrating in digital gradients show directional migration towards higher ECM protein densities when the Golgi is positioned behind the nucleus. Scale bar is 10 μm. B: Human dermal fibroblasts follow gradients of platelet-derived growth factor BB (PDGF-BB). However, this response is lost when the cells are cultured with blebbistatin, an inhibitor of myosin and contractility. C: Microscopic images showing a fibroblast with its edges exposed to different concentrations of ECM protein. Membrane protrusions extend more in areas

with higher protein concentrations compared to lower protein areas. D: Fibroblasts exhibit increased Arp2/3 at the cell edge exposed to higher protein concentrations, aligning with their direction of movement. Scale bar is 50 μm. E: Axons from rat hippocampal neurons tend to grow in the direction of increasing laminin density. F: T lymphocytes display different haptotaxis modes, depending on the type of adhesion they form. When the gradient is made of vascular cell adhesion molecule (VCAM-1), lymphocytes adhere through α4β1 and migrate towards higher VCAM-1 concentrations. In contrast, when the gradient is made of intercellular adhesion molecule (ICAM-1), lymphocytes adhere through αLβ4 and migrate towards lower ICAM-1 concentrations. Scale bars is 200 μm. (Figure adapted from: panel A – Autenrieth et al., 2016; panel B – Moreno-Arotzena et al., 2015; panel C – King et al., 2016; panel D – King et al., 2016; panel E – Dertinger et al., 2002; panel F – Luo et al., 2020)

Upon encountering an external cue, directed cell migration occurs through distinct steps: 1) sensing the cue; 2) interpreting and transducing the cue by coordinating the migration machinery accordingly. The role of the physical forces is central to these steps. These forces are not only integrated into signal sensing, but also act in transmitting information throughout the cell to coordinate a response. Therefore, forces play a crucial role in the directed migration mechanisms. The following sections introduce these migratory steps with a focus on forces.

3. Sensing mechanical gradients

To directly migrate, cells must first sense the gradient. In some types of directed cell migration, physical forces play a minor role in gradient

sensing. For instance, chemotaxis sensing is primarily mediated by G-protein-coupled or tyrosine kinase receptors. However, when cells move in response to mechanical cues, such as stiffness or substrate-bound proteins, physical forces become crucial for sensing external cues. This specific sensing process is referred to as mechanosensing. Mechanosensing involves cell detection and interpretation of mechanical cues from their surroundings. During migration, this occurs through cell-ECM contacts, known as focal adhesions (FAs). FAs not only enable cells to detect changes in ECM properties but also allow them to exert pushing and pulling forces on the ECM. Initially, the ECM resists these forces because of stiffness, which varies from an elastic modulus of hundreds (e.g., lung) to tens of kilopascals (e.g., skeletal muscle) to thousands of kilopascals (e.g. bone) (Figure 7A) (Levental et al., 2007; Swift et al., 2013; Saraswathibhatla et al., 2023; Helvert et al., 2018). As cell forces intensify, ECM resistance increases nonlinearly, or ECM stiffness, known as nonlinear elasticity (Storm et al., 2015; Saraswathibhatla et al., 2023). Over time, sustained cell forces cause ECM resistance to relax through stress relaxation, resulting in creep under loading (Saraswathibhatla et al., 2023). This behavior is defined by the ECM viscoelasticity. Eventually, upon the release of cellular forces, permanent deformations occur due to ECM mechanical plasticity (Saraswathibhatla et al., 2023).

Thus, this section will focus on the two main elements of mechanosensing: the different ECM components and the assembly, maturation, disassembly, and transport mechanisms of FAs.

3.1 Extracellular matrix (ECM)

Extracellular matrix (ECM) is a complex and dynamic network that surrounds cells (Figure 7B). ECM provides structural support, regulates cellular behavior, and participates in numerous physiological processes, including tissue development, homeostasis, and wound healing (Mouw et al., 2014; Saraswathibhatla et al., 2023). Moreover, ECM serves as a scaffold for cell adhesion, migration, and differentiation (Saraswathibhatla et al., 2023). The ECM also acts as a reservoir for growth factors, cytokines, and other signaling molecules, regulating their availability and activity (Gattazzo et al., 2014). This dynamic network is composed of various macromolecules such as collagen, fibronectin, laminin, elastin, and hyaluronic acid (HA).

Collagen is the most abundant protein in the ECM and is essential for tissue integrity and mechanical strength (Figure 7B) (Fratzl, 2008; Svensson et al., 2010). It forms fibrils, networks, and filaments that contribute to the structural framework of tissues, such as skin, bone, cartilage, and tendons (Birk & Bruckner, 2005; Shadwick, 1990; Shoulders, 2009). Collagens are characterized by their triple-helical structure, which is stabilized by hydrogen bonds and other interactions between amino acid residues (van der Rest & Garrone, 1991). These collagenous structures provide tensile strength and resilience to the tissues, allowing them to resist mechanical stress and deformation. Collagen turnover and remodeling are tightly regulated processes essential for tissue repair, regeneration, and homeostasis. Dysregulation of collagen metabolism is associated with various pathological conditions including fibrosis, arthritis, and cancer (Tang et al., 2020).

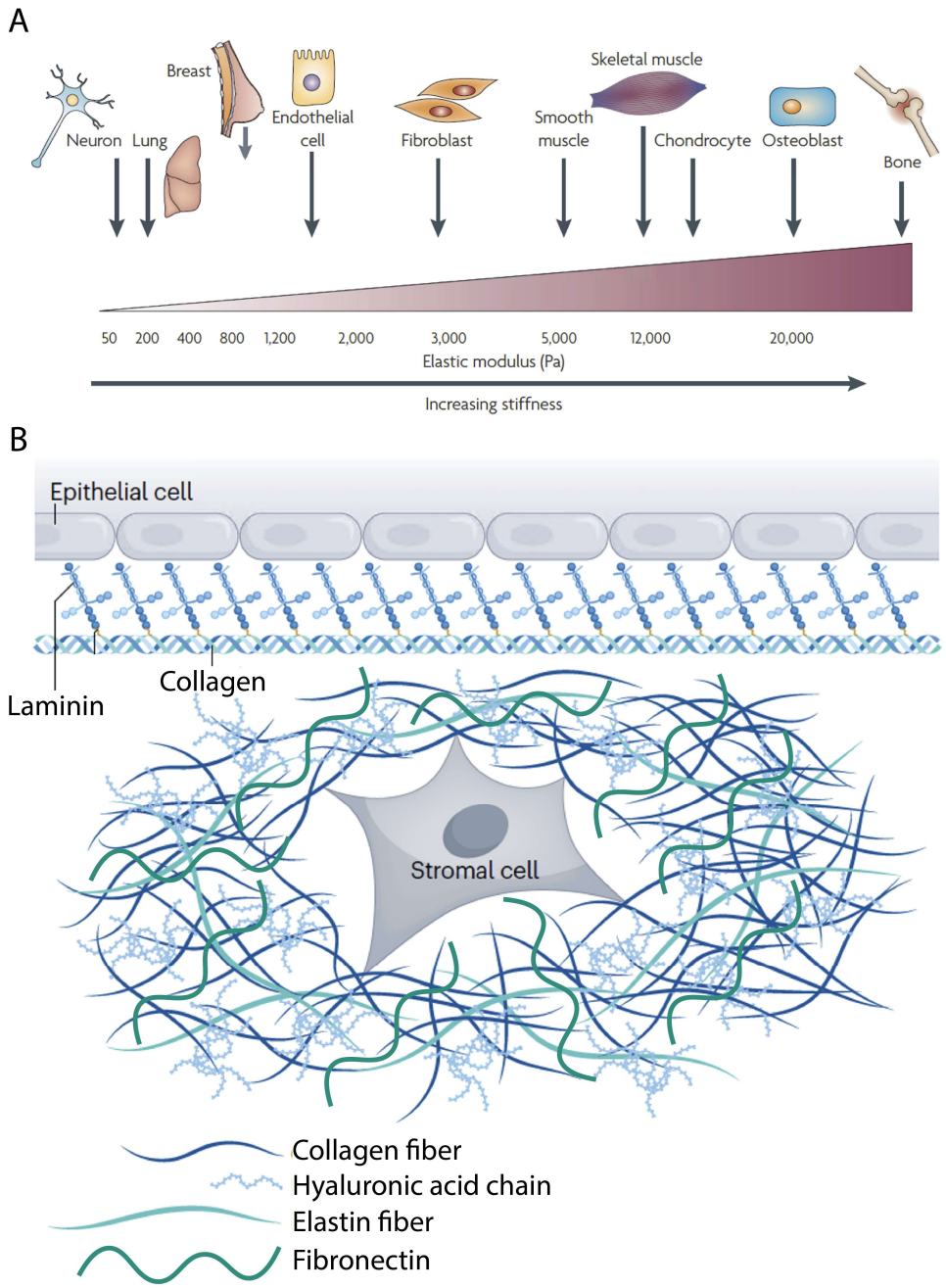

Figure 7 – ECM stiffness ranges and its components. A: The stiffness of the ECM varies significantly across different tissues. For example, lung ECM stiffness is in the range of hundreds of pascals, smooth muscle ECM stiffness is in the

range of thousands of pascals, while skeletal muscle ECM stiffness reaches tens of thousands of pascals. B: Epithelial cells have varying ECM components with different spatial organizations on their basal side. Stromal cells, such as fibroblasts, are responsible for producing and maintaining the ECM suitable for the requirements of the tissue. (Figure adapted from: panel A – Butcher et al., 2009); panel B – Saraswathibhatla et al., 2023)

Fibronectin is another important ECM protein that mediates cell adhesion and signaling (Figure 7B) (Vogel, 2006). It exists in both soluble and insoluble forms and interacts with integrin receptors from FAs via its two arginine–glycine–aspartate (RGD) sequences (Lemańska-Perek & Adamik, 2019; Humphries et al., 2006). It also binds to other ECM components such as collagen and fibrin, forming a scaffold that supports cell migration and tissue organization (Kubow et al., 2015). Fibronectin plays a key role in tissue morphogenesis, wound healing, and embryonic development (Bonnans et al., 2014; Lemańska-Perek & Adamik, 2019). Dysfunctional fibronectin signaling has been implicated in cancer metastasis, cardiovascular diseases, and developmental disorders (Bonnans et al., 2014).

Laminin is a glycoprotein and a major component of the basement membrane, a specialized ECM structure that separates epithelial and endothelial cells from the underlying connective tissue (Figure 7B) (Yurchenco, 2011; Chang & Chaudhuri, 2019). Laminin plays an important role in cell adhesion, migration and differentiation, providing a scaffold for tissue organization and integrity (Hamill et al., 2009). It also interacts with other ECM components, such as collagen and proteoglycans, to modulate cell behavior and signaling (Dzobo &

Dandara, 2023). Mutated laminin has been implicated in various diseases including muscular dystrophy and kidney disorders (Nelson et al., 2015; Vijayakumar et al., 2014).

Elastin provides elasticity and resilience to tissues such as the skin, blood vessels, and lungs (Figure 7B) (Huang et al., 2021). It forms elastic fibers that recoil after stretching to maintain tissue shape and function. Elastin molecules are cross-linked to each other and to other ECM proteins such as fibrillin, originating a network which promotes mechanical stability and tissue flexibility (Cocciolone et al., 2018; Chaudhuri et al., 2020). Elastin synthesis and assembly are tightly regulated processes essential for tissue development and repair (Wang et al., 2021). Mutated elastin is associated with hereditary connective tissue disorders such as Marfan syndrome (Thomson et al., 2019).

HA is a non-proteinaceous ECM component that regulates tissue hydration, lubrication, and viscoelasticity (Figure 7B) (Huang et al., 2021). It forms a high molecular weight glycosaminoglycan that binds to water molecules, creating a hydrated gel-like matrix that fills the interstitial spaces within tissues (Balazs et al., 1986). HA also interacts with cell surface receptors, such as CD44 and the receptor for hyaluronan-mediated motility (RHMM) (Saraswathibhatla et al., 2023). Dysregulated HA metabolism is associated with inflammatory diseases, osteoarthritis, and cancer metastasis (Wolf & Kumar, 2019).

ECM production and remodeling are mainly performed by fibroblasts and pericytes (Huang et al., 2021), also known as stromal cells (Figure 7B). Fibroblasts are widely distributed in connective tissues and tumors (Huang et al., 2021; Kalluri & Zeisberg, 2006). Fibroblasts secrete structural ECM proteins, such as collagen and fibronectin, as well as enzymes involved in ECM modification and degradation (Lynch & Watt,

2018; Voloshenyuk et al., 2011; Brilla et al., 1995). These cells respond to various signaling cues, including cytokines, growth factors and mechanical forces, regulating ECM composition and stiffness (Voloshenyuk et al., 2011; Siwik et al., 2000; Balestrini & Billiar, 2006). Pericytes are located around endothelial cells and contribute to their vascular stability and function. Pericytes interact with ECM and other cell types within the vessel wall (Payne et al., 2019).

3.2 Focal adhesions (FAs)

FAs are dynamic protein complexes that connect the actin cytoskeleton of cells to ECM components such as RGD and collagen. These adhesions facilitate bidirectional transmission of mechanical signals between cells and their microenvironment. Therefore, in addition to anchoring the cells, FAs also function as cell mechanosensors of ECM characteristics, which are essential for translating cytoskeletal forces into migration and cell signaling (Riveline et al., 2001; Geiger et al., 2009). FAs are composed of several proteins including integrins, FAK, paxillin, talin, vinculin, zyxin, and α-actinin (Figure 8) (Hynes, 2002; Geiger et al., 2009; Winograd-Katz et al., 2014).

FAs assembly is characterized by the sequential recruitment of adhesion proteins around a central nucleation site (Figure 8A). This process is initiated beneath small membrane protrusions by the engagement of integrin receptors. Integrins are transmembrane heterodimers containing α- and β-subunits (Saraswathibhatla et al., 2023). The α- and β- subunits preferentially combine according to the ECM protein. For example, α1β1 integrin is the main receptor for collagen,

whereas α5β1 integrin usually links RGD sequences present in fibronectin (Hynes & Naba, 2012). The extracellular domain of integrin is directly linked to ECM components and the intracellular domain links cytoplasmic adhesion proteins. Therefore, upon binding to the ECM, integrins undergo conformational changes that initiate intracellular signaling pathways. This leads to the recruitment and activation of adaptor proteins such as FAK, paxillin, and talin (Figure 8) (Geiger et al., 2009; Winograd-Katz et al., 2014). Talin is a key FA protein because it not only links integrins to actin filaments but also plays a role in integrin activation (Zhang et al., 2008; Geiger et al., 2009). Similar to integrins, talin unfolds under force. Mechanical forces generated by actin polymerization, the actin movement from the interior to the cell edge, or contraction increase the association of talin with integrin and promote talin unfolding. Previous studies have shown that talin unfolding occurs when ∼5pN of force is reached (Yao et al., 2014). Association of integrin with FAK, paxillin, and talin results in the formation of nascent focal adhesions (Figure 8A) (Beningo et al., 2001). These nascent adhesions serve as initial anchoring points that stabilize the leading edge and reinforce the formation of membrane protrusions (Ban et al., 2018).

Over time, these stabilized adhesions undergo maturation owing to intracellular contraction and actin movement from the edge to the cell interior, known as actin retrograde flow. This enhances the generation of traction and tension at the FAs. Consequently, vinculin unfolds and engages with stretched talin, maintaining talin in an open conformation (Figure 8A) (Atherton et al., 2016). As vinculin also binds to actin, the association of this protein stabilizes and reinforces FAs (Atherton et al., 2016). The recruitment of zyxin and α-actinin is also critical for FA maturation (Figure 8) (Grashoff et al., 2010). α-Actinin accumulates with

actin and reorients it, promoting FAs growth and elongation (Choi et al., 2008). This process leads to clustering of integrins and FAs strengthening, resulting in mature focal adhesions (Figure 8) (Calderwood et al., 2013; Sun et al., 2016). Therefore, traction and tension directly influence the maturation of focal adhesions, with different adhesion proteins displaying variable sensitivity to mechanical forces (Ban et al., 2018).

When the tension at the integrins reaches high levels, FAs disassembly occurs at both the trailing and leadings edges. At the leading edge, disassembly is facilitated by actin depolymerization and actin reorganization (Webb et al., 2002). This promotes the formation of new protrusions and adhesions at the leading edge. Disassembly at the leading edge is also facilitated by modulating local contractility due to the constant extension and retraction cycles of cell protrusions. At the trailing edge, disassembly is mainly facilitated by the weakening of local contractility and involves the dissociation of paxillin and α-actinin from FAs (Choi et al., 2008; Laukaitis et al., 2001). This leads to trailing retraction and inward movement of the cell edge, accompanied by slipping of the adhesions. Interestingly, FAs disassembly is not a simple reversal of the sequential assembly mechanism (Giannone et al., 2004). For example, paxillin and α-actinin assemble sequentially, but disassemble simultaneously.

During both assembly and disassembly, FAs proteins are dynamically transported within the cell to and from adhesion points. Photobleaching experiments revealed distinct dynamics in trailing adhesions, slipping ones, compared to leading adhesions, stationary ones (DeMali et al., 2002; Gupton & Waterman-Store, 2006). Specifically, integrin diffusion appears to increase slipping adhesion, indicating a

potential decrease in the affinity of integrins for one or more proteins with which they link (Ballestrem et al., 2001). This turnover mechanism seems to be orchestrated by microtubules, which regulate the localization of adhesion points and dynamics of FAs proteins in response to the ECM (Kaverina et al., 1999).

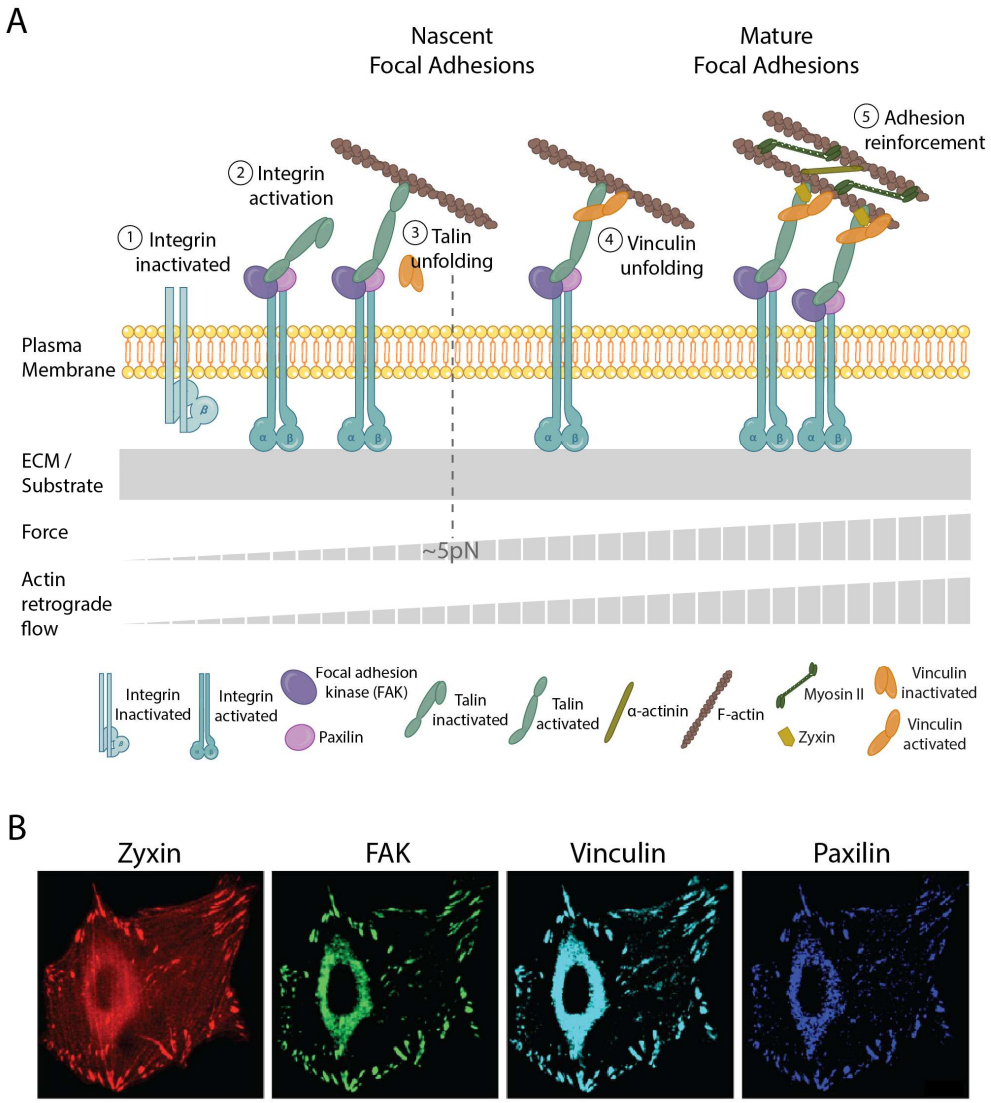

Figure 8 – FAs composition and maturation in response to force. A: Above 5pN of force, talin unfolds to promote the link between the integrin and actin. This unfolding expose protein binding sites and recruit vinculin to the adhesion complex. Upon the recruitment, integrin clusters, adhesions grow and become reinforced, passing from nascent to mature FAs. B: Microscopic images of rat embryonic fibroblasts (REF52) stained for zyxin, FAK, vinculin, and paxillin, revealing the morphology of mature focal adhesions. (Figure adapted from: panel A – Fortunato & Sunyer, 2022; panel B – Malik-Sheriff et al., 2018)

4. Downstream effects of mechanosensing

After mechanosensing a gradient via FAs, cells respond internally by integrating these external signals. This process is known as mechanotransduction, where a mechanical signal is transduced into a biochemical response within the cell.

A clear example is the subcellular translocation of Yes-associated protein (YAP) due to force. YAP functions as a pivotal mechanosensitive regulator within cells, primarily dictated by its localization—in either the cytoplasm or nucleus (Figure 9A) (Zanconato et al., 2016; Porazinski et al., 2015). In the nucleus, YAP acts as a transcriptional coactivator, binding to TEAD transcription factors to modulate gene expression patterns crucial for various cellular functions (Figure 9A) (Zhao et al., 2008). YAP's nuclear localization is regulated by mechanical signals, such as ECM stiffness (Elosegui-Artola et al., 2016), and involves cell cytoskeleton integrity (Das et al., 2016) and FAs arrangement (Elosegui-Artola et al., 2016). Thus, high force directs YAP translocation from the cytoplasm to the nucleus by changing the mechanical limitation of nuclear pores, thereby regulating its activity and downstream gene expression

(Figure 9A) (Elosegui-Artola et al., 2017). Moreover, force-induced YAP translocation also depends on nuclear transport (Andreu et al., 2022; Driscoll et al., 2015; Elosegui-Artola et al., 2017).

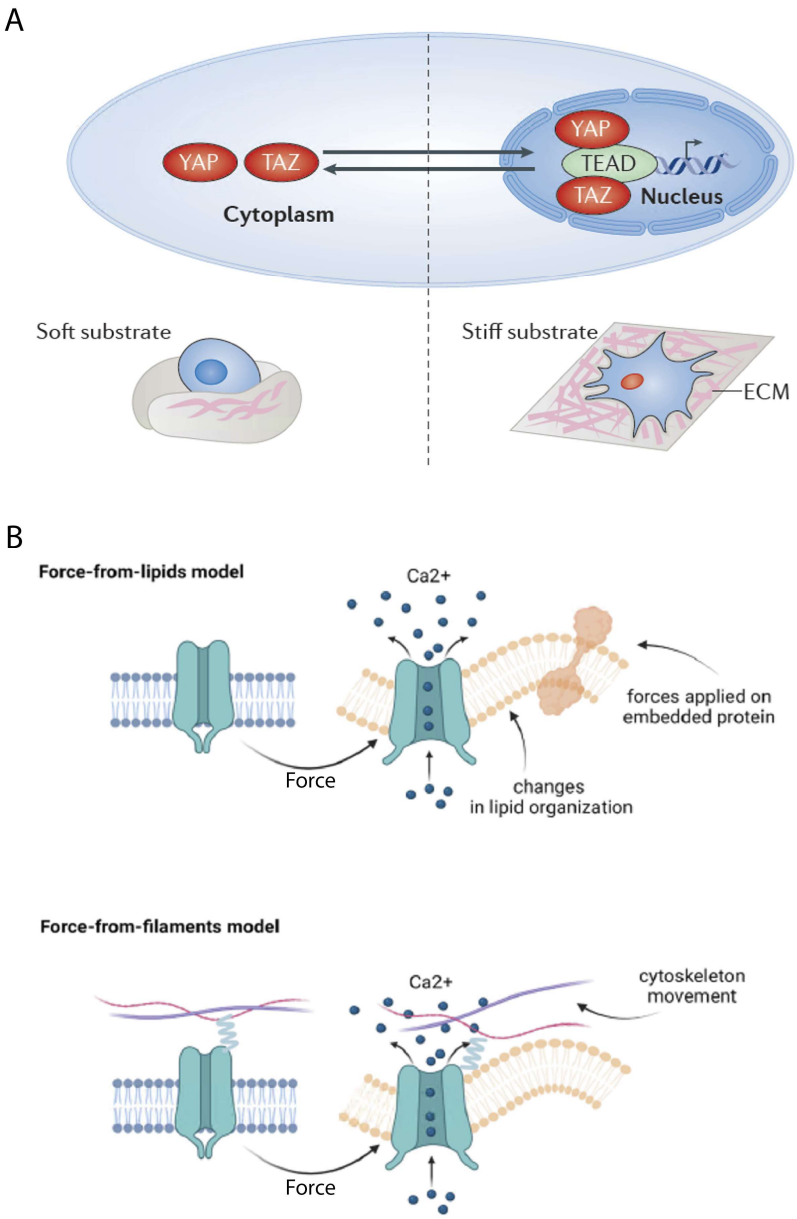

Figure 9 – Examples of biochemical signals driven by force. A: Cells seeded on soft substrates exhibit YAP localization in the cytoplasm. However, when seeded on stiff substrates, higher traction forces are generated, causing YAP to translocate from the cytoplasm to the nucleus. This translocation leads to expression of important genes. B: Force can activate ion channels, such as Piezo, either through direct forces within the lipid membrane due to changes in lipid organization or through intracellular forces driven by cytoskeleton filaments. Both activation approaches result in an increased influx of Ca2+. (Figure adapted from: panel A – Panciera et al., 2017; panel B – Karska et al., 2023)

Another example of a biochemical process driven by force is the non-selective ion channel Piezo1. Piezo1 detects changes in membrane tension and regulates the influx of several cations, such as Ca2+, across the cell membrane (Figure 9B) (Coste et al., 2010; Yao et al., 2022; Syeda et al., 2016). Activation of Piezo1 not only leads to Ca2+ influx but also subsequent activation of calcium-dependent signaling pathways, including those involving NFATs, Calcineurin, and PKCs (Aglialoro et al., 2020). This cascade results in the inside-out activation of integrins, increasing cellular adhesion and influencing cell behavior (Aglialoro et al., 2020; Liu et al., 2024). Therefore, the mechanotransduction process mediated by Piezo1 involves its interaction with FAs assembly.

Even though various biochemical reactions can occur, the most crucial response is the establishment of cell polarity, particularly front-to-rear polarity. Key proteins that define this polarity regulate the actin cytoskeleton, thereby controlling the generation and organization of actin structures essential for migration. Thus, this section will explore different

types of cell polarity and the general role of the cell cytoskeleton, with a particular focus on front-to-rear polarity and the actin cytoskeleton.

4.1 Cell polarity

Cell polarity represents the asymmetric distribution of cytoplasm, organelles, and proteins within a cell, a fundamental aspect crucial for various physiological processes. While cell polarity has been demonstrated to be crucial for cell persistent migration (Vaidžiulytė et al., 2022), its integration with the sensing of gradient cues remains unknown.

Cell polarity manifests in multiple forms, including apicobasal, planar, and front-to-rear polarity. Apicobasal polarity refers to the epithelial organization in an apical membrane facing the outside of the body and a basal membrane oriented towards the underlying tissue. This polarity is critical for maintaining the functional and structural integrity of epithelial tissues. Key apical polarity regulators include Crumbs, aPKC, PTEN, and Par3, which are involved in forming the apical junctional complex and segregating the junctional domain from the apical membrane (Tepass, 2012). Conversely, the basolateral polarity module includes proteins like Dlg, Lgl, Scrib, and Par-1, essential for regulating intercellular junctions (Mysh & Poulton, 2021).

Planar cell polarity (PCP) involves the coordinated polarization of cells within the plane of a tissue. PCP is essential for processes like tissue elongation, proper orientation of hair follicles, and collective migration. Thus, a core PCP pathway, including Wnt-Frizzled/PCP signaling, promotes cellular orientation and coordination of collective cell movements (Koca et al., 2022). Other PCP proteins include Vang, Pk, and

Dsh, which are conserved across species and crucial for establishing PCP through their asymmetric distribution within cells (Montcouquiol et al., 2008; Gray et al., 2011; Ossipova et al., 2022).

Front-to-rear polarity establishes an asymmetry within the cell, where the localization of specific proteins and organelles, along with distinct morphological features, define the cell's front and rear. This polarity enables cells to orient themselves and move in the right direction. Therefore, the establishment of front and rear polarity is essential for directed cell migration.

4.1.1 Front-to-rear polarity

Front-to-rear polarity in directed cell migration refers to the asymmetric organization of cellular components, establishing a leading edge (front) and a trailing edge (rear) within a migrating cell (Figure 10). For example, organelles such as the nucleus, Golgi apparatus (GA), and microtubule-organizing center (MTOC) exhibit front-to-rear polarity. The MTOC and GA typically position themselves between the nucleus and the leading edge (Maninová et al., 2013). Contrarily, the nucleus is often located at the trailing edge. Nuclear reorientation and polarity are mediated by the LINC complex, which physically connects the nucleus and the cytoskeleton. This process is further regulated by signaling pathways such as the LPA-mediated activation of Rho GTPases and integrin-FAK-Src-p190RhoGAP signaling at the leading edge (Maninová et al., 2013). Although the front-to-rear polarity of organelles is relevant, the key role of this polarity in directional movement is to coordinate the signaling

pathways and cytoskeletal dynamics essential for propulsion and guidance. (Maninová et al., 2013; Vassilev et al., 2017).

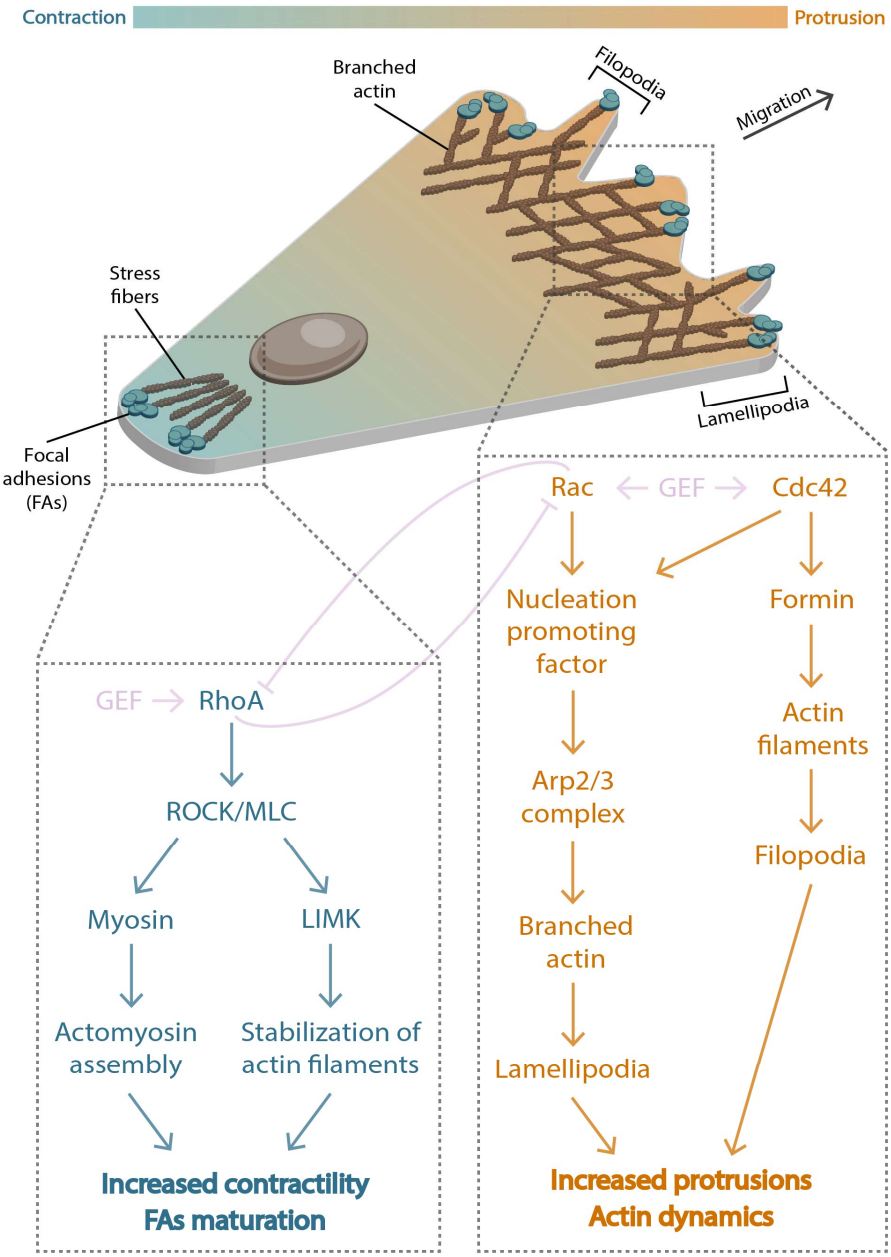

Figure 10 – Regulation of front-to-rear polarity. During cell migration, a gradient of Rho GTPase activity is established. At the front of the cell (orange zone), active Rac1 and Cdc42 stimulate actin polymerization through the Arp2/3 complex and formin, generating cell protrusions such as lamellipodia and filopodia. Conversely, at the rear of the cell (blue zone), active RhoA promotes contractility by enhancing the maturation of focal adhesions and the formation of stress fibers. (Figure from: Fortunato & Sunyer, 2022)

The establishment of front-to-rear polarity is mainly coordinated by the Rho family of GTPases. Rho GTPases are regulated by guanine nucleotide exchange factors (GEFs) (e.g., Vav2, ARHGEF2 and ARHGEF40) and GTPase-activating proteins (GAPs) (e.g., ARHGAP24 and ARHGAP35), which control the active (GTP-bound) and inactive (GDP-bound) states of the GTPases (Ohashi et al., 2017; Schmidt & Hall, 2002; Bai et al., 2015). Interestingly, while there is plenty of GEFs and GAPs, only a subset have well-characterized functions, and the loss of even a single GEF or GAP can have profound effects on cellular behavior and actin cytoskeleton organization (Duman et al., 2015; Bai et al., 2015). Moreover, the specificity of GEF and GAP interactions with Rho GTPases is complex, involving multiple sites on the GTPases for regulation and activation (Li & Zheng, 1997).

Rho GTPases are necessary to facilitate the formation of distinct cellular structures, such as membrane protrusions (e.g., filopodia and lamellipodia), stress fibers and FAs maturation (Figure 10) (Arthur et al., 2000; Aspenström, 2019; Nobes & Hall, 1995). Thus, these proteins act as molecular switches that regulate actin polymerization, depolymerization, and myosin activity, ensuring directional movement. This regulation is

mainly promoted by Rac1, Cdc42 and RhoA small GTPases (Figure 10) (Zegers & Friedl, 2014). At the leading edge, Rac1 and Cdc42 activate actin cytoskeleton polymerization and remodeling, promoting the formation of actin-based protrusions (Hall, 2005; Zegers & Friedl, 2014). Specifically, Rac1 activates the Arp2/3 complex, a key player in the nucleation of branched actin filaments essential for the formation and dynamics of lamellipodia (Figure 10) (Steffen et al., 2004; Ten Klooster et al., 2006; Yang et al., 2022). The interplay between Rac1 and the Arp2/3 complex leads to a rapid polymerization of actin and promotes the extension of the cell membrane forward. Interestingly, Rac1 activation can be induced by calcium influx through mechanosensitive ion channels (e.g., TRP family) (Becker et al., 2009; Fiorio et al., 2012). Cdc42 regulates the formation of filopodia, small, stick-like protrusions that extend from the cell surface. Cdc42 activates formins such as mDia2, which nucleate and elongate unbranched actin filaments necessary for filopodia formation (Figure 10) (Grobe et al., 2018; Fu et al., 2022; Pellegrin & Mellor, 2005). Formation of these membrane protrusions are essential to drive cell movement. At the trailing edge, RhoA controls assembly and adhesion of actomyosin, a protein complex formed by the interaction between actin and myosin. RhoA activation leads to the stimulation of Rho-associated kinase (ROCK), which phosphorylates myosin light chain (MLC), promoting actomyosin contractility (Figure 10) (Chang et al., 2008; Choraghe et al., 2020; Chrzanowska-Wodnicka & Burridge, 1996). This contractility is essential for the maturation of focal adhesions and the generation of mechanical forces. Moreover, it facilitates trailing retraction and forward cell propulsion (Zegers & Friedl, 2014; Hall, 2005; Lambrechts et al., 2004).

Interestingly, the regulation of front-to-rear polarity by Rho GTPases involves complex feedback loops and crosstalk between

different members of the family (Figure 10). For example, inhibition of ROCK, a downstream effector of RhoA, can indirectly reduce RhoA activity by stimulating Tiam1-induced Rac1 activity. This finding suggests that ROCK not only mediates downstream effects but also influences the balance between RhoA and Rac1 activities (Tang et al., 2012). Moreover, the cross-linking and bundling of myosin generates large, stable actin filaments and FAs, which inhibits adhesion signaling to Rac1 (Parsons et al., 2010). This feedback loop between Rho and Rac pathways ensure that Rho GTPases activities are finely tuned spatially and temporally, which is crucial for proper organization of the actin cytoskeleton and the formation and maturation of FAs (Mack & Georgiou, 2014; Arthur et al., 2000; Aspenström, 2019; Nobes & Hall, 1995). Rho GTPases can also be modulated by other signals, including those from FAs. FAs are known to interact with GEFs, GAPs but also RhoA (Joo & Olson, 2021; Nalbant et al., 2009). Although the direct control of GEFs and GAPs is not clear, some insights about RhoA modulation have been shown. For instance, the role of GEF-H1 in localized activation of RhoA at the leading edge of migrating cells, which seems to be influenced by FAs (Nalbant et al., 2009).

4.2 Cell cytoskeleton

Whether random or directed, single or multicellular, cell migration requires the cell cytoskeleton to move. The cell cytoskeleton mainly consists of three primary polymers: intermediate filaments (IFs), microtubules, and actin (Figure 11A). These polymers provide structure, organization, mechanics, and shape to the cells, and they are organized into networks that can resist deformation in response to external forces.

The architecture of these networks is regulated by various proteins, including nucleation-promoting factors (NPFs), capping proteins, polymerases, depolymerization factors, and cross-linkers (Fletcher & Mullins, 2010). The activity of these regulatory proteins is influenced by internal or external mechanical forces, which can also affect the local organization of filaments in the networks.

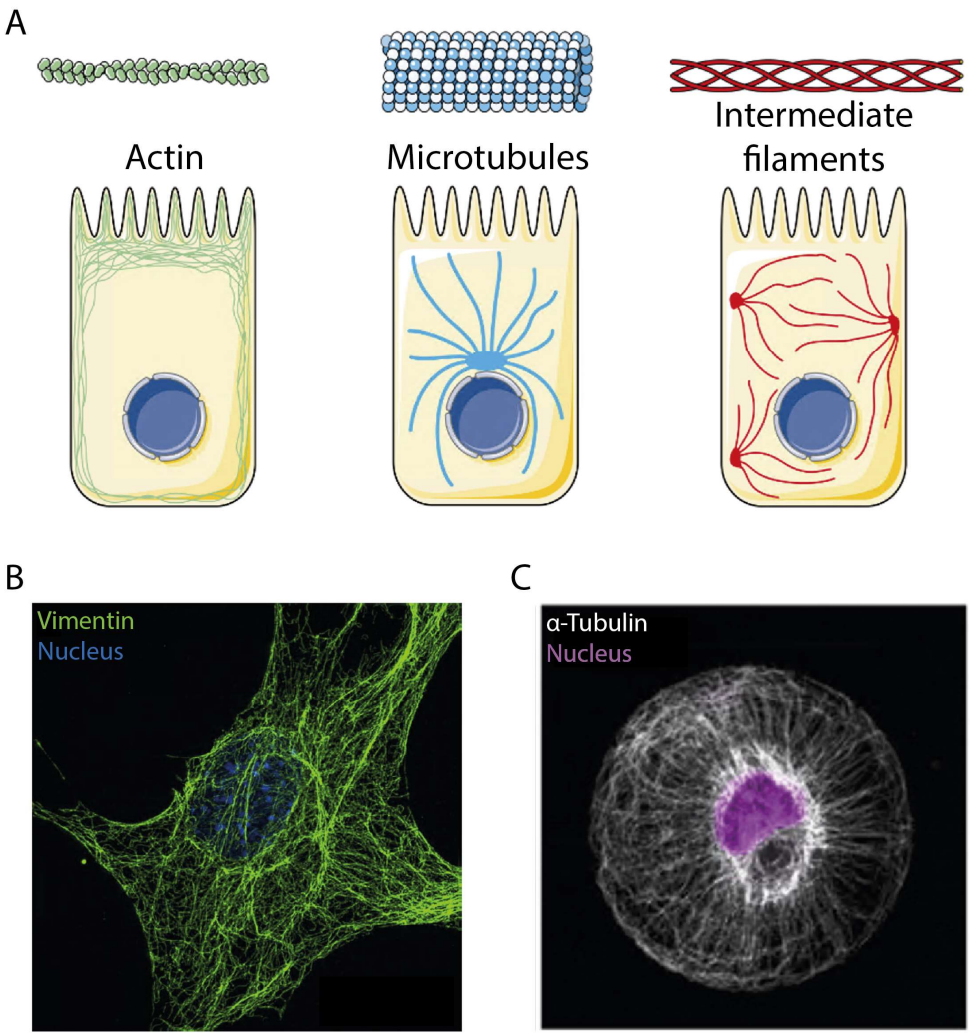

Figure 11 – Cytoskeletal biopolymers. A: The cell cytoskeleton is primarily composed of actin filaments, microtubules, and intermediate filaments. These biopolymers exhibit distinct spatial organizations and fulfill various functions within the cell. B: Microscopic image of mouse embryonic fibroblasts (MEFs) stained for vimentin (green), an important protein in intermediate filaments, and the nucleus (blue). C: Microscopic image of retinal pigment epithelial (RPE1) cells stained for α-tubulin (white), a key protein in microtubules, and the nucleus (magenta). (Figure adapted from panel A – drawn using images from Servier Medical Art. Servier Medical Art by Servier is licensed under a Creative Commons Attribution 3.0 Unported License (https://creativecommons.org/licenses/by/3.0/); panel B – Eibauer et al., 2024; panel C – Li et al., 2023)

The main differences between cytoskeleton polymers are polarity, the type of associated molecular motors, assembly dynamics, and mechanical stiffness. Nevertheless, contrary to the traditional view of distinct functions for each cytoskeletal component, emerging evidence proposes that they interact and support each other. For instance, vimentin IFs have been shown to stabilize microtubules against depolymerization. They also support microtubule rescue, indicating a direct physical interaction that influences microtubule dynamics (Schaedel et al., 2021). Similarly, the crosstalk between IFs and actin has been implicated in modulating cell migration, mechanoresponsiveness, and signaling transduction (Li et al., 2019), For instance, IFs contribute to migration speed, nuclear integrity, and resilience to compressive forces by regulating actomyosin-generated forces, which are essential during cell migration in both two-dimensional (2D) and three-dimensional (3D)

environments (Van Bodegraven & Etienne-Manneville, 2020; Sakamoto et al., 2013). Moreover, the protein Mip-90 has been identified as a microtubule-interacting protein that also interacts with actin filaments. This suggests a role in coordinating the interplay between these two cytoskeletal networks (González et al., 1998). This intercommunication between actin, microtubules, and IFs is crucial for the mechanical integrity and functionality of cells. The interactions between these cytoskeletal components are not merely supportive but are actively involved in regulating and coordinating cellular activities.

Besides directed cell migration, the cell cytoskeleton is also important for the maintenance of intracellular compartments, cell division and intracellular transport (Fletcher & Mullins, 2010).

4.2.1 Intermediate filaments (IFs)

IFs play a significant role in maintaining cellular integrity and are distinguished by their unique mechanical properties (Figure 11A; Figure 11B). IFs exhibit a combination of flexibility and extensibility, allowing them to withstand large deformations while maintaining tensile strength. This is crucial for protecting cellular structures, such as the nucleus, from mechanical stresses encountered *in vivo* (Pogoda & Janmey, 2023; Petitjean et al., 2024). Atomic force microscopy studies have revealed that stabilized IFs have a higher bending modulus compared to non-stabilized ones, suggesting a Young's modulus of around 900 MPa or higher for vimentin IFs (Guzmán et al., 2006). Furthermore, the tensile strength and extensibility of IFs, such as desmin in muscle fibers, indicate a

pronounced strain-hardening regime and a tensile strength of at least 240 MPa (Qin et al., 2009).

The assembly and disassembly of IFs involve the hierarchical organization of their protein subunits. Unlike actin filaments and microtubules, which rely on ATP and GTP hydrolysis, respectively, IF assembly is driven by interactions between coiled-coil dimers. These dimers assemble into tetramers, which then associate laterally and longitudinally to form the mature filament. This hierarchical assembly confers to IFs the above unique mechanical properties (Petitjean et al., 2024).

IFs play a crucial role in mechanotransduction. The phosphorylation and reorganization of IFs, such as vimentin, regulate FAs dynamics and cell contraction (Kraxner et al., 2021; Tang & Gerlach, 2017). Recent evidence suggests that IFs contribute to mechanosensitivity and the regulation of cytoskeletal stability and organization (Ndiaye et al., 2022). For instance, vimentin IFs structure and align microtubules, supporting them against compressive forces and potentially enhancing intracellular transport (Blob et al., 2023). In keratinocytes, the keratin network of IFs adapts to increased matrix stiffness by forming a more rigid network, working in conjunction with actin stress fibers to increase cell stiffness (Laly et al., 2021). Mutations in keratin, such as the R416P mutation in keratin 14, disrupt this mechanical response, impairing mechanotransduction to the nuclear lamina and affecting chromatin remodeling (Laly et al., 2021). Additionally, proteins like plectin connect IFs to other cellular structures, modulating their response to mechanical stimuli and contributing to the maintenance of nuclear integrity under mechanical stress (Laly et al., 2021; Almeida et al., 2015).

4.2.2 Microtubules

Microtubules are the most rigid components of the cytoskeleton (Figure 11A; Figure 11C) (Nasrin et al., 2021). These structures behave as viscoelastic materials, and their mechanical properties can be influenced by the presence of microtubule-associated proteins (MAPs) or conditions that inhibit microtubule assembly (Sato et al., 1988). Tubulin, the building block of microtubules, has similar mechanical properties as microtubules and contributes to the structure of cytoplasm even in nonpolymerizing conditions (Sato et al., 1988).

Microtubules serve as tracks for the transport of organelles and other cellular components by motor proteins such as kinesin and dynein. Post-translational modifications of tubulin, such as acetylation, influence motor protein interactions with microtubules. Acetylated microtubules enhance kinesin mediated transport, crucial for organelle positioning and cell migration (Monteiro et al., 2023). *In vitro* studies suggest that acetylation alone does not directly affect kinesin motility but rather influences it through microtubule bundling, which increases the number of available binding sites for kinesin (Balabanian et al., 2017). Therefore, mechanical forces, such as bending, can impede the translocation dynamics of kinesin along the microtubules (Mirvis et al., 2018; Nasrin et al., 2021). Additionally, MAPs like tau also modulate motor protein activity (Chaudhary et al., 2018).

Microtubules seem to also be involved in mechanotransduction (Luo & Robinson, 2011; Saidova & Vorobjev, 2020). Recent studies reveal that talin- and actomyosin-dependent response to substrate rigidity facilitates the recruitment of α-tubulin acetyltransferase 1 (αTAT1) to FAs, thereby controlling microtubule acetylation (Seetharaman et al.,

2022). This process is critical for the mechanosensitivity of FAs and the subsequent translocation of YAP to the nucleus in response to mechanical cues (Seetharaman et al., 2022). Additionally, the mechanical stability of the talin-KANK1 complex seems to play a role in the mechanosensitive recruitment of microtubule-stabilizing complexes to FAs (Yu et al., 2019). Thus, talin and actomyosin contractility can control microtubule acetylation through αTAT1 recruitment to FAs (Seetharaman et al., 2022). Moreover, the interaction between talin and KANK1, and the mechanical stability of their complex, may contribute to the crosstalk between the actin and microtubule cytoskeletons at FAs, influencing cellular responses to mechanical stimuli (Yu et al., 2019).

4.2.3 Actin

Actin is a highly conserved protein crucial for various cellular functions, existing in a monomeric globular form (G-actin) and a polymeric filamentous form (F-actin) (Figure 11A). The transition between these forms happens by processes known as polymerization (assembly) and depolymerization (disassembly). Actin polymerization is a dynamic process driven by the addition of ATP-G-actin subunits at the barbed ends of growing filaments, while depolymerization occurs at the pointed ends following ATP hydrolysis and phosphate release (Fujiwara et al., 2018; Shekhar et al., 2020). The regulation of these processes involves a complex interplay of proteins that either promote or inhibit actin filament assembly and disassembly. Capping protein (CP) is a key regulator that binds to the barbed ends of actin filaments, preventing both polymerization and depolymerization, with twinfilin facilitating CP's

dissociation from these ends (Hakala et al., 2021). Actin filament turnover is traditionally associated to cofilin-mediated disassembly of actin (Brieher, 2013). Moreover, cyclase-associated proteins have been identified as a critical factor that synergizes with cofilin to significantly enhance the rate of actin filament depolymerization and monomer recycling (Kotila et al., 2019). The interplay between actin assembly and disassembly is further complicated by the involvement of proteins like profilin. Profilin binding to oxidized G-actin, inhibits polymerization and promotes disassembly, thus facilitating cellular remodeling (Grintsevich et al., 2021).

Structurally, formins facilitate the assembly of linear actin filaments, while the Arp2/3 complex promotes branched filament formation, regulated by nucleation-promoting factors (NPFs) such as neuronal Wiskott-Aldrich syndrome protein (N-WASP) and WASP-family verprolin-homologous protein (WAVE) (Figure 10). Actin structural organization and interactions with actin-binding proteins (ABPs) determine the mechanical properties of actin networks. For instance, branched actin networks exhibit increased elasticity and resistance to deformation under mechanical stress, indicating a history-dependent alteration in mechanical properties (Bieling et al., 2016; Chen et al., 2020). ABPs like filamin play a crucial role in these interactions, contributing to the strength and resilience of the network (Lee et al., 2009).

Besides filopodia and lamellipodia, the actin cytoskeleton is composed of several other distinct structures, such as lamellae, stress fibers, the cortex, radial fibers, and transverse arcs (Figure 12) (Hotulainen & Lappalainen, 2006; Nemethova et al., 2008). Each actin

structure has its specific function. Lamellae and lamellipodia are regions at the leading edge involved in movement, with lamellipodia being broad, flat extensions and lamellae the more stable regions behind them (Figure 12A). Filopodia are thin, stick-like projections that can guide migration and contribute to stress fiber formation (Figure 12A) (Nemethova et al., 2008). Stress fibers are contractile actomyosin bundles crucial for adhesion and motility, including different types such as dorsal and ventral (Figure 12A) (Hotulainen & Lappalainen, 2006; Labouesse et al., 2012). Transverse arcs are part of the actin stress fiber network interacting with intermediate filaments like vimentin (Jiu et al., 2015). The actin cortex refers to a thin layer of actin under the plasma membrane, while radial fibers are actin bundles within the lamellipodium (Katoh et al., 1999).

The dynamic nature of actin structures is fundamental to their function. Actin filaments undergo continuous turnover, with a balance between assembly and disassembly to maintain the cell's overall architecture (Théry & Blanchoin, 2024). This dynamic steady state (DSS) is essential for cellular remodeling and migration, as the actin network is constantly renewed (Figure 12B). In each structure, the rates of assembly and disassembly result in a turnover of actin subunits, with lifetimes ranging from seconds for lamellipodia or filopodia to minutes for stress fibers (Goode et al., 2023). The average rate of assembly of actin filaments in all subcellular structures must precisely match the average rate of filament disassembly to maintain a steady state (Mohapatra, 2016). A small mismatch would lead to cell extension and fractionation in the case of excessive assembly or to cell retraction and collapse in the case of excessive disassembly levels (Théry & Blanchoin, 2024). Interestingly, local growth within a structure compensates for shrinkage in other areas

of the same structure, ensuring addition and release of a similar number of monomers. This implies that the DSS of cellular networks is composed of multiple DSSs, with a balance of assembly and disassembly rates at both the cell and structures levels (Théry & Blanchoin, 2024).

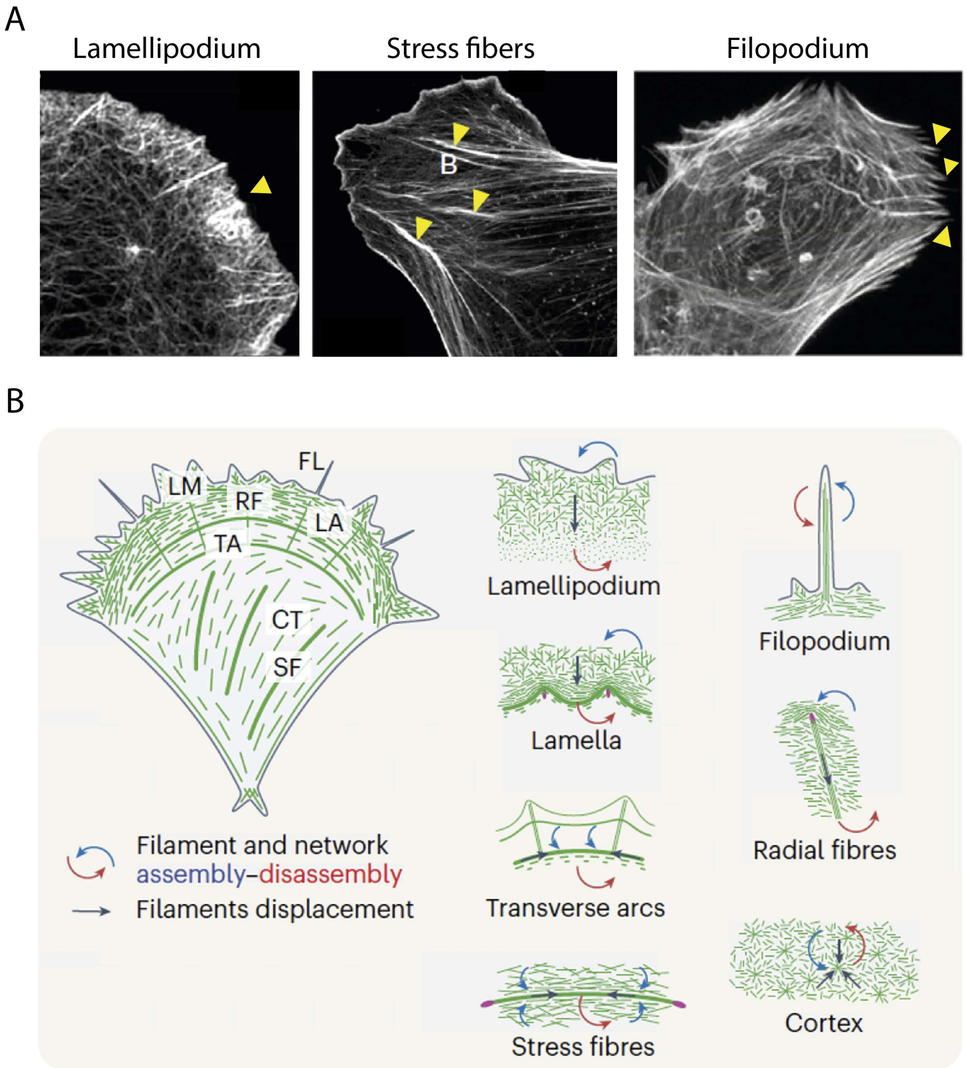

Figure 12 – Actin structures and dynamics. A: Microscopic images of actin, labeled with phalloidin. Different actin structures are indicated by the yellow arrows. Cell type from left to right: macrophages; MEFs and RPE1. B: Each of these actin structures are dynamic and have their own steady state, which integrates with the overall dynamic steady state of the cell. (Figure adapted from: panel A – Théry & Blanchoin, 2024; panel B – Lehne et al., 2022; Cagigas et al., 2022; Li et al., 2018)

For a proper mechanotransduction, actin and myosin interact to form the actomyosin complex. Myosin motors use ATP hydrolysis to produce mechanical work, pulling on actin filaments. This generates actin retrograde flow and contractile forces that are required for cell movement (Gardel et al., 2008; Koenderink et al., 2011; Matsuda et al., 2018; Pepper & Galkin, 2022). Therefore, the actin cytoskeleton, through its retrograde flow and interaction with myosin, produces mechanical forces that are transmitted to the ECM by pulling the FAs (Sun et al., 2016). The assembly and force generation of actomyosin are regulated by various factors, including accessory proteins like Caldesmon and the catch-bond behavior of actin-myosin interactions, which influence the kinetics of actomyosin formation (Inoue & Adachi, 2013; Kokate et al., 2022).

FAs are necessary to the process of actin mechanotransduction, serving as the connection between the ECM and the actin cytoskeleton (Ciobanasu et al., 2013; Sun et al., 2016). Interestingly, the composition and mechanical properties of the ECM can influence the formation and disassembly of FAs, thereby modulating the mechanotransduction

pathways. Moreover, the force transmission through FAs can lead to allosteric changes in function of mechanosensitive proteins within these adhesions, eliciting cellular responses that range from immediate mechanical adjustments to long-term changes in gene expression (Sun et al., 2016). The complexity of these interactions is further highlighted by the fact that the local stress distribution within FAs can determine the recruitment of specific proteins, which in turn can modify the stress distribution and affect the mechanotransduction process (Shams et al., 2018). The linker of nucleoskeleton and cytoskeleton (LINC) complex also plays a pivotal role in actin mechanotransduction by connecting the nucleus to the plasma membrane via the actin cytoskeleton. This complex, comprising inner nuclear membrane-spanning SUN proteins and outer nuclear membrane-spanning nesprin proteins, facilitates the transmission of forces from the ECM to the nucleus (Ueda et al., 2022). SUN1, a component of the LINC complex, is essential for the activation of integrin β1 and the maturation of FAs by affecting the incorporation of vinculin and zyxin (Ueda et al., 2022).

In addition to FAs force, actin influences other critical forces for directed migration. For instance, the membrane tension that propagates across the plasma membrane (Sitarska & Diz-Muñoz, 2020). Traditionally, actin was viewed as the primary source of forces that deform the membrane. However, recent findings suggest a bidirectional relationship where the membrane actively organizes actin filaments (Liu et al., 2008). This dynamic interplay makes membrane tension a global and local regulator of cell behavior, influenced by cytoskeletal dynamics and actin network organization (Simon et al., 2018; Sitarska & Diz-Muñoz, 2020). Although membrane tension was once seen as an obstacle to

filament growth and cell migration, it is now understood to potentially enhance motility by promoting polymerization in the direction of movement (Batchelder et al., 2011). This highlights the complex role of membrane tension in cell motility and its influence on actin polymerization and cell boundary dynamics.

5. Computational models to study directed cell migration

Computational models are crucial for studying directed cell migration because they provide a framework to dissect complex cellular processes and predict outcomes of various biological scenarios. These models help bridge the gap between molecular mechanisms and observable cell behaviors, offering insights that are challenging to obtain through experimental studies alone. Various models have been developed to address different aspects of cell movement at multiple biological scales (Figure 13). Some examples of computational models are random walk model, polygonal model, the vertex-based model and agent-based models (ABMs).

Random walk model is one of the simplest models for describing cell migration. It captures the stochastic nature of cellular movement, where cells move in a series of random steps. This model has been adapted to account for different environmental conditions, such as protein gradients and geometrical confinement (Dickinson, 2000; Brückner et al., 2019). However, in complex environments like 3D extracellular matrices, cell migration often deviates from a purely random walk, necessitating modifications to the model to incorporate anisotropy and cell heterogeneity (Wu et al., 2014; Wu et al., 2015).

Polygonal models focus on the geometric aspects of cell shape and movement. These models represent cells as polygons and are useful for simulating cell boundaries' discrete nature. They incorporate physical principles such as cytoskeletal dynamics, membrane tension, and cellular adhesion, which are fundamental to cell migration (Prahl & Odde, 2018). To be effective, these models must integrate detailed molecular and biophysical data, capturing the forces generated by cellular movements (Lee, 2018).

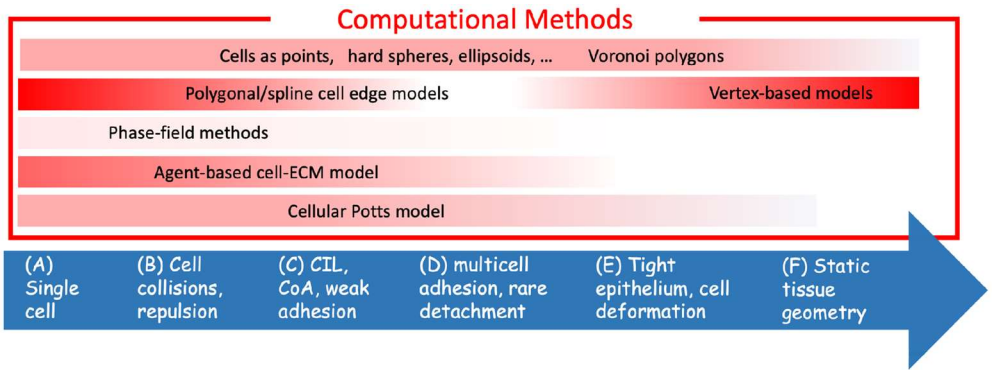

Figure 13 – Computational methods used across scales. Different models are employed to study cell migration based on the scale: intracellular, cellular, or multicellular. For example, vertex-based models are typically used for tissue migration, while polygonal models are primarily applied to single cells. (Figure adapted from: Buttenschön & Edelstein-Keshet, 2020)

The vertex-based model represents multicellular systems as polygons or polyhedral, where cells correspond to vertices. This model simulates mechanical aspects of cell migration, such as cell shape changes, rearrangements, and force exertion. It relies on principles of force balance

at the vertices, determined by the mechanical properties of cells and their interactions with the environment (Khataee et al., 2020). While it primarily captures mechanical interactions, it can be coupled with biochemical signaling pathways to simulate collective cell behaviors (Jensen & Revell, 2023).

ABMs simulate the interactions between cells and the ECM. These models incorporate biophysical processes like mechanosensing, force generation, adhesion dynamics, and ECM remodeling (Campbell et al., 2021; He & Jiang, 2018). A remarkable agent-based approach that explains how cells interact with the ECM is the molecular clutch model.

5.1 Molecular clutch model

The molecular clutch model is a powerful tool for understanding the mechanics of cell migration. This model explains the transmission of force from the actin cytoskeleton to the ECM through FAs, acting like a clutch in a vehicle that engages and disengages to transmit power. Therefore, it integrates concepts of force transmission, loading rates, actin flows, and FAs reinforcement to explain how cells interact with their environment and respond to mechanical cues (Fortunato & Sunyer, 2022).

The origins of the molecular clutch model were formalized in 1988 by Mitchison and Kirschner, who likened the interaction between the cytoskeleton and ECM to a clutch mechanism (Mitchison & Kirschner, 1988). This model was later mathematically adapted and experimentally validated by Chan and Odde, and further refined by others to incorporate

adhesion reinforcement mechanisms (Chan & Odde, 2008; Elosegui-Artola et al., 2014, 2016).

In the molecular clutch model, cells exert forces on their ECM by contracting their actin cytoskeleton through myosin molecular motors (Figure 14A). This force is transmitted through integrins and adaptor proteins, called clutches, that link integrins to actin filaments. The rate at which force builds up in the clutches, known as loading rate, is fundamental to control the amount of force transmitted to the substrate (Elosegui-Artola et al., 2018). This rate depends on factors like substrate stiffness and the number of myosin motors involved (Bangasser et al., 2013). Higher loading rates increase force transmission to the ECM (Figure 14B). Myosin-driven contraction also generates actin retrograde flow and opposes actin polymerization, which pushes the cell membrane outward.

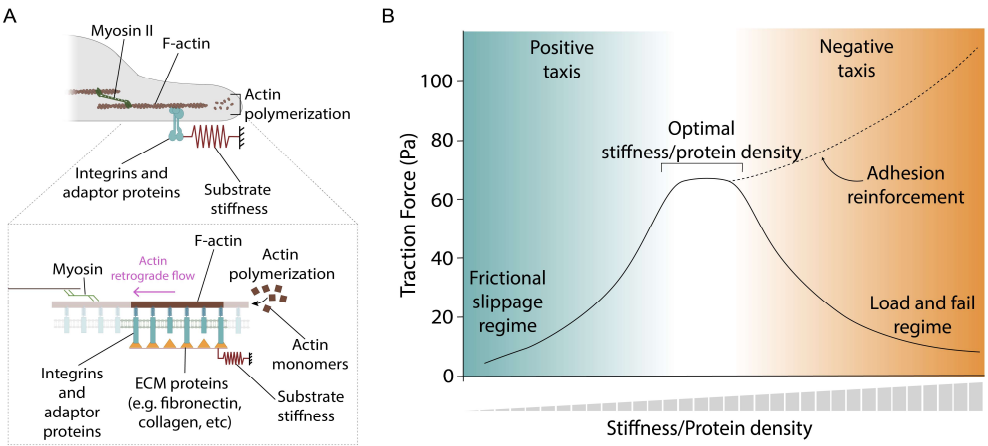

Figure 14 – Molecular clutch model in directed cell migration. A: Representative scheme of the clutch model. (Inset) The clutch model shows substrate deformation as a spring, with integrins acting as clutches with specific

binding and unbinding rates. Myosin contraction creates a retrograde flow opposing actin polymerization, which extends the cell membrane outward. B: clutch model predicts an optimal stiffness where cell force and migration are maximized (solid line). However, this is often overshadowed by talin/vinculin-mediated reinforcement (dashed line). Adhesion reinforcement has been measured as a function of stiffness, but not protein density. However, it is expected that protein density gradients will mimic the predictions observed with stiffness gradients. (Figure adapted from: Fortunato & Sunyer, 2022)

One clear example of the strength of this model's predictions has been demonstrated in durotactic responses (Bangasser et al., 2013). Cells migrate towards stiffer regions of a substrate due to differential force transmission. Force balance within the cell, either globally or locally, leads to migration towards stiffer areas where the retrograde flow is slower, and force transmission is higher. The model predicts not only single but also collective durotaxis (Sunyer et al., 2016).

The model also predicts that cells exhibit biphasic migratory behavior, moving fastest at an optimal substrate stiffness where the traction force is maximized (Figure 14B) (Fortunato & Sunyer, 2022; Bangasser et al., 2017; Elosegui-Artola et al., 2014). At low stiffness, clutches experience "frictional slippage" with high retrograde flow and low forces. At high stiffness, clutches go through cycles of force buildup and catastrophic disengagement, known as "load and fail" or "stick-slip," resulting in low net force transmission. Beyond a certain stiffness threshold, talin unfolding and vinculin binding reinforce FAs, increasing the clutch binding rate and obscuring the optimal stiffness predicted by the model (Figure 14B) (Kechagia et al., 2019; Elosegui-Artola et al., 2014,

2018). For instance, cells like U-251MG glioma cells, which lack adhesion reinforcement, can exhibit "negative durotaxis" and migrate towards softer regions when seeded on substrates stiffer than their optimal stiffness (Isomursu et al., 2022).

Cells also sense protein gradients through differential clutch dynamics, where one set of clutches engages with higher density regions, leading to asymmetric force transmission and actin retrograde flows (Fortunato & Sunyer, 2022). Therefore, like durotaxis, haptotaxis and an optimal protein density could also be explained using the molecular clutch model.

6. Methodologies to study directed cell migration

The study of directed cell migration employs both *in vivo* and *in vitro* techniques, each offering unique insights and advantages.

In vivo studies use model organisms like *Drosophila melanogaster* and zebrafish to investigate cell migration within a complex, 3D environment. These models allow researchers to observe the role of specific genes and proteins in real-time within living tissues. For instance, advanced imaging techniques such as two-photon microscopy enable high-resolution tracking of cells within tissues (Kardash et al., 2010; Moreira et al., 2013; Takeda et al., 2018).

In vitro methodologies offer a controlled environment where variables can be systematically manipulated, facilitating the dissection of complex cellular behaviors. Moreover, these methodologies enable faster and high-throughput experimentation compared to *in vivo* studies. Techniques such as micropatterned substrates help study the effects of

mechanical cues on cell motility, while scratch-wound assays and Matrigel invasion assays allow researchers to assess the roles of specific proteins and signaling pathways (Caballero et al., 2015; Boudreau & Leto, 2019; Goulimari et al., 2005).

One significant advantage of *in vitro* approaches is the ability to generate gradients and control cell polarity.

6.1 Generate *in vitro* mechanical gradients

Given the numerous signals promoting directed migration, a variety of methodologies have been developed to generate these signals (Figure 15). This subsection will focus on the fabrication of stiffness gradients (to study durotaxis) and substrate-bound protein gradients (to study haptotaxis), as these are the main types of directed cell migration that rely on mechanosensing.

Methods to generate stiffness gradients initially used steep gradients by polymerizing adjacent drops of soft and stiff acrylamide, resulting in a sharp transition analyzed only at the interface (Lo et al., 2000). However, this method fails to produce long-range, continuous stiffness gradients as found *in vivo*. A more precise approach uses microfluidic devices to blend polyacrylamide solutions, creating smooth rigidity gradients (Zaari et al., 2004). Despite its precision, this method is costly, labor-intensive, and limited to pathological stiffness ranges. A more accessible technique involves differential diffusion between a pre-polymerized gel of varying thickness and a second gel polymerized on top (Hadden et al., 2017). While reliable, this method provides a small stiffness range, and the thick gels limit microscopic observation.

Variations using microfabricated molds can create steeper gradients but introduce potential artifacts from gel swelling and topological cues (Pieuchot et al., 2018). Photolithography, which patterns stiffness gradients using graded or sliding masks, offers a versatile method for obtaining wide stiffness ranges relevant to physiological and pathological conditions (Figure 15A) (Tse & Engler, 2011; Jiang et al., 2005; Sunyer et al., 2016). However, issues with light transmission and diffusion limit gradient resolution.

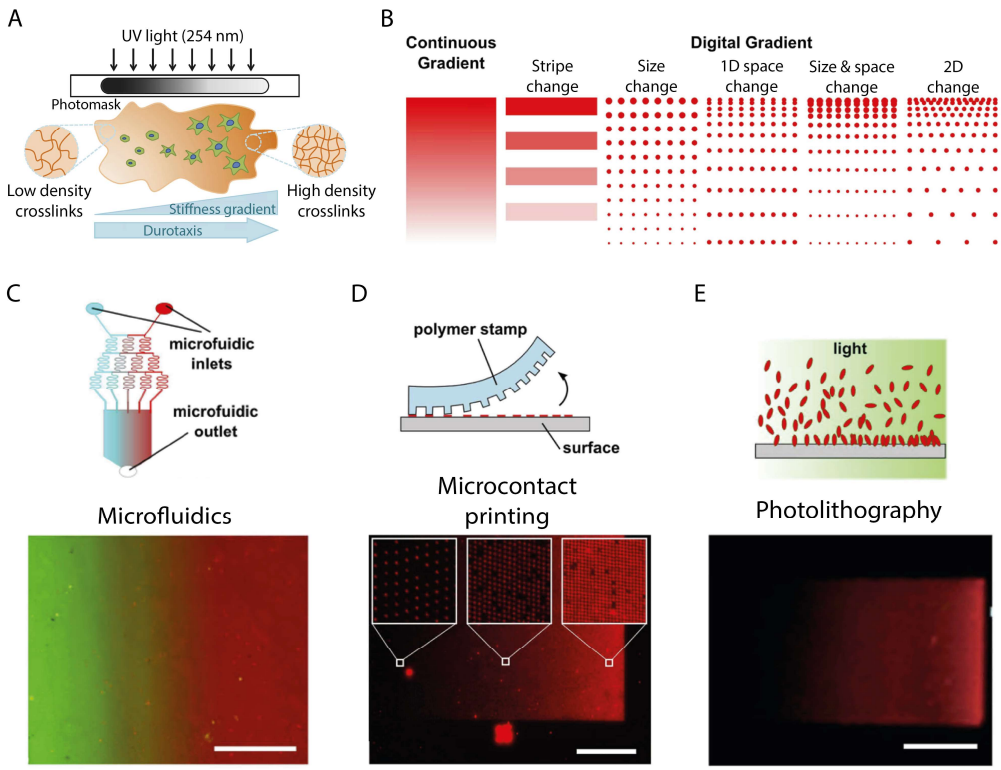

Figure 15 – Experimental techniques to generate gradient cues for directed cell migration. A: This method utilizes a free radical photoinitiator and patterned nitrocellulose photomasks to achieve gradient stiffness through

selective crosslinking. B: Types of substrate-bound protein gradients. C: Microfluidics generate a dilution series flowing into a wide chamber to create a gradient, where proteins adsorb onto the substrate surface. Scale bar is 100μm. D: Microcontact printing utilizes polymer stamps with topography, inked with a protein solution, to create gradient protein patterns by selectively limiting contact regions between the stamp and the surface. Scale bar is 1mm. E: As panel A, this methos uses photomask to achieve gradients of immobilized proteins. Scale bar is 25μm. (Figure adapted from: panel A – Richards et al., 2019; panel B, C, D, E – Ricoult et al., 2015)

Methods to generate gradients of substrate-bound proteins can be categorized into continuous and digital gradients. Continuous gradients change protein density smoothly across a substrate (Figure 15B). Microfluidics is a common method for creating continuous gradients. This method manipulates minute volumes of liquid to produce diffusible protein gradients that are imprinted onto surfaces by protein adsorption (Figure 15C) (Whitesides, 2006; Jiang et al., 2005). However, microfluidic devices can be compromised by obstructions such as air bubbles. Additionally, accurately characterizing the immobilized gradients is challenging, as fluorescence intensity measurements often do not reliably reflect protein concentration (Squires et al., 2008). Another technique for generating continuous gradients is microcontact printing. This method employs a polymer stamp with relief features, which is inked with a protein solution, incubated to allow protein adsorption, and then contacted with the substrate to transfer the protein pattern (Figure 15D) (Baier & Bonhoeffer, 1992; Lang et al., 2008). Photolithography also allows for the creation of continuous protein gradients by using UV light

to pattern surfaces. This technique involves coating a surface with a photopolymer and selectively exposing it to UV light through a graded photomask (Figure 15A; Figure15E). This process alters the crosslinking level and thus the protein binding capacity in a controlled manner (Hynes & Maurer, 2012; Herbert et al., 1997). While photolithography can pattern large surfaces in one step, it typically requires a costly cleanroom environment and has resolution limitations due to light diffraction.

Digital gradients consist of discrete patches of proteins arranged in a specific pattern to form a gradient (Figure 15B). These patches can be dots, dashes, or lines, with the gradient formed by varying the spacing or size of these patches (Lang et al., 2008; Fricke et al., 2011). Digital gradients can be created using microcontact printing by forming lines or dots with increasing protein concentrations through a series of parallel channels on a silicon stamp, which are then transferred onto a substrate (Figure 15D) (Lang et al., 2008). This method allows for precise control over protein placement and concentration, but typically results in gradients with limited dynamic ranges and large areas without guidance cues.

While there are numerous techniques for creating substrate-bound protein gradients, each method has limitations. Continuous gradients are difficult to quantify accurately, and digital gradients, although more precise, do not perfectly mimic natural protein aggregates. Despite advancements, the field still lacks a controlled and precise approach for accurately generating gradients of immobilized proteins, crucial for studying haptotaxis and related cellular mechanisms (Ricoult et al., 2015).

6.2 Optogenetics to control cell polarity

Among the diverse methods to manipulate cellular signaling, optogenetics stands out for its unprecedented spatiotemporal resolution (Valon & de Beco, 2021). Specifically, optogenetic tools enable the precise modulation of Rho GTPases, the pivotal regulators of cell polarity (Machacek et al., 2009). By genetically introducing light-sensitive proteins called opsins into target cells, optogenetics controls the activity of GEFs, thereby modulating Rho GTPase activity at the subcellular level (Valon et al., 2015; Toettcher et al., 2011). Temporal control over protein activity. This precise manipulation allows for the imposition of intracellular gradients of polarity signals, guiding cell migration in a quantitative manner (de Beco et al., 2018).

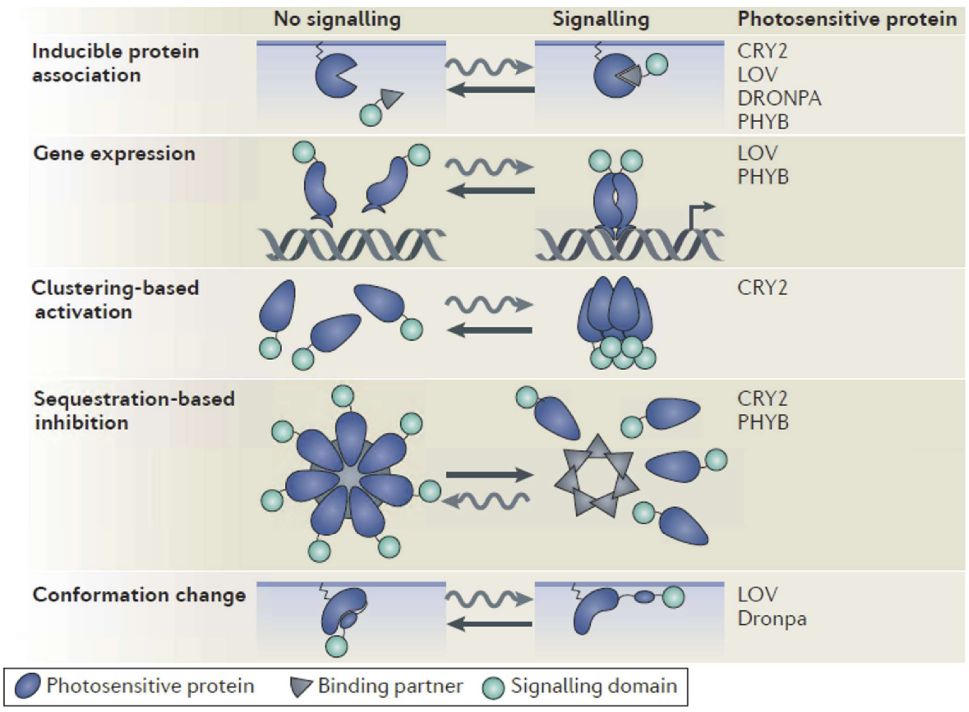

Figure 16 – Cell signaling control using optogenetic tools. Photosensitive proteins, known as opsins, can be used to control various cellular activities, such as gene expression, protein association, or protein clustering. Opsins enable the activation of these processes when they are stimulated by light. Thus, these proteins provide spatial and temporal control over cellular processes, including cell polarity. (Figure adapted from: Tischer & Weiner, 2014)

A range of optogenetic systems has been developed, providing spatial and temporal resolutions, as well as control over diverse cellular signaling pathways (Figure 16) (Valon & de Beco, 2021). For example, The CIBN/CRY2 system is based on the interaction between cryptochrome 2 (CRY2) and the CIBN fragment of the photolyase homology region. Upon blue light illumination, CRY2 undergoes a conformational change that allows it to bind to CIBN, enabling light-inducible dimerization and manipulation of protein localization (Figure 16) (Mehdi & Goss, 2018). Another system is the improved Light-Inducible Dimer (iLID), which uses a mutated LOV domain from *Avena sativa* phototropin 1. Upon blue light exposure, the LOV domain binds to a small peptide, SspB, inducing dimerization and enabling the spatial and temporal control of protein-protein interactions (Figure 16) (Achimovich et al., 2023; Natwick & Collins, 2021). Other systems include PHYB and Dronpa (Figure 16).

Despite its remarkable potential, optogenetics also poses challenges. Achieving subcellular activation smaller than 4–5μm remains challenging with some systems due to limitations in dimer dissociation times (Valon, 2015). Additionally, while systems like iLID offer superior

spatial resolution, others require more frequent illumination, leading to increased phototoxicity and photobleaching (Levskaya et al., 2009).

6.3 Geometry to control cell polarity

Geometry exerts a profound influence on cell motility and polarity, shaping the spatial and temporal coordination of cytoskeletal elements, adhesion complexes, and signaling pathways during migration (Caballero et al., 2015). Microtubules and the PCP pathway are particularly sensitive to geometric cues, highlighting the intricate relationship between geometry and cell polarity (Kaverina & Straube, 2011; Koca et al., 2022). Despite the established roles of actin in cell polarity, the mechanisms by which geometry governs these processes remain incompletely understood (Thapa et al., 2023).

Experimental studies have shed light on the impact of geometry on cell migration. For example, it was shown that cells confined to adhesive micropatterns mimicking polarized morphology, preferentially migrated towards wider regions (Figure 17) (Jiang et al., 2005). Moreover, cells also respond differently to anisotropic substrates based on their morphologies (Figure 17A) (Isomursu, 2024). Further investigations revealed that cell motility on repeating micropattern ratchets depends on individual pattern shapes and their relative positions, highlighting the refined responses of cells to geometric cues (Figure 17B) (Ko et al., 2013; Caballero et al., 2014).

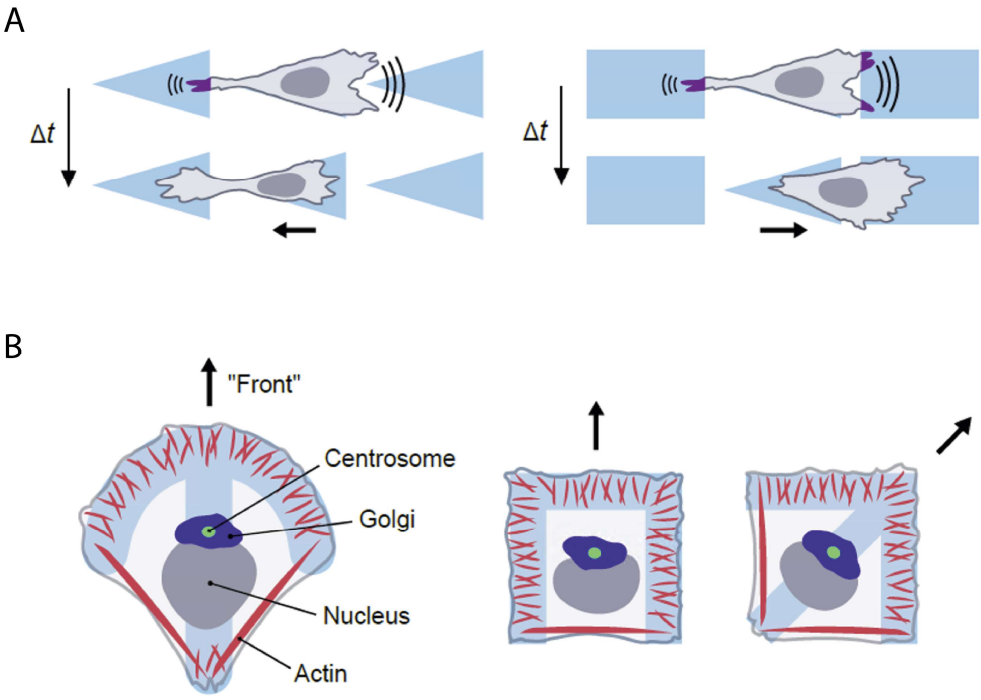

Figure 17 – Cell polarity and migration is regulated using micropatterned ratchets and diverse geometries. A: Cells seeded on various micropatterned shapes, such as teardrops, squares, and arrows, exhibit distinct anisotropies, resulting in varied migration directions. B: Cells subjected to micropatterned ratchets (intermittent confinement) tend to migrate towards higher probability of protrusions with new and more stable adhesions. Migration direction is further influenced by the shapes and spacing of the micropatterns. (Figure adapted from: Isomursu, 2024)

The ECM microenvironment also plays a significant role in the geometric control of cell polarity. Distribution of ECM components influence front-rear polarization and intracellular organization, guiding cell migration towards regions with higher ligand density (Théry et al., 2006). For instance, this phenomenon is evident in cells adhered to

teardrop-shaped micropatterns. This geometry favors cell movement towards the wider end of the micropattern. However, by altering the distribution of fibronectin, with higher concentrations at the narrow end of the micropattern compared to the blunt end, cells show reverse polarity and shift the migratory behavior (Lee et al., 2021; Isomursu, 2024). Therefore, altering ligand distribution can reverse cell polarity. This experiment highlights the remarkable plasticity of cell behavior in response to geometric cues. It also suggests that the spatial distribution of ECM ligands influences cell polarity during migration, with cells dynamically adjusting their migratory trajectories based on the local ligand environment (Lee et al., 2021; Isomursu, 2024).

Chapter 2 – General and specific aims

Directed cell migration along gradients of immobilized proteins – a process called haptotaxis – is crucial for morphogenesis, the immune response, and cancer metastasis. Despite its significance, the mechanisms underlying haptotaxis remain poorly understood. This gap in knowledge is primarily due to the challenges associated with generating precise and controlled protein gradients *in vitro*. Therefore, we believe that fabrication of accurate and reliable gradients is essential for studying the cellular responses involved in haptotaxis. In addition to molecular signals, mechanosensing and mechanotransduction processes are essential to how cells interpret and respond to these gradients. Therefore, the mechanical forces are expected to play a critical role in haptotaxis. However, these mechanical aspects have not been investigated, leaving a significant gap in our understanding of how physical forces really characterize this type of directed migration. Moreover, the cellular microenvironment is highly complex, not only presenting cells with a multitude of different and often opposing cues but also various geometric constraints. These constraints within the environment have been shown to significantly impact cell behavior, as referred to in Chapter 1 – Introduction. Therefore, understanding how physical constraints affect haptotaxis is important for replicating a more physiological context in experimental settings.

Hence, in this thesis we aimed to understand how cells sense and respond to gradients of immobilized protein with the following specific aims:

1. To develop a system to fabricate well-controlled fibronectin gradients within precise geometric patterns.

    1.1 To develop a system to fabricate well-controlled fibronectin patterns on flexible elastomers.

    1.2 To develop a method to spatially quantify the amount of fibronectin within these protein gradient patterns.

    1.3 Elaborate an experimental and computational workflow to monitor cell migration on haptotactic and homogeneous patterns.

2. To quantify the migration of cells on homogeneous patterns of different fibronectin densities.

3. To study how cells integrate haptotactic cues with cell polarity during migration.

3.1 To study the haptotaxis of single MCF10A cells on symmetric patterns of fibronectin density.

3.2 To investigate the effect of substrate stiffness on haptotatic response.

3.3 To characterize how the pharmacological disruption of various cytoskeletal components alters cell haptotactic response.

3.4 To characterize actin dynamics of single cells migrating on homogeneous and gradient patterns.

3.5 To measure membrane tension of single cells migrating on homogeneous fibronectin and on symmetric fibronectin gradients.

3.6 To quantify the traction forces generated by cells during haptotaxis.

3.7 To study the impact of confinement on haptotatic response with patterns of different widths.

By addressing these specific aims, this thesis seeks to advance our understanding of the mechanical and molecular mechanisms driving haptotaxis. Hence, contributing to the broader fields of cell migration, tissue engineering, developmental biology and cancer metastasis.

Chapter 3 – Materials and methods

1. Stable cell line generation

MCF10A-LifeAct-GFP cells were produced by transduction of MCF10A cells with lentiviral particles generated in HEK293T after transient transfection of pLenti.PGK.LifeAct-GFP.W (Addgene, #51010) using Lipofectamine 3000 (Invitrogen, #L3000008). Afterwards, the stable MCF10A-LifeAct-GFP cell line was obtained from a single cell colony expressing medium GFP fluorescence intensity sorted through flow cytometry (FACS) using BD FACSDiva 8.0.1 software.

2. Cell culture

HEK293T cells were routinely maintained in filter-cap Nunc™ EasYFlask™ 25 cm^2 (Thermo Scientific, #156367) or 75 cm^2 Cell Culture Flasks (Thermo Scientific, #156499) at 37ºC and 5% CO_2 to guarantee a steady environment for optimal cell growth. HEK293T cells were cultured in DMEM (1X) + 4.5 g/L D-glucose + L-glutamine + pyruvate media (Gibco, #41966029) supplemented with 10% fetal bovine serum (Life Technologies, #10270098) and 100 U/ml penicillin-streptomycin (Invitrogen, #10378016).

MCF10A, MCF10A-H2B-GFP (gift from G. Charras - London Center for Nanotechnology, UK) and MCF10A-LifeAct-GFP cells were routinely maintained in filter-cap Nunc™ EasYFlask™ 25 cm^2 or 75 cm^2 Cell Culture

Flasks at 37ºC and 5% CO_2 to guarantee a steady environment for optimal cell growth. MCF10A, MCF10A-H2B-GFP and MCF10A-LifeAct-GFP cells were cultured in DMEM-F12 media (Gibco, #21331020) supplemented with 5% horse serum (Invitrogen, #16050122), 100 U/ml penicillin-streptomycin, 20 ng/ml hEGF (Peprotech, #AF-100-15), 0.5 mg/ml hydrocortisone (Sigma-Aldrich, #H0888), 100 ng/ml cholera toxin (Sigma-Aldrich,#C8052) and 10 µg/ml insulin (Life Technologies,#12585014). When passing cells to maintain culture, cells were washed once with sterile PBS 1X (Sigma-Aldrich, #D1408) and incubated in Trypsin/EDTA (Gibco, #11590626) at 37ºC and 5% CO_2 for 5 minutes, in case of HEK293T, or 15-20 minutes, in case of MCF10A, MCF10-H2B-GFP and MCF10-LifeAct-GFP cells. When all cells detached, complete media was added to the T25 or T75 flask and the cell suspension was transferred to a falcon tube. Then, cells were centrifuged for 3.5 minutes at 300 xg and further resuspended in complete media. Cells were seeded in a new T25 or T75 previously filled with complete media and properly diluted to keep passing them every 2-3 days.

3. Cell seeding for experiments

For migration experiments, 24 hours before imaging, MCF10A-H2B-GFP cells were cultured in DMEM-F12 serum-free media (DMEM-F12 media + 100 U/ml penicillin-streptomycin, 20 ng/ml hEGF, 0.5 mg/ml hydrocortisone, 100 ng/ml cholera toxin and 10 µg/ml insulin) supplemented with 2 mM thymidine (Sigma-Aldrich, #T1895) to inhibit cell proliferation. When passing cells for experiments, MCF10A-H2B-GFP cells were washed once with sterile PBS 1X and incubated for 15-20

minutes in Trypsin/EDTA at 37ºC and 5% CO_2. When all cells were detached, DMEM-F12 serum-free media + 2 mM thymidine was added to the T25 or T75 flask and the cell suspension was transferred to a falcon tube. Then, MCF10A-HB2-GFP cells were centrifuged for 3.5 minutes at 300 xg and further resuspended in 4-6 mL DMEM-F12 serum-free media + 2 mM thymidine. Then 1000-6000 cells were seeded under the microscope on 35 mm MatTek glass bottom dishes (MatTek, #P35G-0-20-C) previously sterile using UV for 10-15 minutes and filled with 2 mL of DMEM-F12 serum-free media + 2 mM thymidine.

For drug experiments, MatTek dishes were previously sterile using UV for 10-15 minutes and filled with 2 mL of DMEM-F12 serum-free media + 2 mM thymidine + drug treatment. The drugs used were 10 μM para-Nitroblebbistatin (motorPharma, #DR-N-111), 5 μM Y-27632 (Tocris Bioscience, #1254) or 15 μM LY294002 (Cell Signaling Technology, #9901S) and dimethyl sulfoxide (DMSO) (Sigma-Aldrich, #D8418) was used as control.

For the actin flows experiments, the protocol was the same as for the migration assay with the exception that MCF10A-LifeAct-GFP were the cells used and they were seeded on 35 mm MatTek glass bottom dishes previously sterile using UV for 10-15 minutes and filled with 2 mL of DMEM-F12 serum-free media + 2 mM thymidine + 0.02 mg rutin (Acros Organics, #132390050) to avoid GFP photobleaching.

For traction force microscopy (TFM) experiments, the protocol was the same as for the migration experiments.

For membrane tension experiments, the protocol was the same as for the migration assay with the exception that MCF10A were the cells used.

4. Preparation of soft PDMS substrates

Soft elastomeric silicone polydimethylsiloxane (PDMS) substrates (Dow, #DOWSIL™ CY 52-276) were prepared mixing solution A and solution B with a ration of 9:10, respectively, to obtain a stiffness of 12.6 kPa. The solution was degassed for 30 minutes and maintained on ice to avoid undesired polymerization. Then, 150 µL of the solution was added to 35 mm MatTek glass bottom dishes pre-cleaned with air and pre-warmed at 65ºC using a standard hot plate. Each dish was then spun using a spin coater (Laurell Tech., model WS-650MZ 23NPP/LITE) with a rotation of 400 rpm and acceleration of 100 rpm for 90 seconds. After the spin, substrates were maintained at 65ºC using a standard hot plate, while other substrates were being prepared. When enough substrates were prepared (between 20-40), substrates were incubated overnight at 65ºC for complete substrate polymerization and then maintained at room temperature. Substrates were used for 1-1.5 months after preparation.

This procedure was inspired by the protocol described in Latorre et al., 2018.

5. Functionalization of soft PDMS substrates for photopatterning

Soft PDMS substrates were incubated with 5% (3-Aminopropyl)triethoxysilane (Sigma-Aldrich,#281778) diluted in absolute ethanol for 3 minutes. The substrates were washed 3X with absolute ethanol and then washed 3X with Milli-Q® water obtained by using Milli-Q® Advantage A10 Water Purification System (Merck

Milipore, #Z00Q0V0WW). Then, substrates were incubated with filtered beads solution containing 1:40 red fluorescent (Invitrogen, #F8810) or blue fluorescent (Invitrogen, #F8805) 0.2 µm FluoSpheres™ Carboxylate-Modified Microspheres diluted in boric acid buffer (3.8 mg/mL sodium tetraborate (Sigma-Aldrich, #221732) + 5 mg/mL boric acid (Sigma-Aldrich, #B1934)) for 10 minutes. The substrates were washed 3X with Milli-Q® water. Then, substrates were incubated with 1% Poly-L-lysine (PLL) (Sigma-Aldrich, #P2636) diluted in borate buffer pH= 8.3 (4.75 g/L sodium tetraborate + 3.1 g/L boric acid) for 1 hour. Substrates were washed 3X with 10 mM HEPES buffer pH= 8.2-8.4 (Sigma-Aldrich, #H3375). Finally, surface of soft PDMS substrates was passivated by incubation with 50 mg/mL solution of PEG coupled with succinimidyl valerate (mPEG-sva) (Laysan Bio, #MPEG-SVA-5000) diluted in 10 mM HEPES buffer pH= 8.2-8.4 for 1 hour. Substrates were washed 3X with Milli-Q® water and preserved at 4ºC. Functionalized substrates were used for photopatterning until maximum 2 days after functionalization.

This procedure was inspired by the protocols described in Latorre et al., 2018 and Strale et al., 2016.

6. Labelling fibronectin with fluorophore

Fibronectin from human plasma (Sigma-Aldrich, #F0895) was labelled with 647 fluorophore using Alexa Fluor™ 647 Antibody Labeling Kit (Life Technologies, #A20186) and following manufacturer's guidelines. The concentration of labelled fibronectin with 647 fluorophore (Fibronectin-647) was quantified using PierceTM BCA protein assay kit (Thermo Fisher Scientific, #23227) also following the

recommendations given by the manufacturer. Then, spectrophotometric measurements of protein were calculated using Infinite M200 Pro reader with i-control software. Fibronectin-647 concentration was defined as the average of 3 independent labelling procedures and respective protein quantifications.

7. Design of fibronectin micropatterns

Patterns were designed using Inkscape software. Drawings had gray scale values from 0 to 255, where 0 (black color) corresponds to 0% protein absorption and 255 (white color) corresponds to 100% protein absorption.

Homogeneous lines had 3 μm, 6 μm, 10 μm, 13 μm, 17 μm, 20 μm, 25 μm, 30 μm and 350 μm widths and 3 mm length with 100% white color. Homogeneous patterns had 20 μm width and 500 μm length with 100%, 80%, 60%, 40% or 20% transparency of white color. Gradient patterns had 20 μm (confined, 1D), 40 μm, 60 μm, 80 μm or 250 μm (unconfined, 2D) widths and 500 μm length with a gray scale gradient from black in the 2 edges to white in the center of the drawing. After designing the drawings, they were calibrated according to the photosensitive component (p-Benzoylbenzyl)trimethylammonium chloride (BocSciences, #B2699-222060) consumption using a custom-made MATLAB (Mathworks, USA) script.

This procedure was inspired by the protocol described in Strale et al., 2016.

8. Generation of fibronectin micropatterns

(p-Benzoylbenzyl)trimethylammonium chloride was added to soft PDMS substrates and degraded under UV illumination (λ= 375 nm) using Nikon Eclipse Ti inverted microscope equipped with PRIMO photopatterning system and Leonardo software (Alvéole, France) with laser power of 4.3 and dose of 900 mJ/mm^2 . Substrates were washed 3X with PBS 1X. Then, substrates were incubated with filtered fibronectin-647 solution containing 100 µg/mL fibronectin and 3.8 µg/mL fibronectin-647 fluorophores diluted in PBS 1X for 5 minutes. For homogeneous lines, 100 µg/mL fibronectin and 30 µg/mL fibrinogen-647 (Invitrogen, # F35200). Protein will absorb only in areas that were previously illuminated with UV and generate the designed micropatterns. Substrates were washed 3X with PBS 1X and preserved at 4ºC. Photopatterned substrates were used for experiments until a maximum of 2 days after photopatterning.

This procedure was inspired by the protocol described in Strale et al., 2016.

9. Fibronectin density quantification

Microfluidic PDMS blocks with channels of 2 mm length, 200 µm width and 50 µm height were offered by Dr. Anna Labernadie (Centro de Investigación Príncipe Felipe (CIPF), Spain). Surface of PDMS blocks were modified using plasma cleaner (Harrick, model PCD-002-CE) to improve bonding of the PDMS with 35 mm MatTek glass bottom dishes. Then, the channels were pretreated with 2% pluronic solution (Sigma-Aldrich,

#P2443) for 1 hour in the case of the control PDMS block (exposed to PBS 1X solution) and for overnight in the case of PDMS block exposed to 25%, 50% and 100% fibronectin-647 solutions. Channels were washed 3X with PBS 1X. Fluorescence images of the channels filled with the different concentrations of fibronectin-647 solutions (PBS 1X, 25%, 50% and 100%) were acquired using 250 ms, 500 ms, 1000 ms, 2500 ms and 5000 ms times of exposure in 10 different fields of view (pre-wash images). Then, channels were washed 3X with PBS 1X and new fluorescence images were acquired using the 5 different exposure times in the same 10 fields of view previously selected (pos-wash images). Fluorescence images of blue homogeneous slides were also acquired with 5 different exposure times in 10 different fields of view. All images acquisition was performed using Nikon Eclipse Ti inverted microscope with MetaMorph software and 10X 0.3 NA, 20X 0.45 NA and 40X 0.75 NA objectives.

For the control PDMS lines filled with PBS 1X solution, a median of the fluorescence intensity in the different 10 images was made for each exposure time, obtaining the noise of the camera. For the blue homogeneous slide, a median of the fluorescence intensity in the different 10 images was made for each exposure time, obtaining the mercury lamp intensity. Then, the noise of the camera was rested from the homogeneous slide median, obtaining the values to normalize fibronectin-647 density with mercury lamp fluctuations. For the PDMS lines filled with 25%, 50% and 100% fibronectin-647 solutions, the pos-washed image was rested from the pre-washed imaged for each field of view from all exposure times. Then, the mean of the resulting fluorescence intensity in the 10 fields of view was made for each exposure time. The mean of PBS 1X (used as 0% fibronectin-647) fluorescence

intensity in the different 10 images was also made for each exposure time. Thus, the mean fluorescence intensity for each percentage of fibronectin-647 solutions with different exposures time was calculated with the following formula:

$$Mean\ fluorescence\ intensity = \frac{< [protein] > - noise\ camera}{mercury\ lamp\ intensity - noise\ camera}$$

According to the fibronectin-647 concentration estimation after using the labelling kit, 0%, 25%, 50% and 100% fibronectin-647 solutions correspond to, respectively, 0 μg/mL, 198.92 μg/mL, 397.84 μg/mL, and 795.68 μg/mL. From this assumption, we correlated the mean fluorescence intensity with fibronectin-647 density by multiplying the height of the channel (50 μm) with each fibronectin-647 concentration. Then, a linear regression was calculated between fibronectin-647 density (ng/cm^2) and mean fluorescence intensity, forcing the line to go through X, Y= (0,0). Since for live imaging experiments the fibronectin-647 micropatterns were imaged using 10X and 20X objectives and 5000 ms exposure time, the equations of the linear regression obtained for the 5000 ms (Y=0.001830X and Y=0.001060X, respectively) were used in the custom-made MATLAB script for fibronectin-647 density quantification calibrated with the noise of the camera and mercury lamp intensity in each experiment.

This procedure was inspired by the protocol described in Versaevel et al., 2021.

10. Imaging for migration and drugs experiments

Before starting the time lapse, images of a blue homogeneous slide were acquired with and without far-red wavelength to further calibrate fibronectin density with the mercury lamp intensity and the noise of the camera, respectively. Additionally, images from the fibronectin-647 micropatterns were acquired before imaging. Then, live imaging started after defining the settings and cell seeding under the microscope with thermal (37ºC), CO_2 (5%) and humidity controls. Images were acquired every 10 minutes for 16-20 hours using a 10X 0.3 NA objective with 3 channels: brightfield (cell), green (nucleus) and far-red (fibronectin-647 micropattern). Multichannel acquisition was performed using Nikon Eclipse Ti inverted microscope with MetaMorph software.

11. Imaging for actin flows experiments

Cells were imaged 4-7 hours after seeding with thermal (37ºC), CO_2 (5%) and humidity controls. Images of each cell were acquired every 4 seconds for 3 minutes using a 60X 1.40 NA objective with 2 channels: green (actin) and far-red (fibronectin-647 micropattern). Multichannel acquisition was performed using a Nikon Eclipse Ti inverted microscope with a CSU-W1 confocal scanner unit.

12. Imaging for TFM experiments

Before starting the time lapse, images of a blue homogeneous slide were acquired with and without far-red wavelength to further calibrate

fibronectin density with the mercury lamp intensity and the noise of the camera, respectively. Images from the fibronectin-647 micropatterns were acquired before imaging. Additionally, images from the red fluorescent beads were acquired before imaging with a z series of 10 z steps of 1 µm (range = 9). Then, live imaging started after defining the settings and cell seeding under the microscope with thermal (37ºC), CO_2 (5%) and humidity controls. Images were acquired every 10 minutes for 12-20 hours using a 20X 0.45 NA objective with 4 channels: brightfield (cell), green (nucleus), red (beads) with the previously described z series and far-red (fibronectin-647 micropattern). Multichannel acquisition was performed using Nikon Eclipse Ti inverted microscope with MetaMorph software.

13. Imaging for membrane tension experiments

3-6 hours after seeding cells, the media was changed to DMEM-F12 serum-free media + 2 mM thymidine + 1 µM of Flipper-TR (Tebu-bio, #SC020). After 15 minutes incubation, Flipper images of each cell and the respective fibronectin-647 micropattern were acquired using a HC PL APO CS2 63x/1.40 OIL objective. Flipper was excited at 488 nm and the emission was collected in the 550-650 nm range. Hyperosmotic shocks were performed by changing the media in the microscope to DMEM-F12 serum-free media + 2 mM thymidine + 1 µM of Flipper-TR + 320 mmol/L sucrose (Sigma-Aldrich, #S9378). After 1 hour incubation, new Flipper images of previously imaged cells and the respective fibronectin-647 micropatterns were acquired. Multichannel acquisition was performed using a Leica TCS SP8 microscope equipped with a white light laser

(WLL), a hybrid detector (HyD) in photon-counting mode and LAS X software.

14. Cell tracking, cell segmentation and migration analysis

Tracking of cells was made with TrackMate plugin from Fiji using as reference H2B-GFP nuclear marker that MCF10A cells are expressing. 2D cell segmentation was made using a custom-made MATLAB script. Then, another custom-made MATLAB script was designed to join information of fibronectin-647 density, cell tracking and cell segmentation to obtain a database that describes quantitatively cell migration during the complete live imaging. Persistence ($\frac{displacement}{track\ distance}$), cell velocity ($\frac{\Delta x}{\Delta t}$), cell length (cell segmentation in x axis), x positions, nucleus positions, x turning points (change in directionality) or gradient (differences in protein density) are some of the parameters that were quantified.

In fibronectin-647 gradient micropatterns displacements were considered positive if cells migrated towards higher protein and negative if cells migrated against higher protein. In homogeneous fibronectin-647 micropatterns, displacements were considered positive if cells migrated towards the center of the micropattern and negative if cells migrated towards the edges of the micropattern. To avoid possible ECM deposition, degradation or remodeling effect, tracks were only analyzed since the cell adhered until the first change in directionality. Additionally, since the

micropatterns are symmetric, data was normalized so that all cells land in the same quadrant of the pattern ($x < 0$).

15. Quantification of actin flows, number of actin filaments and protrusions rate

Acquired images of actin were opened using Fiji. Afterwards, kymographs were generated in 4 regions of the trailing and 4 regions of the leading edges. To each region, actin retrograde flow (actin movement from the edges to the cell center), membrane retraction and edge velocities were manually measured by converting the angle of actin movement vectors into velocity. Actin polymerization velocity was calculated with the following formula:

$$v_{edge} = v_{polymerization} + v_{retrograde\ flow}$$

Cell masks were made with LifeAct-GFP signal as reference and using Otsu threshold in Fiji. Masks and pattern images were oriented to have the leading edge on the right side of the images and the trailing edge on the left side. Cell leading and trailing edges were defined, respectively, as the right and the left extremes with 4 μm length of the masks.

To measure actin filaments, we first manually defined the trailing edge as a radial 10 μm area with the center in the most back membrane of the cell. Then, manually measured the number of actin filaments in the trailing edge after applying Bandpass Filter and Unsharp Mask from Fiji.

The protrusions rate was manually measured by quantifying the number of actin peaks in generated kymographs of the leading edge and then dividing it by the total time of imaging (3 minutes).

Fibronectin fluorescence in the leading edge was defined by the mean fluorescence in the first 4 μm of the edge.

16. Traction force and traction asymmetry analysis

All traction computations and the following analyses of traction forces were carried out with custom-written MATLAB scripts. Fourier transform traction microscopy was used to measure traction forces (Trepat et al., 2009; Butler et al., 2002; Serra-Picamal et al., 2015). The displacement fields of the fluorescence microspheres were obtained using a self-written particle imaging velocimetry (PIV) algorithm using square interrogation windows of side length 24 pixels (corresponding to about 7.8 μm) with a relative overlap of 0.75 window length.

Segmented binary masks of the phase contrast images were used to extract the tractions under each cell at each time point. To include the traction profiles as complete as possible, segmentation was dilated by 15 μm in all directions. Axial traction profiles T_x were calculated by averaging the x-component of the tractions across the width of the segmentation at every time point. The axial lengths of these profiles were normalized to unit length for each time point, and these length-normalized tractions were averaged together in groups according to the cell trajectory (haptotactic motion, anti-haptotactic motion, or motion on homogeneous fibronectin) to form the averaged profiles $\langle T_x \rangle$.

The normalized second moment Q_x of the 1D-traction profiles was calculated as $Q_x = \frac{\int x^2 T_x dx}{\int |x|^2 T_x dxc}$, analogously to (Rossetti et al., 2024), where x is the spatial coordinate relative to the center of mass of the traction segmentation. The moments were then averaged over the corresponding times for each cell.

17. Membrane tension analysis

Lifetime measurements and analysis of membrane tension were performed using LAS X software and a custom-made MATLAB script. Cell masks were made with Flipper signal as reference and using Moments threshold in Fiji. Masks and pattern images were oriented to have the leading edge on the right side of the images and the trailing edge on the left side. Cell leading and trailing edges were defined, respectively, as the right and the left extremes with 11 μm length of the masks.

18. Statistical analysis

Graphs and statistical analysis were made using MATLAB, GraphPad Prism 8.0.2, RStudio and Microsoft Excel. Figures and figure legends describe the following statistical details: number of cells, error bars, number of independent experiments, statistical tests, and corresponding p-values. We considered the result significant when p-value < 0.05.

Chapter 4 – Results

1. Fabrication of a system with precise and well-controlled fibronectin gradients

Until now, technical limitations have created a gap in our understanding of haptotaxis. To address this, we developed a minimal *in vitro* system that allows for precise control over fibronectin density and geometry. Our system uses PRIMO technology with the Light-Induced Molecular Adsorption of Proteins (LIMAP) method to create fibronectin micropatterns on soft elastomeric substrates (E = 12.6 kPa) (Figure 18) (Strale et al., 2016; see methods). These substrates are also coated with fluorescent beads to measure cell traction. Therefore, this setup provides a controlled environment for studying how fibronectin gradients influence cell migration, offering clear insights into the mechanisms of haptotaxis.

1.1 Calibrate pattern drawings

When using PRIMO technology, drawings are first uploaded into Leonardo software and then sent to the PRIMO module for patterning (see methods). We noticed that when uploading drawings of linear gradients, the resulting gradient patterns were not as linear as intended (Figure 19A). These nonlinear gradients could impair cells' ability to constantly sense a gradient due to its low magnitude. The underlying

issue is that as the photoinitiator is consumed, it generates reactive species that have a finite lifetime and diffuse in the surrounding fluid. This diffusion leads to degradation of the passivation over a short distance, which in turn disrupts the linearity of the gradient. To solve this, we calibrated the drawings uploaded into the software by creating a calibration curve that represents the inverse profile of multiple patterned gradients (Figure 19B). Using this calibration curve, we adjusted the drawings accordingly and improved the linearity and magnitude of the gradients (Figure 19C-D). Consequently, it also enhanced the accuracy and reliability of our haptotatic system.

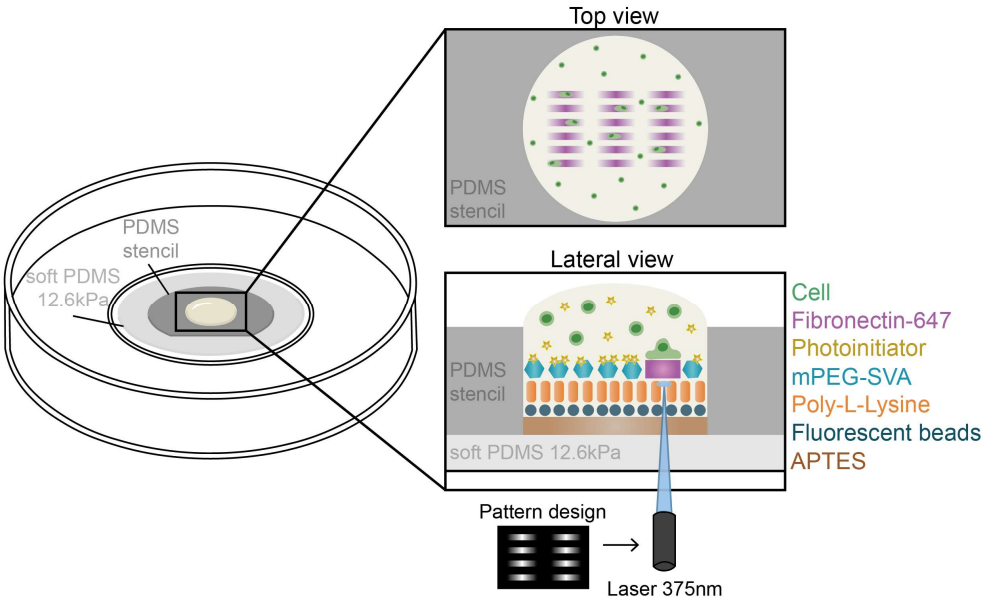

Figure 18 – Micropatterning of soft elastomeric substrates using PRIMO technology. Illustration of a glass-bottom dish coated with a PEG-decorated soft elastomer. Zoomed regions show the schematics of the functionalization of the patterned surface (see methods).

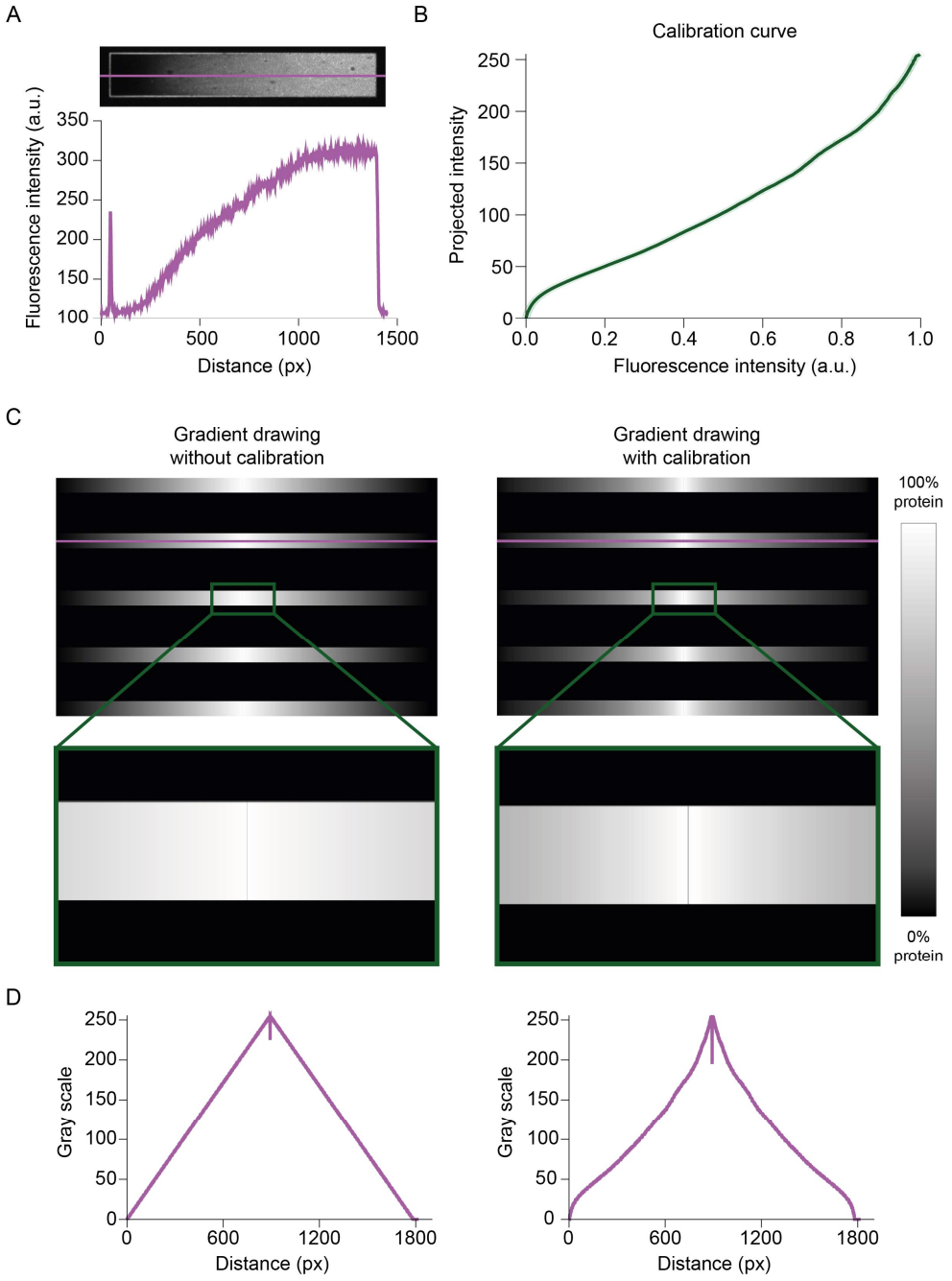

Figure 19 – Calibration of drawings to improve gradient linearity. A: Representative image of a gradient pattern used to calculate the calibration curve (up) and its respective fluorescence intensity profile (down). Profiles

were generated from the pink line in the upper image of panel A. B: Calibration curve calculated using multiple gradient patterns (N = 15). C: Drawings of gradients with and without custom-made calibration. White (gray value = 255) and black (gray value = 0) colors correlate with 100% protein and 0% protein absorption, respectively. D: Gray scale profiles for one drawing of gradients with and without custom-made calibration. Profiles were generated from the pink lines in panel C.

1.2 Development of a method to spatially quantify fibronectin density within haptotatic and homogeneous patterns

One of the challenges of micropatterning is translating fluorescence intensity to fibronectin density experienced by cells. To address this, we were inspired by the work of Versaevel et al. (Versaevel et al., 2021). We flowed fluorescently labeled fibronectin solutions with concentrations ranging from 0% (0 µg/mL) to 100% (795.68 µg/mL) through PDMS channels measuring 200 µm x 2 mm x 50 µm (Figure 20A; Figure 20C). Then, we acquired images before and after washing the channels for every protein concentration. Using these images, we developed a linear equation that correlates fluorescence intensity with fibronectin density for our imaging settings, i.e. 5000 ms of exposure time and 10X objective (Figure 20D-E). This equation allowed us to accurately convert fluorescence intensity into fibronectin density. However, it is known that the intensity of microscope's mercury lamp fluctuates over time, complicating comparisons between independent experiments (Heynen, Gough and Price, 1997). To overcome this issue, we accounted

for these fluctuations by capturing images of a blue auto-fluorescent slide prior to each experiment (Figure 20B). We then used these images to normalize the fluorescence intensity. Additionally, we subtracted the camera noise to improve measurement accuracy. This approach enabled us to reliably convert fluorescence into protein density and make consistent comparisons across independent experiments.

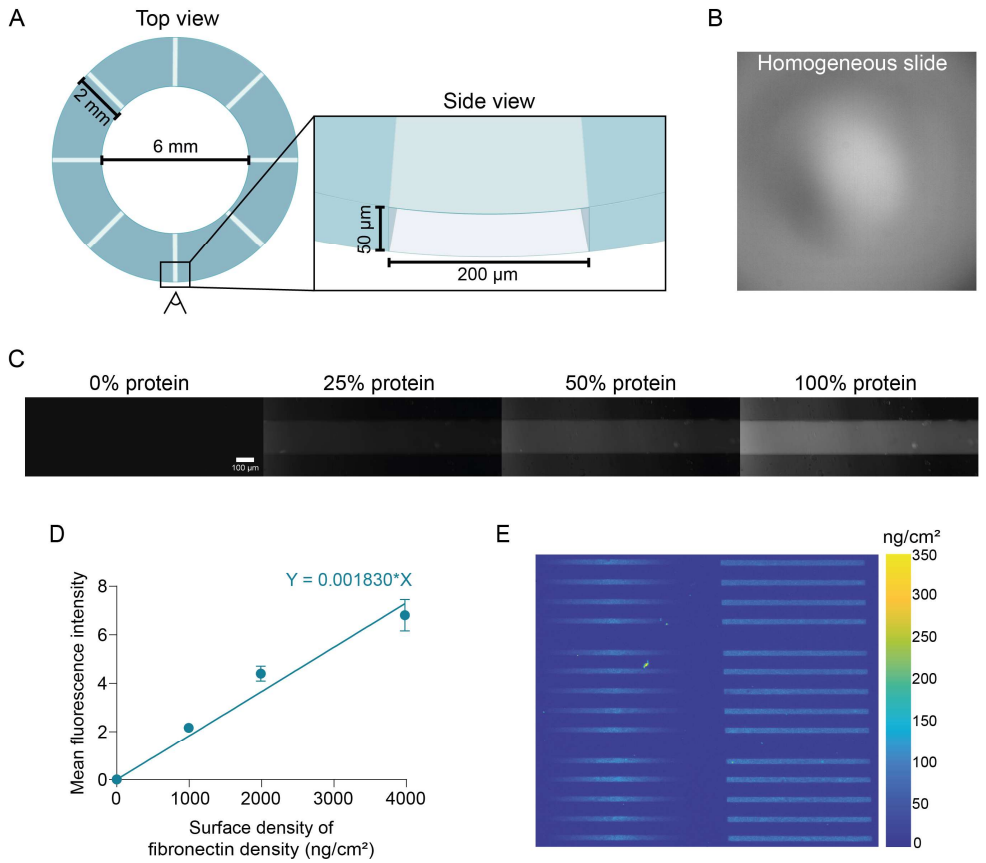

Figure 20 – Experimental approach to convert fluorescence intensity to fibronectin density. A: Illustration of microfluidic PDMS block design. B: Representative image of homogeneous slide image acquired with 10X objective

and 5000 ms exposure. C: Representative images of channels with different percentages of fibronectin-647 solutions acquired with 10X objective and 5000 ms exposure. D: Linear regression for 5000 ms of exposure time correlating fluorescence intensity with fibronectin-647 density using 10X objective. Error bars are SD. E: Representative image of fibronectin-647 density quantification in experimental homogeneous and gradient patterns using the equation correspondent to 5000 ms exposure (Y = 0.001830X). Data from one independent experiment.

1.3 Determination of the optimal pattern dimensions for our cell model

Then, we aimed to determine the optimal pattern dimensions for studying migration in our cell model, the MCF10A cells, which are well-characterized and frequently used in cell migration studies (Sunyer et al., 2016; Palamidessi et al., 2019; Gross et al., 2022; Gilles et al., 1999; Cai et al., 2022). To address this, we created homogeneous fibronectin lines that were 3 mm in length with varying widths (Figure 21A). The widths tested ranged from 3 μm to 350 μm (Figure 21A). We then performed 12-20 hours timelapse imaging of MCF10A cells expressing histone 2B labelled with GFP to facilitate nucleus detection and cell tracking. After tracking the cells' nuclei, we measured cell persistence ($\frac{displacement}{track\ distance}$) and velocity ($\frac{\Delta x}{\Delta t}$), which are standard parameters used to characterize migratory behaviors (Figures 21B-C). Cells on 17 μm and 20 μm lines exhibited faster and more directed movement, while cells on 3 μm and 6 μm lines showed slower and more random movement. These results indicate that micropattern width significantly impacts cell motility, with 17-20 μm

widths providing optimal conditions. Based on these findings, we decided to use 20 µm width patterns to study haptotaxis. Moreover, the patterns were set to 500 µm in length to ensure that cells remained within the microscope's field of view and allow complete tracking of cells (Figure 20E).

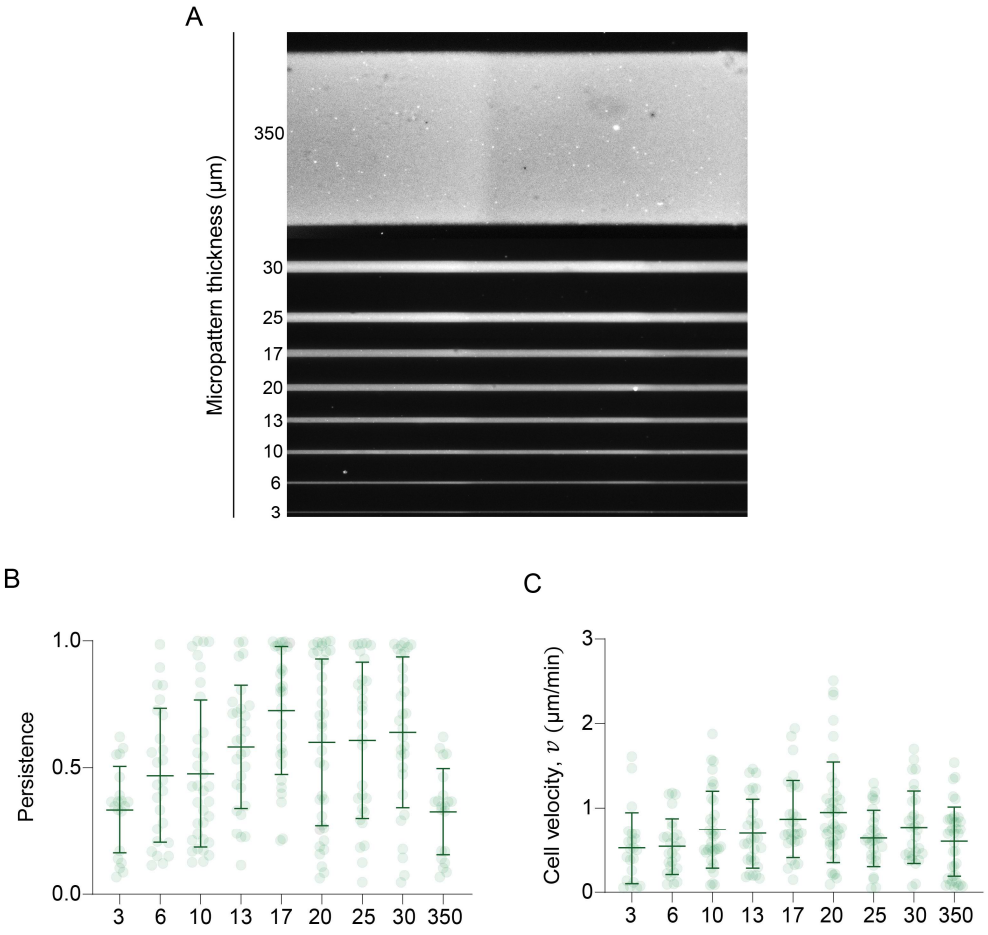

Figure 21 – MCF10A cells exhibit faster and more persistent migration on micropatterned lines with intermediate widths. A: Representative fluorescence image of homogeneous lines with 3 mm length and 3 µm, 6 µm, 10 µm, 13 µm, 17 µm, 20 µm, 25 µm, 30 µm and 350 µm widths. B: Mean persistence

of cells migrating in homogeneous lines with 3 μm (N = 20), 6 μm (N = 26), 10 μm (N = 34), 13 μm (N = 29), 17 μm (N = 29), 20 μm (N = 37), 25 μm (N = 29), 30 μm (N = 30) and 350 μm (N = 21) widths. Error bars are SD. C: Mean velocity of cells migrating in homogeneous lines with 3 μm (N = 22), 6 μm (N = 26), 10 μm (N = 34), 13 μm (N = 29), 17 μm (N = 29), 20 μm (N = 40), 25 μm (N = 29), 30 μm (N = 30) and 350 μm (N = 37) widths. Error bars are SD. Data of homogeneous lines with 3 μm, 6 μm and 10 μm from four independent experiments. Data of homogeneous lines with 13 μm, 17 μm and 20 μm from five independent experiments. Data of homogeneous lines with 25 μm, 30 μm and 350 μm from two independent experiments.

1.4 Experiment and analysis of cell migration in haptotactic and homogeneous patterns

With the methodology optimized, we established the experimental and analysis workflow for the upcoming experiments. To analyze single cell migration, MCF10A cells were seeded under the microscope to precisely monitor the processes of cell adhesion and initial polarization. We inhibited cell proliferation with thymidine to ensure only a single cell was present in each pattern. Then, we selected only patterns with a single, viable, and non-dividing cell for further analysis. Each cell's nucleus was tracked to record its trajectory over time, and phase-contrast image segmentation was employed to monitor the leading and trailing edges, as well as cell length. Fluorescently labeled fibronectin was used to measure the exact fibronectin density experienced by each cell at various time points. This data was compiled into a comprehensive database detailing

single cell migration numerically, both in homogeneous and gradient patterns.

After adhering to the patterns, cells exhibited oscillatory trajectories. Since cells can deposit, degrade, and remodel ECM proteins, we focused on the initial cell movement — from adhesion to the first turn. Moreover, we took advantage of pattern's symmetry to normalize the trajectories, ensuring that all of them started on the left half of the pattern ($x < 0$). Movements toward the center were considered positive, while movements away were negative. This methodology allowed us to map cell behavior, including cell length, velocity, traction forces, and actin dynamics, as functions of fibronectin density. Therefore, we established a well-controlled 1D system to precisely understand haptotaxis.

2. Cell length and velocity show a biphasic response to fibronectin density

To study the impact of fibronectin density on cell migration, we began by seeding MCF10A cells onto substrates with homogeneous fibronectin patterns, varying in density from 20% to 100% (Figure 22A). We assessed migratory response by analyzing cell length and velocity, as these parameters are expected to vary with changes in adhesiveness (Schreiber et al., 2021). Confirming the technique accuracy, patterns with lower protein concentrations exhibited reduced fluorescence intensity, while those with higher concentrations showed increased fluorescence intensity (Figure 22B). We found that higher fibronectin densities

resulted in more cells adhering to the patterns, indicating that cells adhere more effectively when more fibronectin is present.

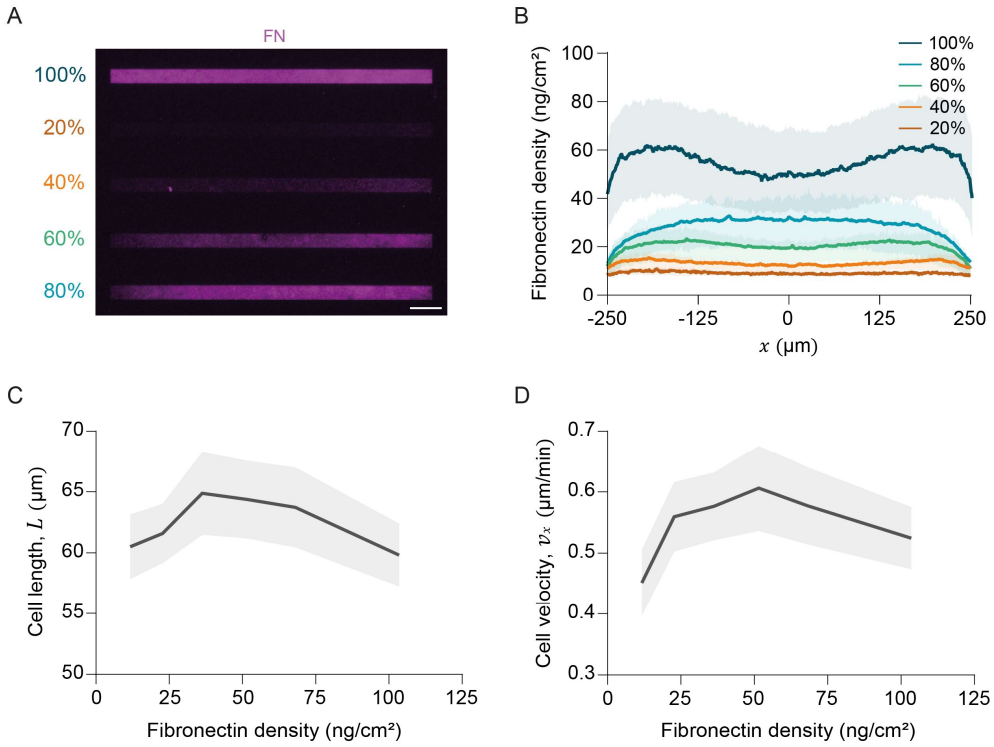

Figure 22 – The response to fibronectin density occurs in a biphasic manner. A: Representative fluorescence images of homogeneous patterns with 20%, 40%, 60%, 80% and 100% fibronectin. Scale bar is 50 µm. B: Median fibronectin density of homogeneous patterns with 20% (N = 23), 40% (N = 39), 60% (N = 83), 80% (N = 75) and 100% (N = 337) fibronectin. Error bars are 25 and 75 percentiles. C: Mean cell length for 6 fibronectin density bins. Bin1 = [6.91; 15.99] (N = 87), bin2 = [16.13; 29.35] (N = 85), bin3 = [29.48; 43.35] (N = 88), bin4 = [43.57; 58.97] (N = 90), bin5 = [59.43; 76.64] (N = 87) and bin6 = [76.68; 185.05] (N = 90). Error bars are 95% CI. D: Mean velocity in x for 6 fibronectin density bins. Bin1 = [6.91; 15.99] (N = 87), bin2 = [16.13; 29.35] (N

= 85), bin3 = [29.48; 43.35] (N = 88), bin4 = [43.57; 58.97] (N = 90), bin5 = [59.43; 76.64] (N = 87) and bin6 = [76.68; 185.05] (N = 90). Error bars are 95% CI. Data of homogeneous patterns with 100% fibronectin from nine independent experiments. Data of homogeneous patterns with 20%, 40%, 60% and 80% fibronectin from four independent experiments.

Furthermore, higher protein densities resulted in larger cell sizes (Figure 22C) and faster cell movement (Figure 22D) up to 36.29 ng/cm^2 and 51.44 ng/cm^2 of fibronectin, respectively. Beyond these densities, both cell length and velocity decreased, revealing a biphasic response. Initially, increased protein density enhanced both adhesion strength and cell motility. However, beyond those thresholds, excessive adhesion possibly led to decreased cell length and velocity as adhesions became overloaded (Fortunato and Sunyer, 2022; Bangasser et al., 2017; Elosegui-Artola et al., 2014). Overall, our data show that fibronectin density modulates MCF10A speed and elongation. However, higher fibronectin density enhances cell adhesion, spreading, and velocity up to an optimal level. This indicates a relationship between adhesion and cell length, as well as between adhesion and velocity.

3. MCF10A cells follow fibronectin gradients

To test the hypothesis that MCF10A cells exhibit haptotaxis, we seeded them on homogeneous patterns with 100% fibronectin (Figure 23A-B) and on symmetric gradient patterns with maximum fibronectin density at the center and decay to zero at both pattern edges (Figure 24A-

B). These symmetric patterns enable us to not only understand haptotactic behavior but also to investigate how cells respond to changes in gradient direction once cell polarity is established.

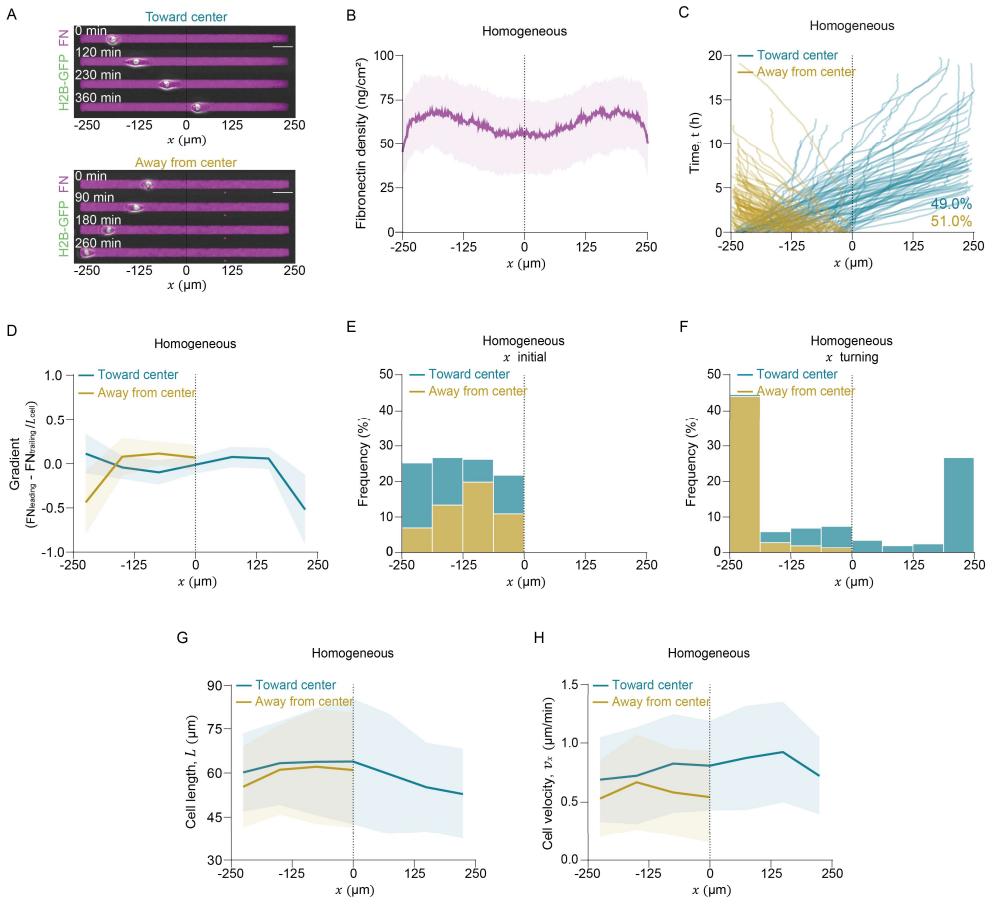

Figure 23 – Cells in homogeneous patterns exhibit increased velocity over time but random directionality. A: Representative fluorescence images of a cell migrating in homogeneous patterns. Scale bar is 50 μm. B: Median fibronectin density of homogeneous patterns. Error bars are 25 and 75 percentiles. N = 202. C: Individual tracks of cells migrating in homogeneous patterns. N = 99 for cells migrating toward center and N = 103 for cells migrating away from center. D: Mean gradient of cells migrating in homogeneous patterns.

N = 70 for cells migrating toward center and N = 103 for cells migrating away from center. Error bars are SD. E: Initial x position of cells migrating in homogeneous patterns. N = 70 for cells migrating toward center and N = 103 for cells migrating away from center. F: Turning x position of cells migrating in homogeneous patterns. N = 70 for cells migrating toward center and N = 103 for cells migrating away from center. G: Mean velocity in x for cells in homogeneous patterns. N = 70 for cells migrating toward center and N = 103 for cells migrating away from center. Error bars are SD. H: Mean cell length for cells migrating in homogeneous patterns. N = 70 for cells migrating toward center and N = 103 for cells migrating away from center. Error bars are SD. Data from four independent experiments.

On homogeneous patterns, cells moved randomly, with 49.0% migrating toward the center and 51.0% moving away from it due to a nearly zero gradient ($\frac{FN_{leading}-FN_{trailing}}{L_{cell}}$) (Figure 23C-D). These cells adhered uniformly across the patterns (Figure 23E) and they mostly turned at the pattern edges (Figure 23F), indicating a persistence length greater than the pattern size. Cell elongation was greatest at the center (Figure 23G), and cell velocity increased continuously from adhesion until repolarization (Figure 23H).

In gradient patterns, an impressive 82.7% of cells migrated toward areas with higher fibronectin density, indicating robust haptotaxis, while only 17.3% moved anti-haptotatically (Figure 24C-D). Interestingly, this anti-haptotactic response is likely due to cell adhesion occurring near the fibronectin peak, where the gradient is almost zero, resulting in random directionality (Figure 24C; Figure 24E). Outside this peak, the gradient

was significantly different from zero, confirming that cells experienced varying fibronectin densities during most of their migration (Figure 24E). As expected, the difference in fibronectin density between the leading and trailing edges was positive for haptotactic cells and negative for anti-haptotactic ones. We also observed that both haptotactic and anti-haptotactic cells predominantly adhered to regions with higher protein density (Figure 24F). Overall, these findings show that MCF10A cells robustly follow fibronectin gradients and suggest that haptotaxis is influenced by the gradient magnitude.

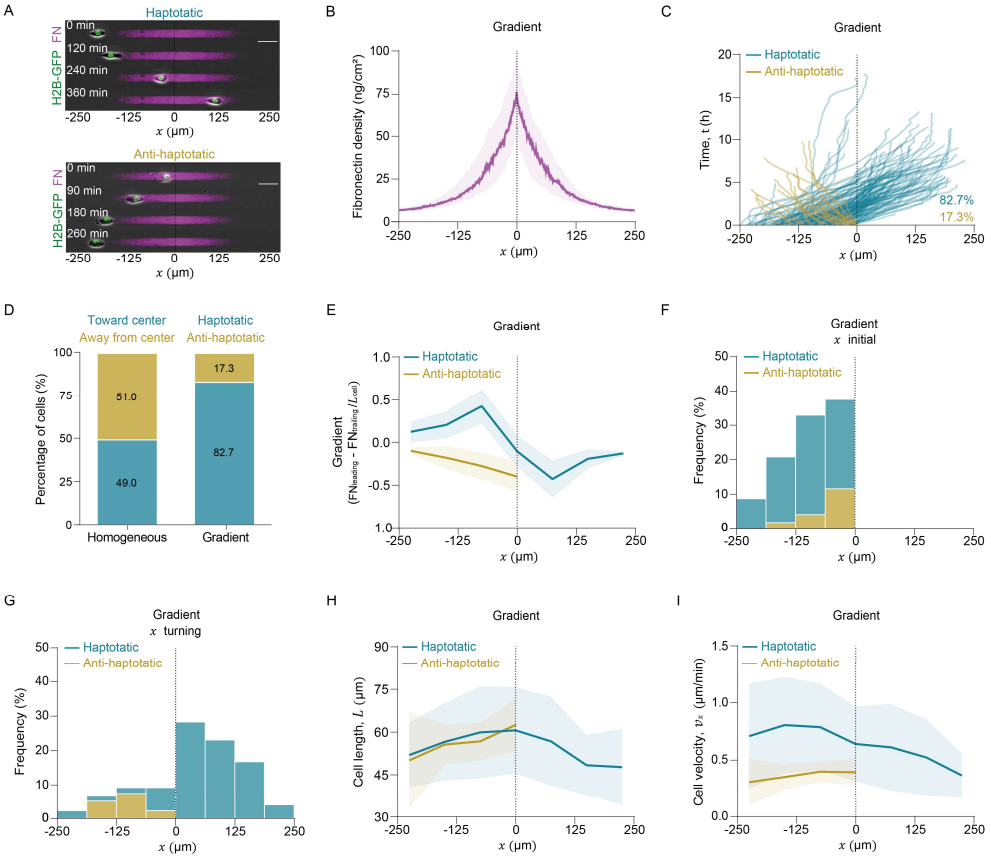

Figure 24 – Polarized MCF10A cells maintain their directionality even

when exposed to a gradient with an opposing direction. A: Representative fluorescence images of a cell migrating in gradient patterns. Scale bar is 50 μm. B: Median fibronectin density of gradient patterns. Error bars are 25 and 75 percentiles. N = 173. C: Individual tracks of cells migrating in gradient patterns. N = 143 for haptotatic cells and N = 30 for anti-haptotatic cells. D: Haptotaxis probability for cells migrating in gradient patterns (N = 173) and probability of cells moving toward center or away from center in homogeneous patterns (N = 202). E: Mean gradient of cells migrating in gradient patterns. N = 125 for haptotatic cells and N = 30 for anti-haptotatic cells. Error bars are SD. F: Initial x position of cells migrating in gradient patterns. N = 143 for haptotatic cells and N = 30 for anti-haptotatic cells. G: Turning x position of cells migrating in gradient patterns. N = 143 for haptotatic cells and N = 30 for anti-haptotatic cells. H: Mean cell length for cells migrating in gradient patterns. N = 125 for haptotatic cells and N = 30 for anti-haptotatic cells. Error bars are SD. I: Mean velocity in x for cells migrating in gradient patterns. N = 125 for haptotatic cells and N = 30 for anti-haptotatic cells. Error bars are SD. Data from five independent experiments.

3.1 Effects of gradient magnitude, substrate stiffness, contractility and lamellipodia expansion in haptotatic responses

Our previous results indicated that gradient magnitude could affect haptotaxis. To further test this hypothesis, we used the inherent heterogeneity in patterns produced by PRIMO technology. This heterogeneity allowed us to divide the data into low, medium, and high gradient magnitudes (Figure 25A). Cells on patterns with higher gradients experienced significantly greater maximum fibronectin

densities (Figure 25B). Cell velocity remained consistent across slopes (Figure 25C), while the probability of haptotaxis increased with steeper gradients (Figure 25D). This demonstrates that the initial response toward higher fibronectin areas is influenced by the gradient magnitude, thereby confirming our hypothesis.

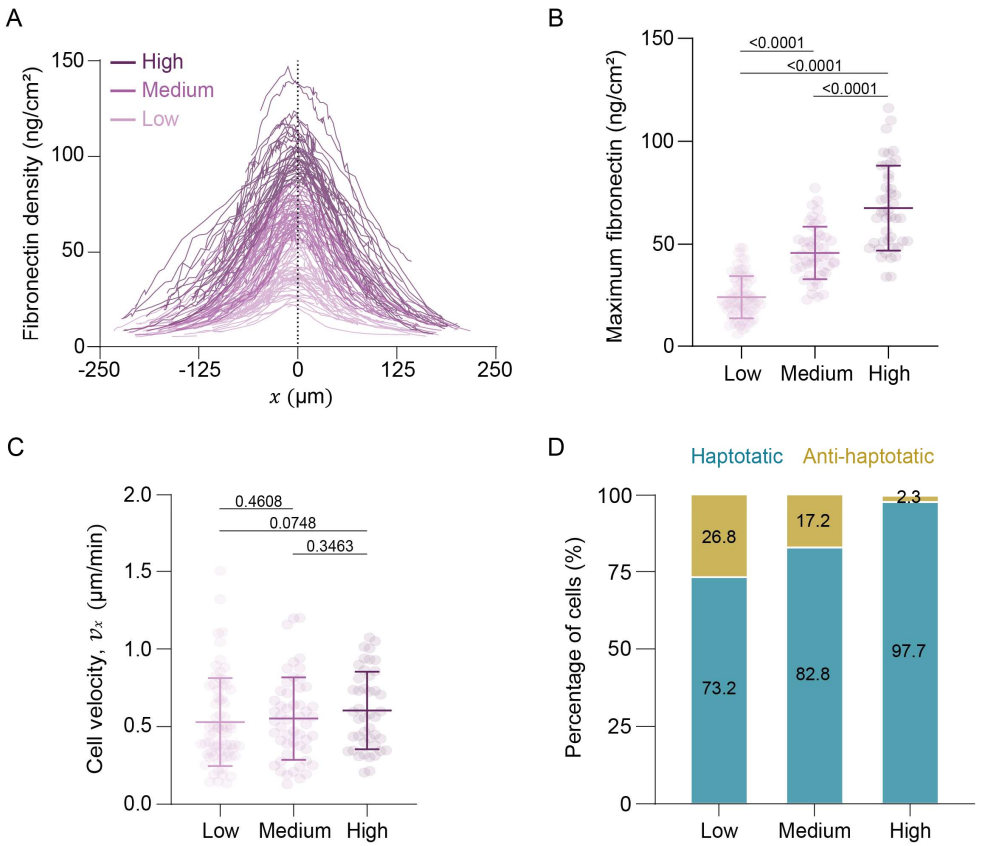

Figure 25 – Higher gradients enhance haptotactic response without affecting cell velocity. A: Fibronectin density profile for each cell migrating in gradient patterns with low (N = 71), medium (N = 48) and high (N = 44) gradients. B: Mean maximum fibronectin density for cells migrating in gradient patterns with low (N = 71), medium (N = 48) and high (N = 44) gradients. Error

bars are SD. P-values obtained using Mann-Whitney test. C: Mean velocity in x for cells migrating in gradient patterns with low (N = 71), medium (N = 48) and high (N = 44) gradients. Error bars are SD. P-values obtained using Mann-Whitney test. D: Haptotaxis probability for cells migrating in gradient patterns with low (N = 71), medium (N = 48) and high (N = 44) gradients. Data from four independent experiments.

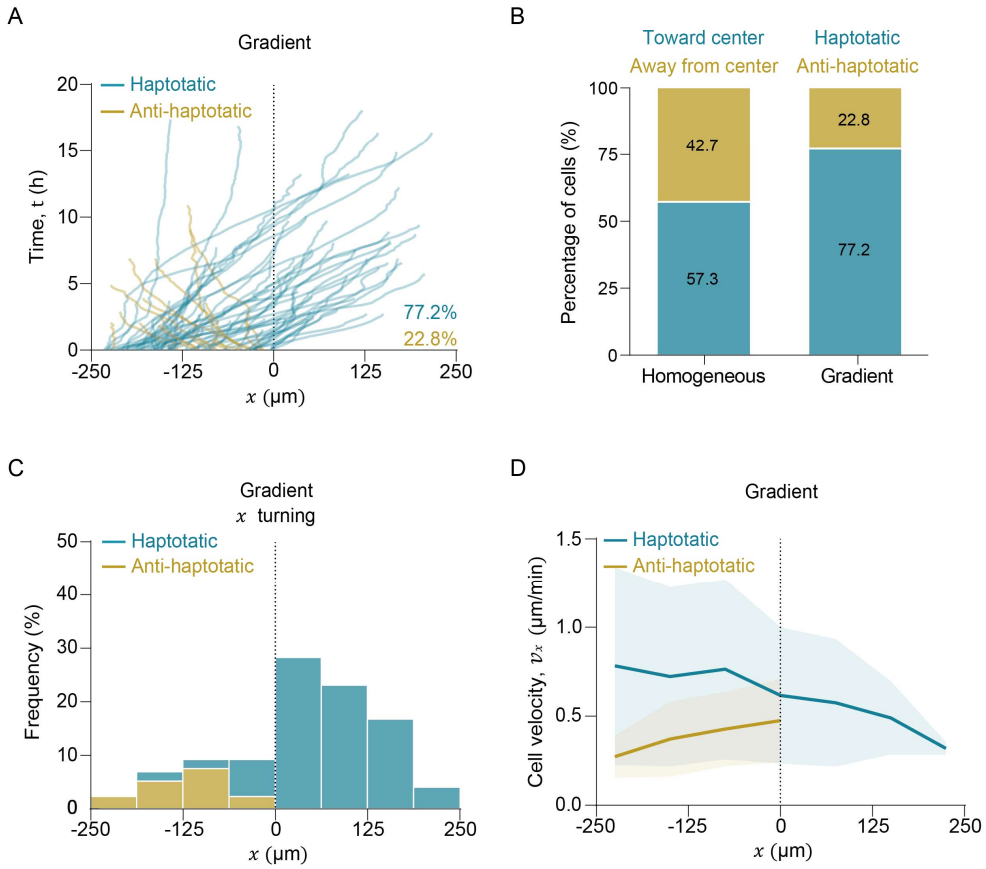

Figure 26 – Haptotatic response remains consistent on stiffer substrates. A: Individual tracks of cells migrating in gradient patterns on glass substrates. N = 61 for haptotatic cells and N = 18 for anti-haptotatic cells. B: Haptotaxis probability for cells migrating in gradient patterns on glass substrates (N = 79)

and probability of cells moving toward center or away from center in homogeneous patterns on glass substrates (N = 82). C: Turning x position of cells migrating in gradient patterns on glass substrates. N = 61 for haptotatic cells and N = 18 for anti-haptotatic cells. D: Mean velocity in x for cells migrating in gradient patterns. N = 39 for haptotatic cells and N = 18 for anti-haptotatic cells. Error bars are SD. Data from one independent experiment.

As cells were seeded on soft substrates, we wondered if haptotaxis would be influenced by substrate stiffness. To test this, we seeded cells on gradients patterned on glass substrates with approximately 60-70 GPa (Figure 26) (Wereszczak & Anderson, 2014). Our preliminary data suggests that haptotaxis efficiency is not affected by substrate stiffness, as cells exhibited similar haptotaxis probabilities on both soft and stiff substrates (Figure 26A; Figure 26B).

We next asked whether haptotaxis depends on cell contractility and lamellipodia spreading as other modes of directed migration such as durotaxis (Yeoman et al., 2021; Ramirez-San Juan et al., 2017; DuChez, 2017). To test this, we decreased cell contractility by inhibiting myosin and ROCK using blebbistatin and Y-27632, respectively. Blebbistatin specifically targets myosin by inhibiting its ATPase activity, which disrupts its interaction with actin (Straight et al., 2003). On the other hand, Y-27632 binds to the ATP-binding site of ROCK, inhibiting its kinase activity (Uehata et al., 1997). This reduces the phosphorylation of MLC, thereby decreasing myosin activity. To reduce lamellipodia spreading, we inhibited PI3K using LY294002. This inhibitor specifically blocks PI3K kinase activity, leading to reduced production of PI(3,4,5)P3 at the

leading edge (Vlahos et al., 1994). DMSO-treated cells served as experimental controls to ensure observed effects were due to the inhibitors.

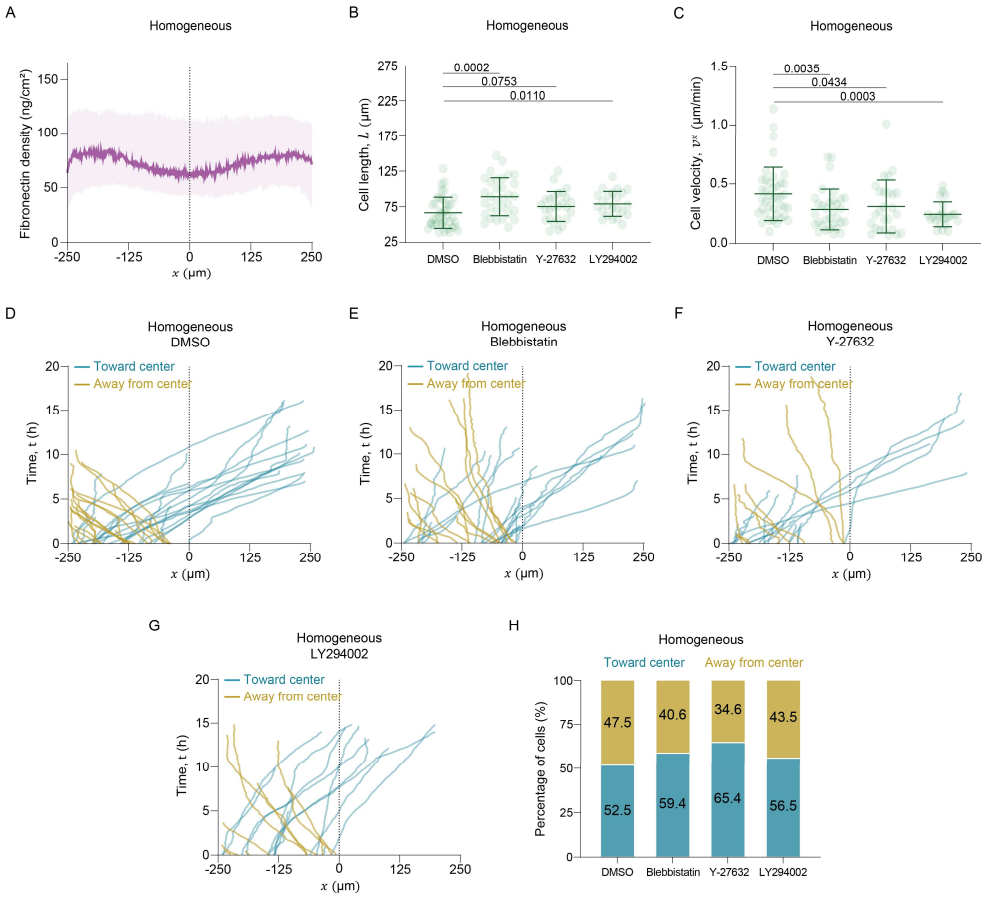

Figure 27 – Inhibition of cell contractility and lamellipodia spreading impacts cell motility. A: Median fibronectin density of all homogeneous patterns incubated with drugs. Error bars are 25 and 75 percentiles. N = 121. B: Mean cell length of cells migrating in homogeneous patterns when incubated DMSO (N = 40), blebbistatin (N = 32), Y-27632 (N = 26) and LY294002 (N = 23). Error bars are SD. P-values obtained using Mann-Whitney test. C: Mean velocity

in x of cells migrating in homogeneous patterns when incubated DMSO (N = 40), blebbistatin (N = 32), Y-27632 (N = 26) and LY294002 (N = 23). Error bars are SD. P-values obtained using Mann-Whitney test. D: Individual tracks of cells migrating in homogeneous patterns when incubated with DMSO. N = 21 for cells migrating toward center and N = 19 for cells migrating away from center. E: Individual tracks of cells migrating in homogeneous patterns when incubated with blebbistatin. N = 19 for cells migrating toward center and N = 13 for cells migrating away from center. F: Individual tracks of cells migrating in homogeneous patterns when incubated with Y-27632. N = 17 for cells migrating toward center and N = 9 for cells migrating away from center. G: Individual tracks of cells migrating in homogeneous patterns when incubated with LY294002. N = 13 for cells migrating toward center and N = 10 for cells migrating away from center. H: Probability of cells moving toward center or away from center in homogeneous patterns. N = 40 for cells incubated with DMSO, N = 32 for cells incubated with blebbistatin, N = 26 for cells incubated with Y-27632 and N = 23 for cells incubated with LY294002. DMSO data from five independent experiments. Blebbistatin and Y-27632 data from three independent experiments. LY294002 data from one independent experiment.

Cells incubated with these inhibitors exhibited reduced cell length and velocity in both homogeneous (Figure 27A-C) and gradient patterns (Figure 28A-C). Cells on the homogeneous patterns displayed random directionality (Figure 27D-H). Surprisingly, cells in gradient patterns moved toward areas of higher fibronectin density, similarly to DMSO-treated control cells (Figure 28D-H). This suggests that individual MCF10A cells can efficiently follow fibronectin gradients independently of contractility and lamellipodia spreading.

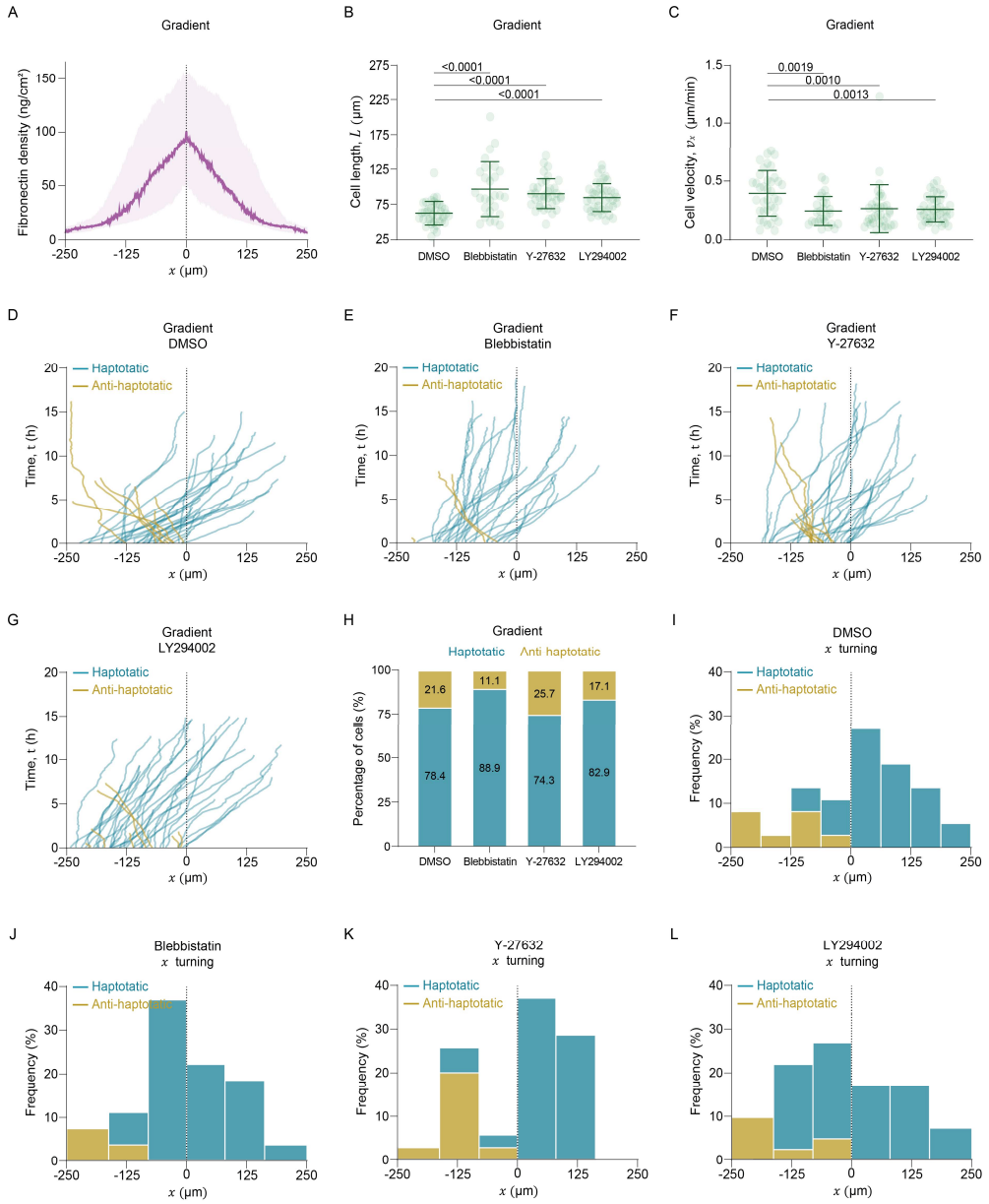

Figure 28 – Haptotaxis is unaffected by contractility and lamellipodia spreading. A: Median fibronectin density of all gradient patterns incubated with drugs. Error bars are 25 and 75 percentiles. N = 140. B: Mean cell length of cells migrating in gradient patterns when incubated DMSO (N = 37), blebbistatin (N = 27), Y-27632 (N = 35) and LY294002 (N = 41). Error bars are SD. P-values obtained using Mann-Whitney test. C: Mean velocity in x of cells migrating in

gradient patterns when incubated DMSO (N = 37), blebbistatin (N = 27), Y-27632 (N = 35) and LY294002 (N = 41). Error bars are SD. P-values obtained using Mann-Whitney test. D: Individual tracks of cells migrating in gradient patterns when incubated with DMSO. N = 29 for haptotatic cells and N = 8 for anti-haptotatic cells. E: Individual tracks of cells migrating in gradient patterns when incubated with blebbistatin. N = 24 for haptotatic cells and N = 3 for anti-haptotatic cells. F: Individual tracks of cells migrating in gradient patterns when incubated with Y-27632. N = 26 for haptotatic cells and N = 9 for anti-haptotatic cells. G: Individual tracks of cells migrating in gradient patterns when incubated with LY294002. N = 34 for haptotatic cells and N = 7 for anti-haptotatic cells. H: Haptotaxis probability for cells migrating in gradient patterns. N = 37 for cells incubated with DMSO, N = 27 for cells incubated with blebbistatin, N = 35 for cells incubated with Y-27632 and N = 41 for cells incubated with LY294002. I: Turning x position of cells migrating in gradient patterns when incubated with DMSO. N = 29 for haptotatic cells and N = 8 for anti-haptotatic cells. J: Turning x position of cells migrating in gradient patterns when incubated with blebbistatin. N = 24 for haptotatic cells and N = 3 for anti-haptotatic cells. K: Turning x position of cells migrating in gradient patterns when incubated with Y-27632. N = 26 for haptotatic cells and N = 9 for anti-haptotatic cells. L: Turning x position of cells migrating in gradient patterns when incubated with LY294002. N = 34 for haptotatic cells and N = 7 for anti-haptotatic cells. DMSO data from five independent experiments. Blebbistatin and Y-27632 data from three independent experiments. LY294002 data from one independent experiment.

4. Haptotatic cells can migrate against fibronectin gradients once polarity is established

After the initial migration and polarization toward high fibronectin, around 70% of haptotactic cells crossed the fibronectin peak and continued migrating persistently against the gradient (Figure 24G). This indicated that MCF10A cells could migrate from high to low fibronectin densities when there was a preexisting front-rear polarity. Therefore, we categorized the trajectories of haptotactic cells into two phases: 1) up the gradient – initial migration toward higher fibronectin until reaching the peak; and 2) down the gradient – movement after crossing the peak until the cell turn. We then focused on these two migration phases.

We measured cell length and velocity during migration. Cell length increased as cells migrated up the gradient, peaking at the highest fibronectin density, and decreased as cells migrated down the gradient (Figure 24H). Moreover, haptotactic cells accelerated after adhering to the gradient and maintained this increased velocity as they migrated up the gradient. Upon reaching the peak fibronectin density, their velocity immediately decreased and then remained constant at slower velocities compared to their migration up the gradient. Nevertheless, even though their velocity decreased, cells migrating down the gradient maintained an average speed of around 0.5 μm/min (Figure 24I). Anti-haptotactic cells showed a similar length profile but had lower velocities compared to haptotactic cells (Figure 24H-I). This highlights the lower efficiency of initially polarizing and migrating against the gradient.

Although stiffer substrates did not affect haptotaxis, we explored their impact on cell migration down the gradient. We analyzed the x turning positions and velocity profiles of haptotactic cells (Figure 26C-D). Similar to soft substrates, most haptotactic cells migrated against the gradient after crossing the peak (Figure 26C). The velocity profile also followed a similar pattern, increasing until the peak and then decreasing afterward, averaging around 0.5 μm/min (Figure 26D).

We also investigated whether contractility and lamellipodia spreading affect cells' ability to migrate down the gradient. To explore this, we analyzed x turning positions for cells treated with the previously described drug inhibitors (Figure 28I-L). DMSO-treated control cells and ROCK-inhibited cells showed similar crossing probabilities (64.86% and 65.71%, respectively) (Figure 28I-J). In contrast, cells with myosin and PI3K inhibition had lower crossing probabilities (44.44% and 41.46%, respectively) (Figure 28K-L). This suggests that myosin and PI3K may facilitate migration down the gradient. However, because these cells move more slowly, they might not have enough time to reach the fibronectin peak and cross it within the imaging time frame. Thus, it is challenging to attribute the decrease in crossing probability specifically to the inhibition of these proteins.

In summary, our data show that once polarity is established, MCF10A cells can migrate long distances down the gradient with slightly decreased cell length and velocity. Moreover, cells lacking myosin and PI3K showed more impaired migration down the gradient compared to those with ROCK inhibition.

4.1 Increased actin dynamics acts as an adaptation mechanism to migrate down the gradient

Cells migrating in fibronectin gradients experience different fibronectin densities at their leading and trailing edges. We hypothesized that this difference could influence the velocities of the leading and trailing edges during migration. To test this, we measured the difference in velocities between the leading and trailing edges during migration up and down the gradient ($v_{down} - v_{up}$) (Figure 29A-B). Values near zero indicate no change in edge velocity, while positive values indicate an increase and negative values a decrease in velocity down the gradient. Our analysis revealed that the trailing edge's velocity remained consistent regardless of the gradient direction (Figure 29B). In contrast, the leading edge was significantly slower when migrating down the gradient (Figure 29B). This explains the observed decrease in cell length and velocity during migration down the gradient.

Since actin contractility occurs at the trailing edge and actin polymerization at the leading edge, we asked whether actin dynamics could explain how cells sustain directed movement and velocity (Bear & Haugh, 2014; Hall, 2005; Zegers & Friedl, 2014; Chang et al., 2008; Choraghe et al., 2020; Chrzanowska-Wodnicka & Burridge, 1996). To investigate actin dynamics at the edges, we used MCF10A cells expressing LifeAct-GFP (Figure 29C). At the trailing edge, we measured actin retrograde flow (v_r) and the number of actin filaments (Figure 29D; Figure 29H). At the leading edge, we measured v_r, edge velocity (v_e), actin polymerization velocity (v_p), and the rate of protrusions (Figure 29D).

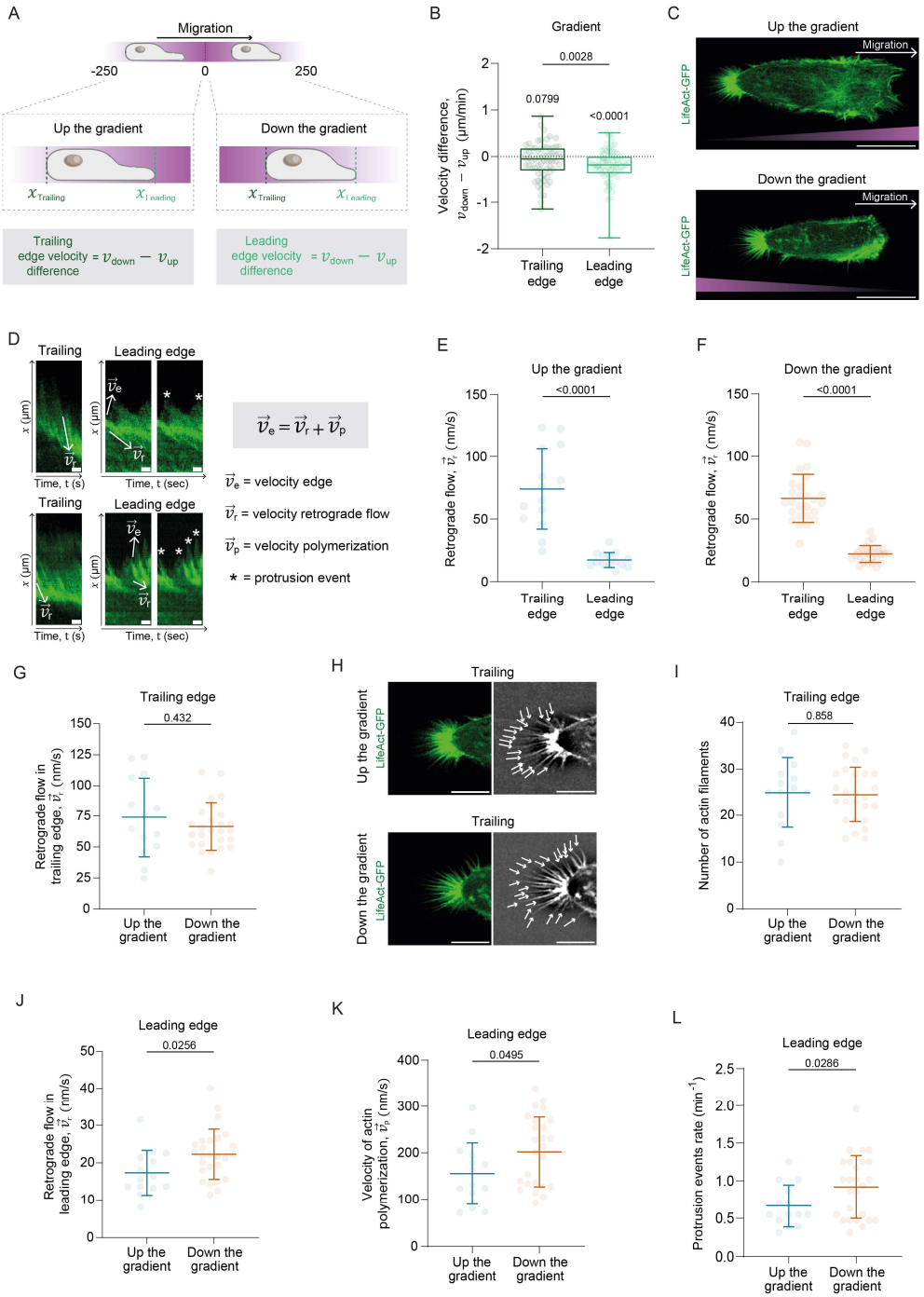

Figure 29 – Migration down the gradient is attributed to increased actin dynamics. A: Scheme illustrating how difference in edge velocities is quantified. B: Edge velocity differences of haptotatic cells migrating up and down the

gradient (N = 70). Error bars are SD. P-values obtained with Wilcoxon test (test if values are different from 0) for each condition and Wilcoxon matched-pairs signed test when comparing conditions. C: Representative fluorescence images of MCF10A-LifeAct-GFP cells migrating up and down the gradient. Scale bar is 20 μm. D: Representative kymographs of trailing and leading edges with the different actin flow vectors and protrusion events. Scale bar is 1 μm. E: Mean retrograde flow in the trailing and leading edges of cells migrating up the gradient (N = 14). Error bars are SD. P-values obtained using Mann-Whitney test. F: Mean retrograde flow in the trailing and leading edges of cells migrating down the gradient (N = 26). Error bars are SD. P-values obtained using Mann-Whitney test. G: Mean retrograde flow in the trailing edge of cells migrating up and down the gradient. N = 14 for cells migrating up the gradient and N = 26 for cells migrating down the gradient. Error bars are SD. P-values obtained using permutation test. H: In the left, representative fluorescence images of actin filaments in the trailing edge of cells migrating up and down the gradient. In the right, actin filaments images after using bandpass filter and unsharp mask to count the number of actin filaments (indicated by the white arrows). Scale bar is 10 μm. I: Mean number of actin filaments in the trailing edge of cells migrating up and down the gradient. N = 14 for cells migrating up the gradient and N = 26 for cells migrating down the gradient. Error bars are SD. P-values obtained using permutation test. J: Mean retrograde flow in the leading edge of cells migrating up and down the gradient. N = 14 for cells migrating up the gradient and N = 26 for cells migrating down the gradient. Error bars are SD. P-values obtained using permutation test. K: Mean velocity of actin polymerization in the leading edge of cells migrating up and down the gradient. N = 14 for cells migrating up the gradient and N = 26 for cells migrating down the gradient. Error bars are SD. P-values obtained using permutation test. L: Mean protrusion events rate in the leading edge of cells migrating up and down the gradient. N = 14 for cells migrating up the gradient and N = 26 for cells migrating down the gradient.

Error bars are SD. P-values obtained using permutation test. Panel B from four independent experiments. Panels C-L from five independent experiments.

We observed actin retrograde flow at both cell edges and used this to analyze asymmetry in actin flows. Our analysis showed that retrograde flows were significantly faster at the trailing edge compared to the leading edge when cells migrated up the gradient (Figure 29E). Interestingly, cells migrating down the gradient also showed asymmetry in actin retrograde flows, though it was slightly less pronounced (Figure 29F). Thus, actin flow asymmetry between leading and trailing edges occurs in cells migrating up and down the gradient.

To investigate this further, we compared actin dynamics at the trailing and leading edges in different cells migrating up and down the gradient. At the trailing edge, we observed similar retrograde flow and number of filaments during both migration phases (Figure 29G; Figure 29I). This suggests that the trailing edge is unaffected by changes in fibronectin density once polarity is established. In contrast, the leading edge showed significant differences. Cells migrating down the gradient had faster actin retrograde flow (Figure 29J). This increased retrograde flow challenges the cells' ability to maintain persistence and high velocity against the gradient. To counteract this, we hypothesize that cells migrating down the gradient would increase actin polymerization. Since edge velocity is the sum of retrograde flow and actin polymerization, we calculated the polymerization velocity to test our hypothesis. Cells migrating down the gradient exhibited a faster polymerization rate (Figure 29K). Additionally, these cells showed more frequent and faster

membrane protrusions (Figure 29L). This indicates enhanced actin dynamics at the leading edge in cells migrating down the gradient, characterized by increased membrane retractions and protrusions.

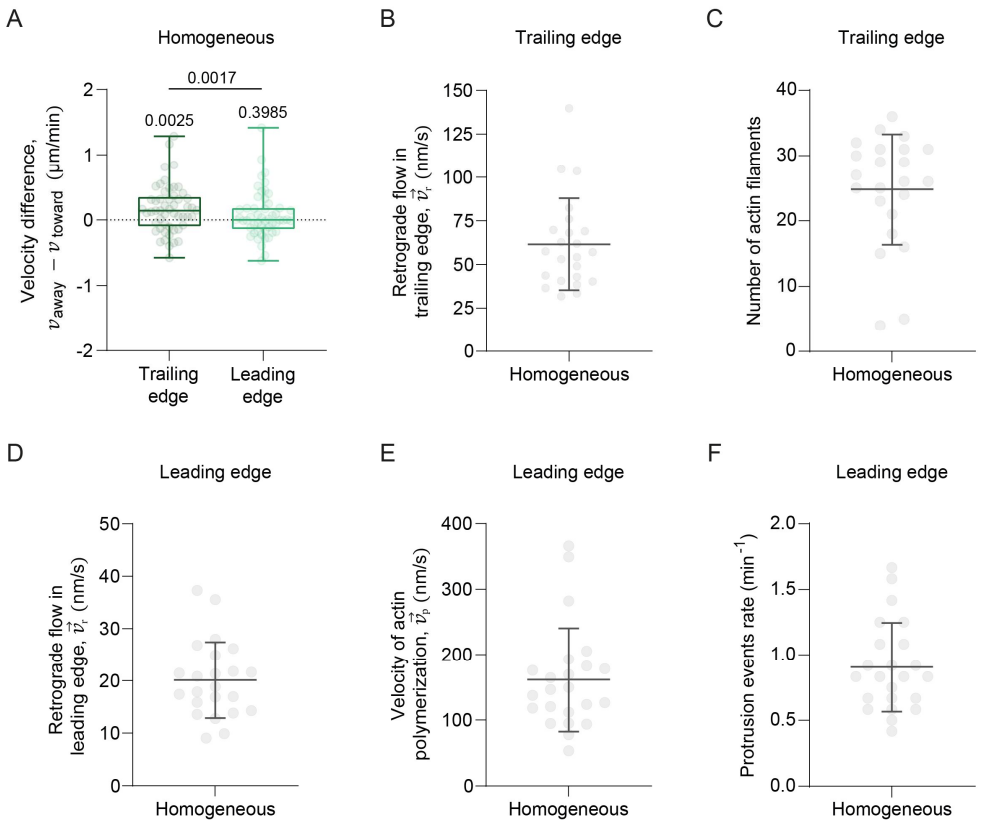

Figure 30 – Trailing edge velocity increases as cells cross the center of homogeneous patterns. A: Edge velocity differences of cells migrating toward or away from center in homogeneous patterns (N = 53). Error bars are SD. P-values obtained with Wilcoxon test (test if values are different from 0) for each condition and Wilcoxon matched-pairs signed test when comparing conditions. B: Mean retrograde flow in the trailing edge of cells migrating in homogeneous patterns (N = 23). Error bars are SD. C: Mean number of actin filaments in the

trailing edge of cells migrating in homogeneous patterns (N = 23). Error bars are SD. D: Mean retrograde flow in the leading edge of cells migrating in homogeneous patterns (N = 23). Error bars are SD. E: Mean velocity of actin polymerization in the leading edge of cells migrating in homogeneous patterns (N = 23). Error bars are SD. F: Mean protrusion events rate in the leading edge of cells migrating in homogeneous patterns (N = 23). Error bars are SD. Panel A from four independent experiments. Panels B-F from five independent experiments.

In homogeneous patterns, where both edges are exposed to the same fibronectin density, the trailing edge increases its velocity after crossing the center of the pattern (Figure 30A). In contrast, the velocity of the leading edge remained unchanged (Figure 30A). This suggests that enhanced retraction at the trailing edge drives the cell movement in these patterns. Notably, the actin dynamics in homogeneous patterns were similar to those observed during cell migration up the gradient (Figure 30B-F). This indicates that both stochastic and gradient-driven migration processes involve similar actin dynamics.

We then investigated how cells' actin dynamics are affected by the same fibronectin density at the leading edge but with different gradient directions. Thus, we analyzed the key actin parameters measured previously and compared both migration phases (Figure 31). Surprisingly, the trailing edge remained unchanged, while the leading edge exhibited faster cycles of membrane retractions and extensions when cells migrate down the gradient, as shown previously (Figure 29G; Figure 29J; Figure 29K-L; Figure 31).

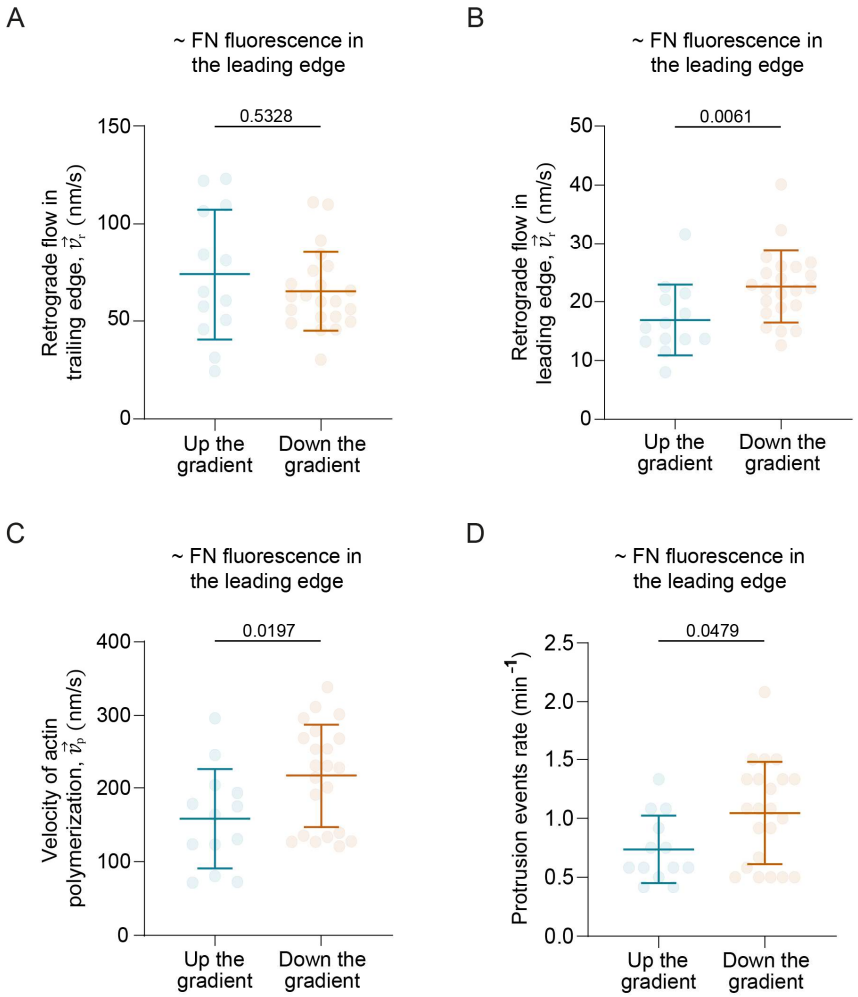

Figure 31 – Actin dynamics are influenced by gradient direction. A: Mean retrograde flow in the trailing edge of cells migrating up and down gradient patterns and exposed to similar fluorescence intensity in the leading edge. N = 13 for cells migrating up the gradient ($\langle F_{Leading} \rangle = 168.61 \pm 31.81$) and N = 22 for cells migrating down the gradient ($\langle F_{Leading} \rangle = 164.84 \pm 45.93$). Error bars are SD. P-values obtained using Mann-Whitney test. B: Mean retrograde flow in the leading edge of cells migrating up and down gradient patterns and exposed to similar fluorescence intensity in the leading edge. N = 13 for cells migrating up the gradient ($\langle F_{Leading} \rangle = 168.61 \pm 31.81$) and N = 22 for cells migrating down the

gradient ($\langle F_{Leading} \rangle = 164.84 \pm 45.93$). Error bars are SD. P-values obtained using Mann-Whitney test. C: Mean velocity of actin polymerization in the leading edge of cells migrating up and down gradient patterns and exposed to similar fluorescence intensity in the leading edge. N = 13 for cells migrating up the gradient ($\langle F_{Leading} \rangle = 168.61 \pm 31.81$) and N = 22 for cells migrating down the gradient ($\langle F_{Leading} \rangle = 164.84 \pm 45.93$). Error bars are SD. P-values obtained using Mann-Whitney test. D: Mean rate of protrusion events in the leading edge of cells migrating up and down gradient patterns and exposed to similar fluorescence intensity in the leading edge. N = 13 for cells migrating up the gradient ($\langle F_{Leading} \rangle = 168.61 \pm 31.81$) and N = 22 for cells migrating down the gradient ($\langle F_{Leading} \rangle = 164.84 \pm 45.93$). Error bars are SD. P-values obtained using Mann-Whitney test. Data from five independent experiments.

Overall, our data show that cells migrating up and down the gradient exhibit different actin retrograde flows between their edges. This reveals that actin retrograde flow is asymmetric in cells migrating along gradients in opposing directions. We also show that cells moving down the gradient had a slower leading edge. However, this edge was more dynamic, with faster membrane retractions and extensions, resulting in a higher frequency of protrusions. We believe these changes in actin dynamics during migration down the gradient help cells to maintain their polarity and persistence when moving against the gradient.

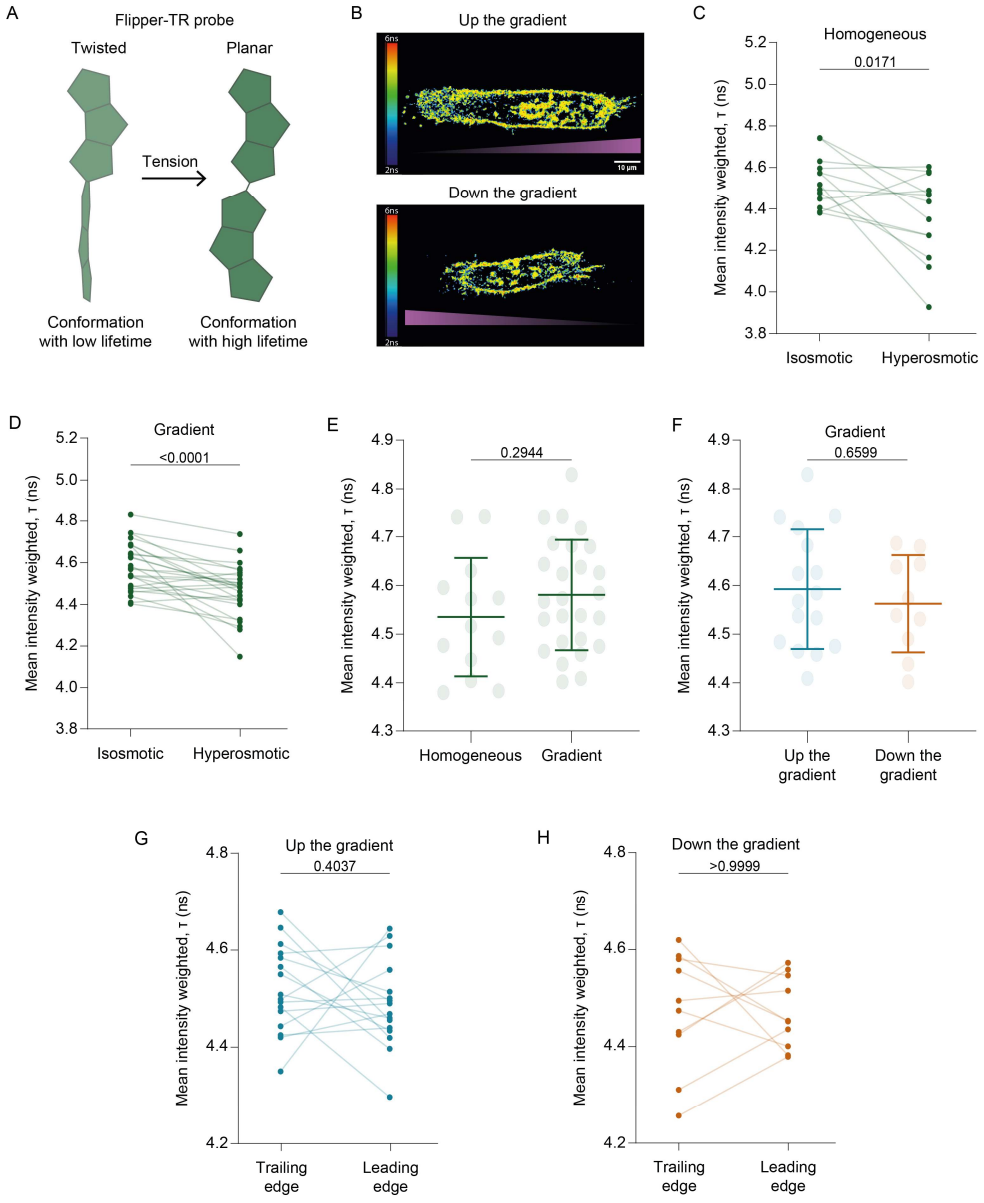

Figure 32 – Membrane tension remains unchanged regardless of fibronectin density. A: Illustration of Flipper-TR conformations. B: Representative lifetime images of cells incubated with Flipper-TR probe migrating up and down gradient patterns. C: Flipper's tau intensities of cells migrating in homogeneous patterns with isosmotic media and hyperosmotic

media (N = 13). P-value obtained using Wilcoxon matched-pairs signed rank test. D: Flipper's tau intensities of cells migrating in gradient patterns with isosmotic media and hyperosmotic media (N = 26). P-value obtained using Wilcoxon matched-pairs signed rank test. E: Flipper's mean tau intensity of cells migrating in homogeneous (N = 13) and gradient (N = 26) patterns. Error bars are SD. P-value obtained using Mann-Whitney test. F: Flipper's mean tau intensity of cells migrating up (N = 16) and down (N = 10) the gradient patterns. Error bars are SD. P-value obtained using Mann-Whitney test. G: Flipper's tau intensities of trailing and leading edges of cells migrating up the gradient pattern (N = 16). P-value obtained using Wilcoxon matched-pairs signed rank test. H: Flipper's tau intensities of trailing and leading edges of cells migrating down the gradient pattern (N = 10). P-value obtained using Wilcoxon matched-pairs signed test. Data from two independent experiments. (Panel A inspired from: Roffay et la., 2022)

4.2 Assessing membrane tension during migration up and down the gradient

Actin polymerization can increase membrane tension (Sitarska and Diz-Muñoz, 2020). Thus, we hypothesized that higher actin dynamics might be linked to increased membrane tension. To test this, we used the Flipper-TR membrane tension sensor (Figure 32A-B). We first validated the sensor's functionality by inducing a hyperosmotic shock in cells migrating on both homogeneous and gradient patterns. As expected, this treatment decreased membrane tension (Figure 32C-D) (Assies et al., 2021). We then compared membrane tension between cells migrating in homogeneous and gradient patterns, and between the two migration phases (Figure 32E-F). Surprisingly, in our preliminary experiments, we

found no significant differences in membrane tension in any of these comparisons, nor between cell edges (Figure 32G-H). These results indicate that increased actin dynamics do not affect plasma membrane tension in our system.

4.3 Traction asymmetry is conserved in cells migrating up and down the gradient

To characterize the mechanics of cell migration in our haptotatic system, we measured the traction forces exerted by cells on both homogeneous and gradient substrates. We found that traction magnitude increased during the first hours of migration on both types of patterns, indicating a transient adaptation to the substrate after adhesion (Figure 33A). To isolate the effect of the fibronectin gradient on traction forces, we normalized the traction forces on gradient patterns by dividing them by the average traction forces on homogeneous substrates. The resulting normalized tractions mirrored the fibronectin density profile, increasing with density, peaking at the center, and decreasing down the gradient (Figure 34A-B). Cells on homogeneous patterns showed constant traction magnitude, likely due to the uniform fibronectin density (Figure 33B-C).

Furthermore, we observed that traction forces were mainly distributed at the leading and trailing edges, forming contractile force dipoles (Figure 33B; Figure 34A). To explore this further, we analyzed the traction profiles along the polarity axis for cells migrating up and down the gradient, as well as on homogeneous fibronectin. All profiles revealed an asymmetric intracellular traction distribution, with high traction

peaks at the leading edge and lower, more dispersed tractions at the trailing edge (Figure 33D; Figure 34C). This asymmetry was more pronounced in cells migrating up the gradient and on homogeneous patterns, suggesting stronger mechanical asymmetry under these conditions.

To quantify traction asymmetry relative to the patterns, we computed the normalized traction quadrupole, Q (Figure 34D; see methods). Negative Q values indicate traction asymmetry toward fibronectin density (polarized), while positive values indicate asymmetry against the gradient. A Q value of zero indicates symmetric tractions (unpolarized). Cells migrating up the gradient had negative Q values, showing increased polarity as they approached the fibronectin peak (Figure 34E). Surprisingly, cells migrating down the gradient also showed asymmetry, although less pronounced, confirming a lower degree of mechanical asymmetry (Figure 34E). Cells on homogeneous patterns exhibited consistent Q values, indicating strong polarity during migration (Figure 33E).

We also found a linear correlation between traction asymmetry and cell velocity in cells migrating on gradient substrates (Figure 34F). Most cells migrating up or down the gradient displayed positive velocity and negative Q values, clustering in one quadrant of the $Q - v$ diagram. In contrast, anti-haptotactic cells showed negative velocity and positive Q values, occupying the opposite quadrant.

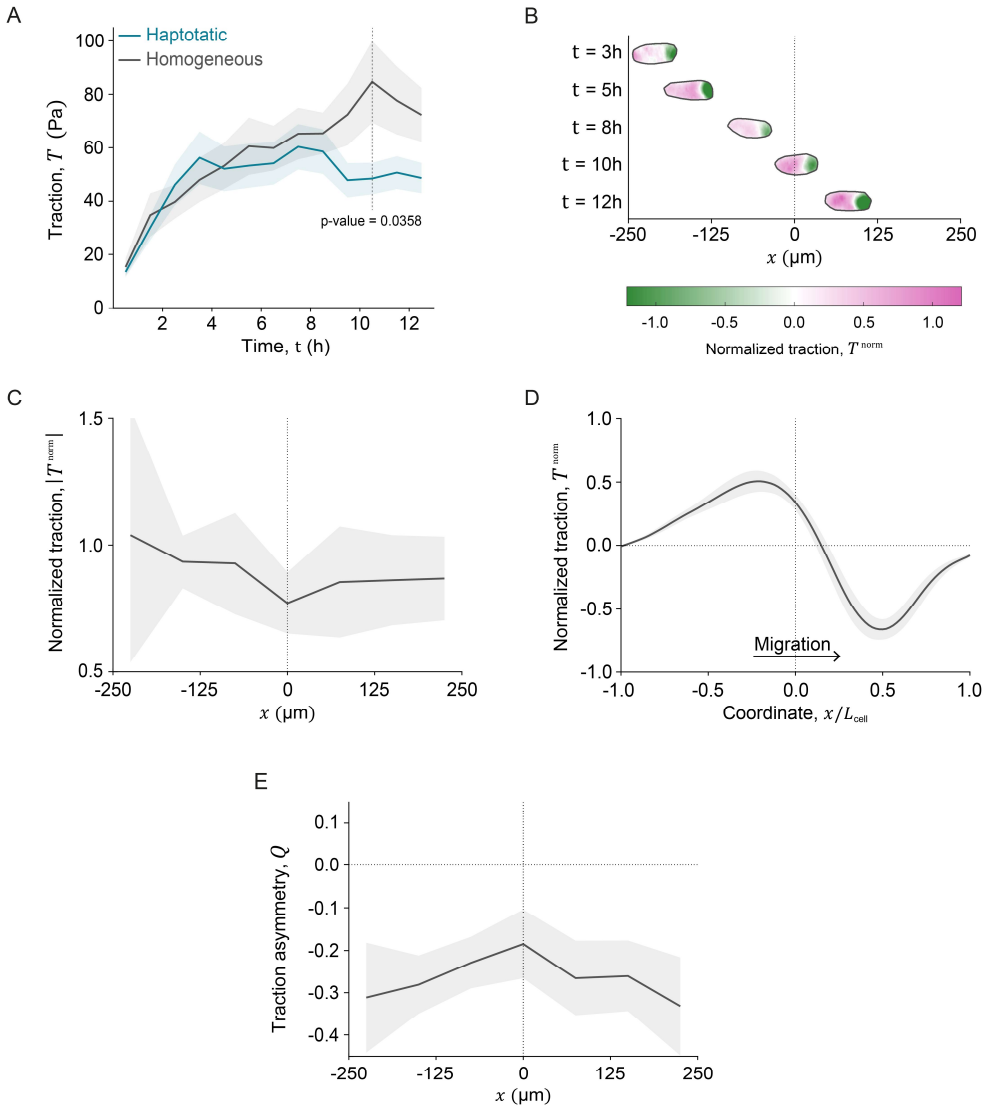

Figure 33 – Traction forces increase over time, while traction asymmetry remains constant in cells migrating in homogeneous patterns. A: Mean normalized traction magnitude for cells migrating in homogeneous patterns (N=11) and haptotatic cells migrating in gradient patterns (N=23). Error bars are SEM. P-value obtained with Wilcoxon rank sum test. B: Representative mean normalized traction images of a cell (grey line) migrating in homogeneous patterns. C: Mean normalized traction magnitude for cells migrating in homogeneous patterns (N=11). Error bars are SEM. D: Mean profiles of x

component of the normalized traction forces for cells migrating in homogeneous patterns (N=11). Error bars are SEM. E: Mean normalized traction asymmetry in cells migrating in homogeneous patterns (N=11). Error bars are SEM. Data from three independent experiments.

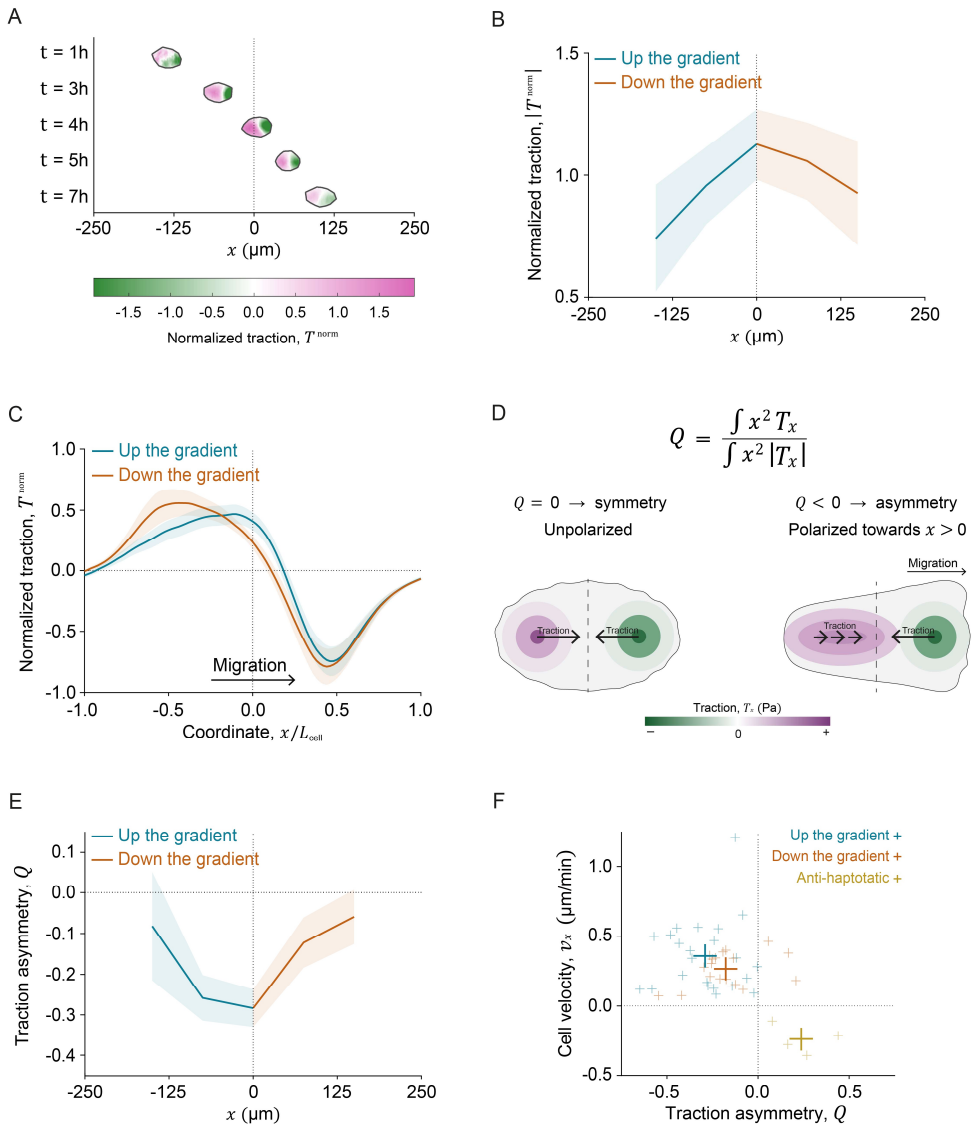

Figure 34 – Traction asymmetry is maintained during both migrations up

and down the gradient, though with lower magnitude. A: Representative mean normalized traction images of a cell (grey line) migrating in gradient patterns. B: Mean normalized traction magnitude for cells migrating up (N=23) and down (N=18) the gradient patterns. Error bars are SEM. C: Mean profiles of x component of the normalized traction forces for cells migrating up (N=23) and down (N=18) the gradient patterns. Error bars are SEM. D: Illustration of mechanical asymmetry through second moment of tractions forces (Q_X). E: Mean normalized traction asymmetry in cells migrating up (N=23) and down (N=18) the gradient patterns. Error bars are SEM. F: Scatter plot of average velocity and normalized traction asymmetry of cells migrating in homogeneous patterns (N=13), up the gradient (N=23), down the gradient (N=18) and anti-haptotatic (N=4). Data from three independent experiments.

In summary, our results reveal traction force asymmetries between the leading and trailing edges of cells during haptotatic migration, with more pronounced asymmetry in cells moving up the gradient. However, cells migrating down the gradient also displayed traction asymmetry, suggesting that cells dynamically adjust their traction distribution to adapt to changes in gradient direction.

5. Confinement influences integration of gradient sensing and persistent polarity dynamics

A key feature of our experimental system is that cells are constrained to migrate along the x-axis while being confined vertically along the y-axis. This setup implies that cells can only change their migration

direction by flipping their front-rear polarity by 180º. So, we wondered how the migration dynamics change as the width of the fibronectin gradient is altered. To test this, we created fibronectin gradients with widths of 20 μm (confined, 1D), 40 μm, 60 μm, 80 μm, and 250 μm (unconfined, 2D) (Figure 35A).

We found that cells consistently followed the fibronectin gradients regardless of confinement (Figure 36). However, once reached the fibronectin peak, cells showed different migratory behaviors. On confined gradients, cells oscillated between both pattern edges and could migrate both up and down the gradient, as previously observed (Figure 36A). At 40 μm, cells were unable to fully repolarize vertically and continued to migrate down the gradient similar to the confined gradients (Figure 36A). In contrast, cells exposed to 60 μm and 80 μm gradients could repolarize vertically, but their migration in the y-direction was restricted as they quickly reached the pattern limits. This led to the emergence of circular trajectories (Figure 36A). On unconfined gradients, most cells repolarized vertically and continued to migrate along the y-axis where the fibronectin density was highest (Figure 36A). This suggests that once cells repolarize in the y-axis, they lose the ability to migrate down the gradient. To characterize these differences, we calculated the standard deviation in x and y, as well as x and y probability histograms (Figure 36B-E). These analyses confirmed that unconfined gradients led to smaller trajectories in the x-axis and larger trajectories in the y-axis, while confined gradients showed the opposite trend.

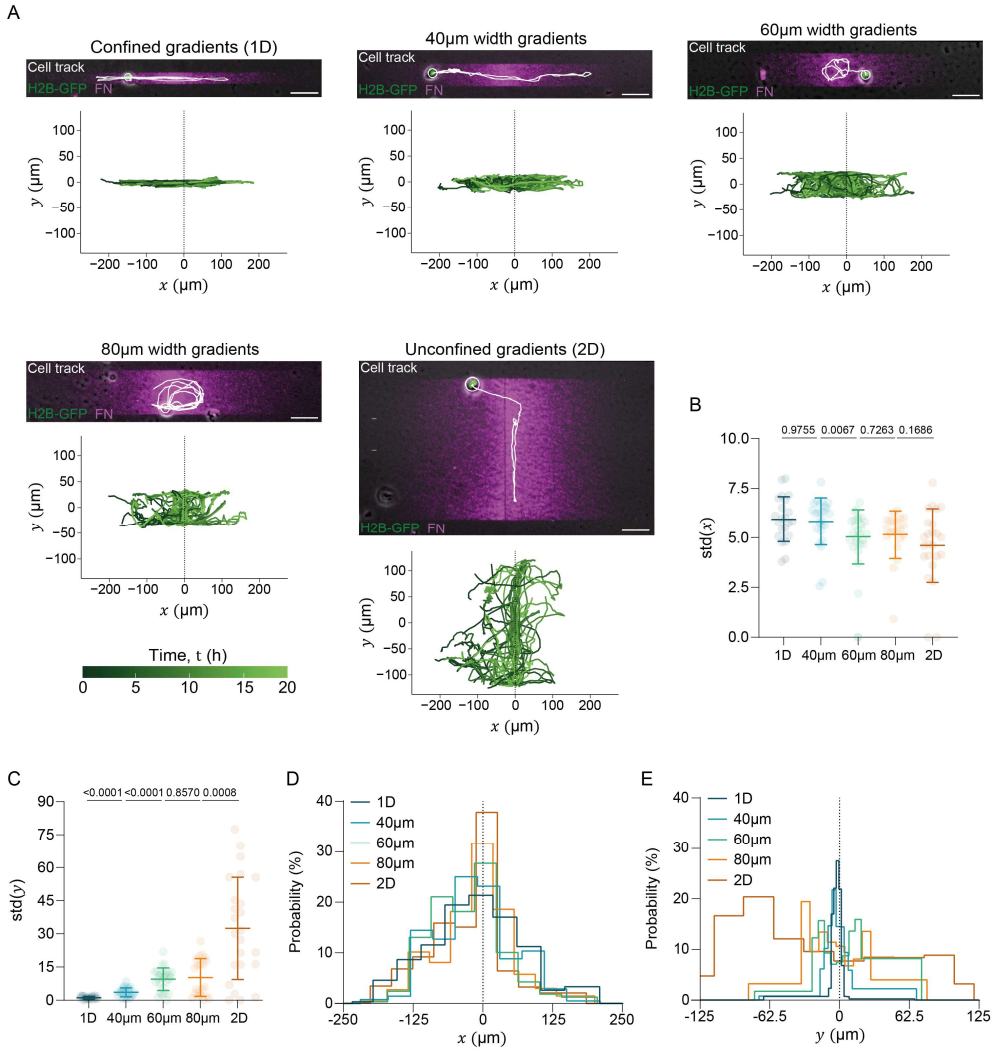

Figure 35 – Migration down the gradient occurs exclusively in confined gradients. A: x and y components of individual cell tracks in gradient patterns with 20 μm width (N = 27), 40 μm width (N = 27), 60 μm width (N = 30), 80 μm width (N = 22) and 250 μm width (N = 25). Scale bar is 50 μm. B: Standard deviation of cells' x positions in gradient patterns with 20 μm width (N = 27), 40 μm width (N = 27), 60 μm width (N = 30), 80 μm width (N = 22) and 250 μm width (N = 25). Error bars are SD. P-values obtained using Mann-Whitney test. C: Standard deviation of cells' y positions in gradient patterns with 20 μm width (N = 27), 40 μm width (N = 27), 60 μm width (N = 30), 80 μm width (N = 22) and

250 μm width (N = 25). Error bars are SD. P-values obtained using Mann-Whitney test. D: Probability of cells' x positions in gradient patterns with 20 μm width (N = 27), 40 μm width (N = 27), 60 μm width (N = 30), 80 μm width (N = 22) and 250 μm width (N = 25). E: Probability of cells' y positions in gradient patterns with 20 μm width (N = 27), 40 μm width (N = 27), 60 μm width (N = 30), 80 μm width (N = 22) and 250 μm width (N = 25). Data from one independent experiment.

Overall, these results indicate that the ability of cells to follow fibronectin gradients is independent of confinement. Remarkably, we found that the integration between gradient sensing and persistent polarity dynamics can lead to unexpected trajectories. In confined gradients, cells fail to repolarize and adapt to migrate against the fibronectin gradient. By contrast, in unconfined gradients, cells can repolarize vertically and keep their movement on higher fibronectin regions. For intermediate confinements, complex trajectories such as circles emerged. These findings reveal how confinement modulates the ability of cells to sense and respond to fibronectin gradients.

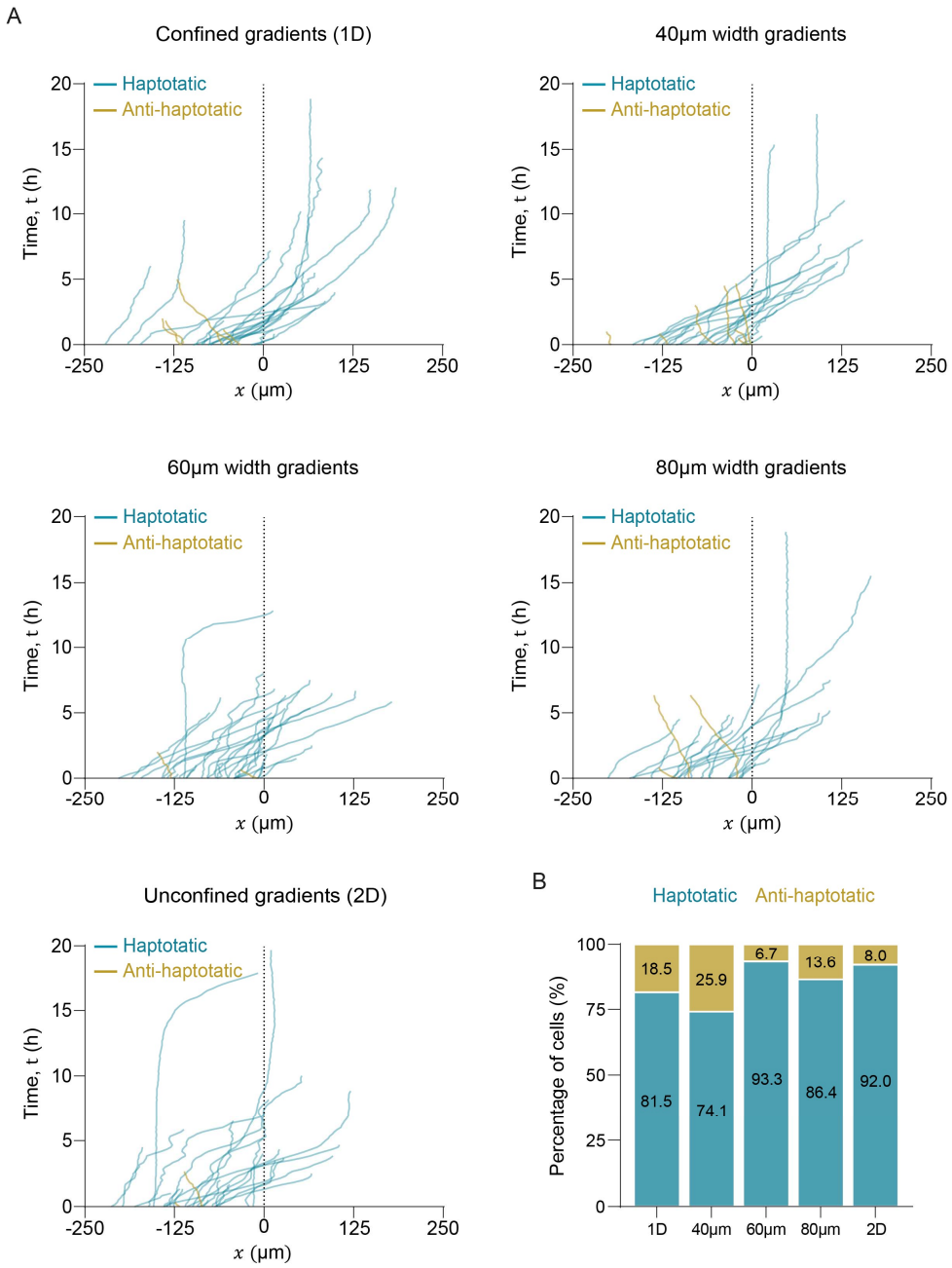

Figure 36 – Haptotaxis efficiency is independent of geometric confinement. A: Individual tracks of cells migrating in gradient patterns with 20 µm width (N = 27), 40 µm width (N = 27), 60 µm width (N = 30), 80 µm width (N = 22) and 250 µm width (N = 25). B: Haptotaxis probability of cells migrating in gradient

patterns. N = 27 for cells in gradient patterns with 20 μm width, N = 27 for cells in gradient patterns with 40 μm width, N = 30 for cells in gradient patterns with 60 μm width, N = 22 for cells in gradient patterns with 80 μm width and N = 25 for cells in gradient patterns with 250 μm width. Data from one independent experiment.

Chapter 5 – Discussion

Cells are commonly believed to migrate toward areas of highest protein density in response to ECM gradients – a process known as haptotaxis (Dertinger et al., 2002; Wen et al., 2015; Moreno-Arotzena et al., 2015; Autenrieth et al., 2016; King et al., 2016). Our study challenges this idea by demonstrating that haptotatic migration changes with confinement. In our experiments, epithelial cells exhibited robust haptotaxis on symmetric fibronectin gradients, initially polarizing and moving toward areas of highest fibronectin density, regardless of cell contractility and lamellipodia spreading. Surprisingly, in confined gradients, most haptotactic cells continued migrating against the gradient upon reaching the peak of fibronectin. This migration against the gradient resulted from increased actin dynamics and a weaker but sustained traction force asymmetry when compared to migration toward the gradient. We further explored this novel migration behavior by tuning the gradient width to create different levels of confinement. We found that cells followed complex trajectories, including circular movements at intermediate widths. In unconfined gradients, cells smoothly repolarized and continued migrating vertically along the fibronectin peak, losing their ability to migrate against the gradient.

Although haptotaxis has a clear relevance in both physiology and disease, the molecular and mechanical mechanisms of haptotaxis remain unclear. This is partly due to the difficulty in developing *in vitro* systems with well-controlled protein gradients (Weber et al., 2013; Oudin et al.,

2016; Ricoult et al., 2015). With the goal of filling this gap, we developed a 1D system that allows precise control and quantification of fibronectin density in homogeneous and gradient patterns. We used PRIMO technology to develop our patterns due to its prior success in creating gradients (Luo et al., 2020; Versaevel et al., 2021). Notably, this work is the first to fabricate symmetric fibronectin gradients for studying single epithelial cell migration. PRIMO technology offers several advantages: 1) flexible pattern design, allowing for easy adjustments, such as changing levels of confinement; 2) high resolution, achieving patterns as fine as 1.2 µm; 3) the creation of complex patterns, including gradients and patterns with multiple proteins; 4) reproducibility; and 5) it is maskless and contactless, saving time and resources (Melero et al., 2019). We created our patterns on elastomeric soft PDMS substrates, which can be tuned to match the stiffness of many tissues, ranging from 3 to 18 kPa (Latorre et al., 2018; Butcher et al., 2009). PDMS is biocompatible, has excellent optical properties and is stable against humidity-induced swelling and temperature fluctuations, making it highly homogeneous and isotropic (Bélanger & Marois, 2001; Piruska et al., 2005; Miranda et al., 2021; Bergert et al., 2016). This substrate is suitable for PRIMO patterning and the addition of fluorescent beads, enabling the effective study of single cell haptotaxis and measurement of traction forces. By analyzing parameters such as cell velocity, length, actin dynamics, and tractions forces, we established a direct correlation between cell behavior and fibronectin density. In summary, we designed a 1D system that offers a clear framework for understanding the molecular and mechanical responses to symmetric fibronectin gradients.

We observed that MCF10A cells become larger and move faster as fibronectin increases in a biphasic manner. The biphasic velocity response has been explained by the interplay between adhesion strength and actin dynamics (Palecek et al., 1997; Schreiber et al., 2021). Stronger adhesions enhance cell velocity by promoting force transmission in actin protrusions at the leading edge. However, when adhesion strength becomes too high, the retrograde flow is insufficient to detach adhesions from the substrate, leading to slower cells (Palecek et al., 1997; Schreiber et al., 2021). Thus, the biphasic nature of adhesion-velocity relationship balances force transmission and friction (Fortunato & Sunyer, 2022; Bangasser et al., 2017; Elosegui-Artola et al., 2014). Adhesion-velocity relationship was observed in other cell lines, suggesting that it is a universal characteristic of cell motility (Palecek et al., 1997; Schreiber et al., 2021; Lemma et al., 2022). Our findings also indicate that the optimal fibronectin density for MCF10A cells migration is similar to MDA-MB-231 malignant breast tumor cell line (Schreiber et al., 2021).

Besides affecting velocity, adhesions failure due to excessive force may also lead to edge slippage and cell shrinking. This would explain the biphasic behavior we observed in cell length. Overall, our findings highlight that cell length and velocity depend on fibronectin density with biphasic relationships. Adhesion-velocity relationship is consistent across various cell types and shows similar optimal fibronectin levels for both epithelial and malignant breast tumor cell lines.

MCF10A cells initially migrated toward areas with higher fibronectin densities when seeded on symmetric gradients. This result reinforces previous observations on the haptotactic responses of

epithelial cells (Versaevel et al., 2021). Moreover, MCF10A cells are commonly used as a cell model for benign tumors (Nikkhah et al., 2011; Rother et al., 2014; Liu et al., 2019; Oudin et al., 2016; Cai et al., 2022). This indicates that tumor cells also exhibit haptotaxis and corroborates previous *in vitro* and *in vivo* studies (Oudin et al., 2016). Notably, over 80% of the single cells initially followed the fibronectin gradient, demonstrating a strong haptotactic response. This robust behavior contrasts sharply with the lower efficiency observed in single cells responding to stiffness gradients (Raab et al., 2012; Sunyer et al., 2016). Therefore, we show that ECM gradients may be a stronger signal for directed migration than stiffness gradients, even though both rely on integrin-based adhesions to sense their environment. We further support this by showing that single haptotactic responses remained unchanged on both soft and stiff substrates. These findings also indicate that efficient integrin-based directed migration does not require collective force transmission as in durotaxis (Sunyer et al., 2016).

Cells are more haptotactic on steeper gradients, as shown previously (Smith et al., 2006). This suggests that a large difference in fibronectin density between the cell edges increases adhesion failure in low adhesion areas, leading to cell polarity toward the gradient. Our experiments also reveal that cell velocity remained constant across different gradient magnitudes, which contrasts with prior studies (Smith et al., 2006). One possibility is that the tested gradient magnitudes were not distinct enough to affect velocity. Nonetheless, our data clearly show that the gradient magnitude more strongly influences initial cell migration toward higher fibronectin densities than it affects cell velocity.

Our study shows that MCF10A cells follow fibronectin gradients independently of contractility effects of ROCK and myosin proteins (Fortunato & Sunyer, 2022; Chang et al., 2008; Choraghe et al., 2020; Chrzanowska-Wodnicka & Burridge, 1996). This implies that differences in adhesion strength caused by gradient magnitude are sufficient to establish initial cell polarity. The role of contractility in haptotaxis has been controversial (Moreno-Arotzena et al., 2015; Autenrieth et al., 2016; King et al., 2016). In studies with continuous protein gradients like ours, where protein density changes smoothly, haptotaxis was observed to occur independently of contractility (King et al., 2016; Ricoult et al., 2015). However, this behavior was not observed with digital gradients, where discrete spots of protein are arranged to form a gradient (Autenrieth et al., 2016; Ricoult et al., 2015). This suggests that the impact of contractility on haptotaxis may depend on the formation, length and spacing of local adhesions. Additionally, while our findings differ from those related to durotaxis, they are consistent with contact guidance. This leads to a new hypothesis that haptotaxis could rely more on detecting gradients through actin protrusions, similar to contact guidance, rather than on cell contractility, as seen in durotaxis (Yeoman et al., 2021; Kubow et al., 2017).

Surprisingly, we also found that haptotaxis is independent of lamellipodia spreading driven by the PI3K (Welf et al., 2012). This contradicts other studies suggesting that lamellipodia are crucial for driving haptotaxis through Arp2/3 activation (King et al., 2016). PI3K signaling usually increases locally at the leading edge after protrusion begins, promoting and stabilizing nascent lamellipodia (Welf et al., 2012). However, lamellipodia spreading can be driven by Rho GTPase Rac1 or

PI3K, as both directly activate the Arp2/3 complex and promote branched actin polymerization (Steffen et al., 2004; Ten Klooster et al., 2006; Yang et al., 2022). Since PI3K is often linked to chemotaxis, we hypothesize that haptotaxis may rely more on Rac1 than on PI3K for initial lamellipodia formation. This would imply that mechanosensitive types of directed cell migration depend on Rho GTPase regulation for leading edge specification, while PI3K plays a large role in non-mechanosensitive migrations (Janetopoulos & Firtel, 2008). Moreover, it reinforces the idea that integrins directly regulate Rho GTPases, a molecular link that remains poorly understood. In summary, haptotaxis appears to be guided by specific molecular pathways that are independent of myosin, ROCK, and PI3K for initial sensing and cell polarity establishment.

One of our key findings occurs when cells reach the peak of fibronectin in symmetric gradients. After initially polarizing and migrating toward higher fibronectin densities, cells continued to move directionally at slower velocities even when exposed to a negative gradient. This contradicts the common idea that haptotactic cells only move toward regions with the highest protein density (Dertinger et al., 2002; Wen et al., 2015; Moreno-Arotzena et al., 2015; Autenrieth et al., 2016; King et al., 2016; Oudin et al., 2016; Weber et al., 2013). A similar observation was made during gap closure of Madin-Darby canine kidney (MDCK) monolayers on circular fibronectin gradients (Versaevel et al., 2021). Those gradients had zero fibronectin density at the centers and maximum density at the edges of the patterned circles. Initially, MDCK cells adhered and spread mostly at the edges with high fibronectin density, creating gaps within the tissue. To close these gaps, MDCK cells collectively migrated against the fibronectin gradient at lower speeds

compared to those observed on uniformly coated substrates. This indicates that different haptotactic cell lines can migrate individually or collectively against a fibronectin gradient, although at reduced speed (Versaevel et al., 2021).

Migration down a gradient is a well-known phenomenon in chemotaxis (Skoge et al., 2014; Hamza et al., 2014). After an initial phase of chemotactic migration along a gradient of cAMP, single *Dictyostelium* cells continue to migrate in the same direction when the gradient is removed or weakly inverted (Skoge et al., 2014). This effective memory has been interpreted in terms of adaptive gradient sensing and bistability of the downstream signaling circuitry. The mechanisms underlying migration against haptotactic gradients identified here have different origin. Unlike chemotaxis, where the machinery for gradient sensing and cell polarity are coupled through biochemical signaling, in haptotaxis directed motion is coupled to gradient sensing through cell adhesions and cytoskeletal mechanics (Wen et al., 2015; King et al., 2016; Roca-Cusachs et al., 2013; Bagorda & Parent, 2008; DesMarais et al., 2009).

We also found that reducing substrate adhesion at the leading edge alone does not trigger repolarization. On uniform protein substrate, a migrating cell stochastically pauses, reorganizes into a less polarized state, and then repolarizes to move persistently in a new direction (Hennig et al., 2020). On a gradient, haptotactic cells are expected to repolarize when encountering a negative gradient. However, repolarization does not occur immediately when the leading edge faces less adhesive areas. Thus, while gradient magnitude affects the initiation and strength of cell polarization, a change in its sign does not directly

cause repolarization. Instead, cells keep their established polarity to persistently migrate against the gradient, despite the decreasing adhesiveness. Taken together, our data unveil that cells can sustain migration against fibronectin gradients due to persistent cell polarity.

Cell polarity can be considered a form of cellular memory because it allows cells to maintain their spatial orientation and functional asymmetry over time. This concept is not new, as different types of cellular memory have been observed during cell migration. For instance, a recent study showed that migrating cells leave permanent "footprints" along their paths, which affect subsequent movements (d'Alessandro et al., 2021). This indicates that cells not only respond to their environment but also actively shape it as they migrate, demonstrating a bidirectional interaction between cells and their ECM (Gagné et al., 2020). In our study, we prevented the impact of these footprints by focusing on the initial run of cells. However, it is important to consider that the leading edge of migrating cells might alter the local fibronectin density by depositing or endocytosing fibronectin. These local changes can subsequently be detected by the trailing edge and complicate our understanding of how trailing edge dynamics correlate with fibronectin density. While this factor represents a limitation in our study, it also highlights an important area for further investigation.

We show that the velocity of the leading edge decreases when cells migrate down the gradient. This decrease is due to reduced friction, which leads to faster retrograde flow (Bergert et al., 2015; Vazquez et al., 2022). As a result, the leading edge's movement slows down and cell length decreases. These observations are also predicted by the molecular

clutch model (Fortunato & Sunyer, 2022; Mitchison & Kirschner, 1988; Bangasser et al., 2017; Chan & Odde, 2008; Elosegui-Artola et al., 2014, 2016). In the model, molecular clutches link actin filaments to the ECM and resist myosin-driven retrograde flow. Moreover, the model predicts that areas with higher ECM density have more engaged clutches, which reduce retrograde flow and increase traction forces. Conversely, in areas with lower ECM density, fewer clutches engage, leading to faster retrograde flow and reduced traction forces. Based on these assumptions, the molecular clutch model predicts that increased friction at the leading edge drives cell migration up the gradient, causing asymmetric retrograde flow and migration toward higher ECM density. However, using the same assumptions, the model fails to predict cell migration down the gradient because friction and retrograde flow differences no longer favor movements toward low protein areas.

In our experiments, we observed that retrograde flow at the leading edge aligns with the clutch model, exhibiting faster flow in low protein areas compared to high protein areas. Interestingly, the trailing edge does not match the model predictions and shows no significant difference between migration up and down the gradient. One hypothesis is that the trailing edge experiences greater resistance to changes in fibronectin density compared to the leading edge. This resistance may result from the trailing edge having more stable and less dynamic FAs, making it less responsive to variations in fibronectin density. Consequently, the trailing edge encounters consistent friction and show more uniform actin flow rates.

Furthermore, we observed that cells migrating down the gradient exhibit enhanced actin polymerization and increased protrusion rates at the leading edge. We believe this increase helps counterbalance the higher retrograde flow observed in these cells, as actin flows at the leading edge are known to influence each other. Actin polymerization generates force that pushes the membrane forward, creating a continuous retrograde flow of actin filaments back toward the cell body (Yamashiro & Watanabe, 2014; De Boer et al., 2023). Conversely, retrograde flow affects the direction and efficiency of actin polymerization by responding to the forces applied at the leading edge (Zimmermann et al., 2012; Betz et al., 2009). Therefore, the interplay between actin polymerization and retrograde flow can determine cell protrusion and persistence (Zimmermann et al., 2012). In summary, cells migrating down the gradient have faster retrograde flow, increased actin polymerization, and higher protrusion rates at the leading edge, while the trailing edge remains unchanged. Moreover, we speculate that the differences in actin dynamics between the edges result from their connection and communication. This allows cells to adapt their actin dynamics and maintain directed migration against fibronectin gradients.

Our data indicate that membrane tension does not change when cells migrate up and down the gradient. Although these preliminary might seem surprising, several factors can explain this finding. Actin polymerization was shown to increase membrane tension by pushing the membrane through the addition of actin monomers (Sitarska & Diz-Muñoz, 2020). This would suggest higher membrane tension when cells migrate down the gradient due to increased actin dynamics. However, membrane tension is also influenced by cell size (Diz-Muñoz et al., 2013;

Togo et al., 2000; Ren et al., 2021). Smaller cells experience less membrane tension than larger cells due to their surface area-to-volume ratio (Togo et al., 2000). Given that cells migrating down the gradient are smaller, we would expect them to exhibit lower membrane tension, which contradicts our earlier hypothesis. Therefore, interpreting membrane tension data is complex, as the effects of actin polymerization and cell size may offset each other. Additionally, our data show that membrane tension is consistent at both the leading and trailing edges. This consistency likely results from the connection between the actin cortex and the membrane, which allows tension to spread rapidly across the cell (Lüchtefeld et al., 2024). Overall, we speculate that membrane tension remains constant during migration up or down the gradient due to balancing effects of actin polymerization and cell size. Moreover, the uniform membrane tension between cell edges may result from a rapid tension distribution, preventing the detection of local differences in response to varying fibronectin densities.

Our study is the first to measure traction forces on protein gradients and offers new insights into the mechanical responses during migration in both up and down the gradient. We observed that traction forces increase with fibronectin density for cells migrating up the gradient. This confirms previous studies that link adhesion strength to traction force generation (Elosegui-Artola et al., 2016; Sarangi et al., 2017). Consistently, cells migrating down the gradient decreased traction forces due to reduced adhesiveness. MCF10A cells also displayed traction asymmetries that align with their direction of migration, whether moving up or down the gradient. Specifically, cells moving up the gradient showed a pronounced peak in traction at the leading edge and lower,

more spread-out traction at the trailing edge. A similar traction profile was observed when cells migrate down the gradient, though with slightly higher traction peaks and less pronounced traction asymmetry. Despite the reduced asymmetry, this suggests that traction asymmetry might serve as an adaptive mechanism to maintain persistent polarity, similar to our previous findings on actin dynamics. Thus, we speculate that actin flow and traction forces are correlated, as already suggested by others (Gardel et al., 2008; Shin et al., 2010; Craig et al., 2012). Specifically, it has been shown that tractions are inversely correlated with actin flow speed at the leading edge (Gardel et al., 2008). Our data reflect this inverse relationship when cells migrate up the gradient, where slower actin flow velocities correspond with higher traction forces. Conversely, when cells migrate down the gradient, the trend is reversed, with faster actin flow velocities and lower traction forces. Moreover, our data also revealed a clear relationship between traction asymmetry and cell velocity. Cells with greater traction asymmetry, particularly those migrating up the gradient, moved faster. In contrast, cells with lower traction asymmetry, such as those migrating down the gradient, moved slower. This observation aligns with previous research that links force distribution to cell movement (Rossetti et al., 2024). In summary, our study found that traction forces are directly related with fibronectin density, with higher forces in areas of high adhesiveness and lower forces in less adhesive areas. Furthermore, cells displayed traction asymmetry regardless of the gradient direction. This asymmetry aligns with the direction of cell movement and suggests an adaptive mechanical response that helps maintain persistent polarity. We also found that this traction asymmetry is closely associated with cell velocity.

Further we investigated how confinement along the y-axis affects cell migration in fibronectin gradients. We found that cells followed the fibronectin gradient regardless of confinement but exhibited different trajectories upon reaching the fibronectin peak. In confined gradients, cells oscillated between the pattern edges, migrating up and down the gradient. In unconfined gradients, cells repolarized their leading edge and migrated perpendicular to the gradient axis where fibronectin density was highest. Intermediate confinements led to more complex trajectories, such as circular paths around the maximum fibronectin area. Thus, migration down the gradient mainly occurred in confined gradients. We believe this happens because repolarization in confined gradients requires a 180º shift of the entire polarity machinery, including proteins, forces, cellular organelles, and structures. This process is energetically costly, so cells adapt their machinery to maintain migration down the gradient (Zanotelli et al., 2021). In contrast, cells in unconfined gradients can repolarize in any direction, allowing them to smoothly turn and migrate toward high fibronectin areas. These findings challenge the idea that gradient sensing alone governs cell polarity and migration. Instead, physical constraints like confinement influence whether sensing or polarity dominates, resulting in complex and unexpected trajectories.

A recent study shows that lateral confinement significantly affects the velocity of epithelial clusters (Vercurysse et al., 2022). Interestingly, we show that confinement has a stronger effect on the persistence of migration than on velocity at the single cell level. Additionally, confinement within a collagen matrix has been shown to affect the migration dynamics of cancer cells (Mosier et al., 2024). In highly confined environments, cancer cells migrate faster and retain

information about the matrix even after leaving the confined area. This suggests that physical constraints, such as geometrical confinement, can promote the formation of cellular memory during migration (Kalukula et al., 2024; Mosier et al., 2024). *In vivo*, cells constantly transition between high and low confinement (Kalukula et al., 2024). Thus, investigating whether cells continue to migrate against the gradient when moving from confined to unconfined patterns could offer valuable insights into how cells navigate complex microenvironments. Overall, our study shows that confinement modulates gradient sensing and polarity integration. This results in the emergence of complex and unexpected trajectories, such as circles and migration against the gradient.

Although our study advances the understanding of haptotaxis, it also has limitations. For example, we focused on single epithelial cells migrating in 1D-2D environments, which may not fully reflect *in vivo* complexities. In a living organism, cells interact with a variety of ECM proteins, respond to multiple guidance cues, and interact with other cells, including different cell types (Yamada et al., 2022; Fortunato & Sunyer, 2022; Frantz et al., 2010; Gumbiner, 1996). Thus, future research should explore a broader range of ECM proteins, such as collagen and laminin, to determine if the migration behaviors we observed are specific to fibronectin. Also, using a similar system to ours in studies of chemotaxis or durotaxis could reveal if our findings under confinement are universal to other types of directed migration. Furthermore, epithelial tissues often migrate collectively. So, understanding the impact of cell-cell adhesions on collective haptotactic responses is crucial. Although we show that they are not fundamental for an effective haptotatic response, changes in cell-cell interactions could significantly impact how cells migrate up and down

a gradient. Another point to explore is the processes of ECM remodeling, deposition, degradation, and endocytosis to elucidate how cells interact and adapt to protein gradients. To further validate our findings, advanced methods like optogenetics could be used to maintain cell polarity in unconfined symmetric gradients. By doing so, we could investigate if this sustained polarity dominates gradient sensing and make cells migrate against the gradient in unconfined gradients. Additionally, labeling FAs and myosin to track adhesions and force dynamics could offer deeper understanding of how molecular responses vary along the gradient. Future research should also focus on assessing cell energy costs to unveil how metabolic activity impacts haptotactic responses, cell polarity, and repolarization. For instance, using ATP/ADP ratio sensors could provide valuable insights, particularly as cells migrate down the gradient (Berg et al., 2009; Zanotelli et al., 2019; Tantama et al., 2013). Lastly, exploring the molecular mechanisms and force dynamics involved in 3D haptotaxis is crucial, though this requires advanced biophysical tools that are currently limited.

Our findings provide a new perspective on haptotaxis and highlight the crucial role of cell confinement in shaping haptotactic migration. This insight is particularly relevant for cancer research. As tumor progresses, its invasive front often becomes much stiffer than the surrounding stroma due to increased ECM deposition and remodeling (Nia et al., 2020; Acerbi et al., 2015). This means that cancer cells must migrate and invade from areas with dense ECM near the tumor to areas with less ECM in the surrounding tissue, which contradicts haptotaxis (Higgins et al., 2021). This contradiction, known as “migration paradox”, suggest that ECM density alone does not determine cell directionality and

that other factors may be involved (Mathieu et al., 2024; Shatkin et al., 2020). Our data indicate that cell confinement could be one such factor. In fact, tumor stroma is characterized by confinement due to its dense ECM network (Mongera et al., 2023; Illina et al., 2020; Saraswathibhatla et al., 2023). So, we hypothesize that cells initially polarize toward the high ECM density at the tumor's invasive front. But once this polarity is established, the strong confinement within the stroma can drive cells to migrate from high to low ECM areas and escape the tumor niche. Thus, confinement may be crucial for understanding the migration paradox and how invasive cancer cells navigate environments with varying ECM densities. In conclusion, future research will improve our understanding of directed migration in complex environments and lead to new therapeutic strategies for diseases with abnormal cell motility, such as cancer. Moreover, we anticipate that our findings open new approaches across several fields, including cell migration, tissue engineering, developmental biology, and cancer metastasis.

Chapter 6 – Conclusions

Based on the results presented in this thesis, the following conclusions can be drawn:

1. We developed a system to fabricate well-controlled and quantifiable fibronectin patterns with arbitrary geometry, suitable for both homogeneous and symmetric protein gradients. This system is ideal for accurately measuring traction forces in adherent cells.

2. We developed an experimental and computational workflow to monitor cell migration on homogeneous and haptotatic patterns. This workflow generates a dataset that correlates cellular descriptors, such as length, velocity, actin dynamics, traction forces and position within the pattern, with fibronectin density.

3. Length and velocity of single MCF10A cells exhibit a biphasic response to fibronectin density.

4. Single MCF10A cells display a robust haptotaxis.

5. Steeper gradients enhance cells' haptotatic response but do not affect their velocity.

6. Upon adhesion, the initial haptotatic response is independent of substrate stiffness, cell contractility, and lamellipodia spreading.

7. On confined symmetric gradients, most cells continue migrating down the gradient at a slightly slower velocity after reaching the peak of fibronectin density.

8. MCF10A cells increase their actin dynamics, such as polymerization velocity and protrusion rate, to migrate against the fibronectin gradient.

9. Membrane tension remains unchanged in MCF10A cells migrating on both homogeneous and haptotatic gradients. It also stays constant when cells migrate up or down the gradient.

10. After accounting for the time-dependent increase, the traction forces in MCF10A cells directly correlate with fibronectin density and reflect the fibronectin density profile.

11. Migration up and down the gradient show actin flows and traction asymmetries that maintain a long-term persistent polarity. These asymmetries are weaker when cells migrate against the gradient.

12. Our system demonstrates the relationship between velocity and traction asymmetry in cells migrating on haptotactic gradients. This relationship is also present whether cells migrate up or down the gradient.

13. Cell confinement modulates gradient sensing and persistent polarity. With intermediate confinements, cells display complex trajectories like circles. In unconfined gradients, cells lose their ability to migrate down the gradient.

Chapter 7 – Contributions to the data presented in this thesis

Chemistry for PRIMO patterning coupled with traction measurements on elastomeric silicon substrates, as illustrated in Figure 18, was optimized by Dr. Raimon Sunyer from the Facultat de Medicina (Hospital Clínic) – Universitat de Barcelona.

The experiments in Figure 19, Figure 20 and Figure 21 were performed and analyzed by Isabela Corina Fortunato. The custom MATLAB code for calibrating pattern drawings and converting fluorescent intensity into protein density was made by Dr. Raimon Sunyer.

The experiments in Figure 20, Figure 21, Figure 22, Figure 23, Figure 24, Figure 25, Figure 26, Figure 27, Figure 28, Figure 29, Figure 30, Figure 31, Figure 35 and Figure 36 were performed and analyzed by Isabela Corina Fortunato. The custom-made MATLAB code to generate numerical databases describing cell migration was made by Dr. Raimon Sunyer.

The experiments in Figure 32 were performed by Isabela Corina Fortunato with the help of Dr. Joaquim Torra from the Institute of Photonic Sciences (ICFO). The analysis was made by Isabela Corina Fortunato.

The experiments in Figure 33 and Figure 34 were performed by Isabela Corina Fortunato. The analysis was made by Isabela Corina Fortunato and Dr. Steffen Grosser from Institute for Bioengineering of Catalonia (IBEC) with the help of Dr. Leone Rossetti from King's College London and Miquel Bosch from IBEC.

Chapter 8 – References

A

Acerbi, I., Cassereau, L., Dean, I., Shi, Q., Au, A., Park, C., ... & Weaver, V. M. (2015). Human breast cancer invasion and aggression correlates with ECM stiffening and immune cell infiltration. *Integrative Biology*, 7(10), 1120-1134.

Achimovich, A. M., Yan, T., & Gahlmann, A. (2023). Dimerization of iLID optogenetic proteins observed using 3D single-molecule tracking in live E. coli. *Biophysical Journal*, 122(16), 3254-3267.

Adler, J. (1966). Chemotaxis in Bacteria: Motile Escherichia coli migrate in bands that are influenced by oxygen and organic nutrients. *Science*, 153(3737), 708-716.

Aglialoro, F., Hofsink, N., Hofman, M., Brandhorst, N., & Van den Akker, E. (2020). Inside out integrin activation mediated by PIEZO1 signaling in erythroblasts. *Frontiers in physiology*, *11*, 562598.

Alanko, J., Uçar, M. C., Canigova, N., Stopp, J., Schwarz, J., Merrin, J., ... & Sixt, M. (2023). CCR7 acts as both a sensor and a sink for CCL19 to coordinate collective leukocyte migration. *Science immunology*, 8(87), eadc9584.

Albuschies, J., & Vogel, V. (2013). The role of filopodia in the recognition of nanotopographies. *Scientific reports*, *3*(1), 1658.

Almeida, F. V., Walko, G., McMillan, J. R., McGrath, J. A., Wiche, G., Barber, A. H., & Connelly, J. T. (2015). The cytolinker plectin regulates nuclear mechanotransduction in keratinocytes. *Journal of cell science*, 128(24), 4475-4486.

Andreu, I., Granero-Moya, I., Chahare, N. R., Clein, K., Molina-Jordán, M., Beedle, A. E., ... & Roca-Cusachs, P. (2022). Mechanical force application to the nucleus regulates nucleocytoplasmic transport. *Nature cell biology*, *24*(6), 896-905.

Arthur, W. T., Petch, L. A., & Burridge, K. (2000). Integrin engagement suppresses RhoA activity via a c-Src-dependent mechanism. Current Biology, 10(12), 719-722.

Aspenström, P. (2019). The intrinsic GDP/GTP exchange activities of Cdc42 and Rac1 are critical determinants for their specific effects on mobilization of the actin filament system. *Cells*, 8(7), 759.

Assies, L., García-Calvo, J., Piazzolla, F., Sanchez, S., Kato, T., Reymond, L., ... & Matile, S. (2021). Flipper Probes for the Community.

Atherton, P., Stutchbury, B., Jethwa, D., & Ballestrem, C. (2016). Mechanosensitive components of integrin adhesions: role of vinculin. *Experimental cell research*, 343(1), 21-27.

Autenrieth, T. J., Frank, S. C., Greiner, A. M., Klumpp, D., Richter, B., Hauser, M., ... & Bastmeyer, M. (2016). Actomyosin contractility and RhoGTPases affect cell-polarity and directional migration during haptotaxis. *Integrative biology*, *8*(10), 1067-1078.

B

Bagorda, A., & Parent, C. A. (2008). Eukaryotic chemotaxis at a glance. *Journal of cell science*, 121(16), 2621-2624.

Bai, Y., Xiang, X., Liang, C., & Shi, L. (2015). Regulating Rac in the nervous system: molecular function and disease implication of Rac GEFs and GAPs. *BioMed research international*, 2015.

Baier, H., & Bonhoeffer, F. (1992). Axon guidance by gradients of a target-derived component. *Science*, 255(5043), 472-475.

Balabanian, L., Berger, C. L., & Hendricks, A. G. (2017). Acetylated microtubules are preferentially bundled leading to enhanced kinesin-1 motility. *Biophysical journal*, 113(7), 1551-1560.

Balazs, E. A., Laurent, T. C., & Jeanloz, R. W. (1986). Nomenclature of hyaluronic acid. *Biochemical Journal*, *235*(3), 903.

Balestrini, J. L., & Billiar, K. L. (2006). Equibiaxial cyclic stretch stimulates fibroblasts to rapidly remodel fibrin. *Journal of biomechanics*, *39*(16), 2983-2990.

Ballestrem, C., Hinz, B., Imhof, B. A., & Wehrle-Haller, B. (2001). Marching at the front and dragging behind: differential αVβ3-integrin turnover regulates focal adhesion behavior. *The Journal of cell biology*, 155(7), 1319-1332.

Ban, E., Franklin, J. M., Nam, S., Smith, L. R., Wang, H., Wells, R. G., ... & Shenoy, V. B. (2018). Mechanisms of plastic deformation in collagen networks induced by cellular forces. *Biophysical journal*, 114(2), 450-461.

Bangasser, B. L., Rosenfeld, S. S., & Odde, D. J. (2013). Determinants of maximal force transmission in a motor-clutch model of cell traction in a compliant microenvironment. *Biophysical journal*, 105(3), 581-592.

Bangasser, B. L., Shamsan, G. A., Chan, C. E., Opoku, K. N., Tüzel, E., Schlichtmann, B. W., ... & Odde, D. J. (2017). Shifting the optimal stiffness for cell migration. *Nature communications*, 8(1), 15313.

Batchelder, E. L., Hollopeter, G., Campillo, C., Mezanges, X., Jorgensen, E. M., Nassoy, P., ... & Plastino, J. (2011). Membrane tension regulates motility by controlling lamellipodium organization. *Proceedings of the National Academy of Sciences*, 108(28), 11429-11434.

Bear, J. E., & Haugh, J. M. (2014). Directed migration of mesenchymal cells: where signaling and the cytoskeleton meet. *Current opinion in cell biology*, *30*, 74-82.

Becker, D., Bereiter-Hahn, J., & Jendrach, M. (2009). Functional interaction of the cation channel transient receptor potential vanilloid 4 (TRPV4) and actin in volume regulation. *European journal of cell biology*, 88(3), 141-152.

Bélanger, M. C., & Marois, Y. (2001). Hemocompatibility, biocompatibility, inflammatory and in vivo studies of primary reference materials low-density polyethylene and polydimethylsiloxane: A review. Journal of Biomedical Materials Research: An Official Journal of The Society for Biomaterials, *The Japanese Society for Biomaterials, and The Australian Society for Biomaterials and the Korean Society for Biomaterials*, 58(5), 467-477.

Beningo, K. A., Dembo, M., Kaverina, I., Small, J. V., & Wang, Y. L. (2001). Nascent focal adhesions are responsible for the generation of strong propulsive forces in migrating fibroblasts. *The Journal of cell biology*, *153*(4), 881-888.

Berg, J., Hung, Y. P., & Yellen, G. (2009). A genetically encoded fluorescent reporter of ATP: ADP ratio. *Nature methods*, 6(2), 161-166.

Bergert, M., Erzberger, A., Desai, R. A., Aspalter, I. M., Oates, A. C., Charras, G., ... & Paluch, E. K. (2015). Force transmission during adhesion-independent migration. *Nature cell biology*, 17(4), 524-529.

Bergert, M., Lendenmann, T., Zündel, M., Ehret, A. E., Panozzo, D., Richner, P., ... & Ferrari, A. (2016). Confocal reference free traction force microscopy. *Nature communications*, 7(1), 12814.

Betz, T., Koch, D., Lim, D., & Käs, J. A. (2009). Stochastic actin polymerization and steady retrograde flow determine growth cone advancement. *Biophysical Journal*, 96(12), 5130-5138.

Bieling, P., Weichsel, J., McGorty, R., Jreij, P., Huang, B., Fletcher, D. A., & Mullins, R. D. (2016). Force feedback controls motor activity and mechanical properties of self-assembling branched actin networks. *Cell*, 164(1), 115-127.

Birk, D. E., & Bruckner, P. (2005). Collagen suprastructures. *Collagen: primer in structure, processing and assembly*, 185-205.

Blob, A., Ventzke, D., Nies, G., Dühmert, J. N., Schmitzer, B., Munk, A., ... & Köster, S. (2023). Vimentin intermediate filaments structure and mechanically support microtubules in cells. *bioRxiv*, 2023-04.

Bonnans, C., Chou, J., & Werb, Z. (2014). Remodelling the extracellular matrix in development and disease. *Nature reviews Molecular cell biology*, *15*(12), 786-801.

Boudreau, H. E., & Leto, T. L. (2019). Model systems to investigate nox-dependent cell migration and invasiveness. NADPH Oxidases: *Methods and Protocols*, 473-485.

Brieher, W. (2013). Mechanisms of actin disassembly. *Molecular biology of the cell*, 24(15), 2299-2302.

Brilla, C. G., Maisch, B., Zhou, G., & Weber, K. T. (1995). Hormonal regulation of cardiac fibroblast function. *European heart journal*, *16*(suppl_C), 45-50.

Brückner, D. B., Fink, A., Schreiber, C., Röttgermann, P. J., Rädler, J. O., & Broedersz, C. P. (2019). Stochastic nonlinear dynamics of confined cell migration in two-state systems. Nature Physics, 15(6), 595-601.

Brzeska, H., Pridham, K., Chery, G., Titus, M. A., & Korn, E. D. (2014). The association of myosin IB with actin waves in dictyostelium requires both the plasma membrane-binding site and actin-binding region in the myosin tail. *PloS one*, 9(4), e94306.

Butcher, D. T., Alliston, T., & Weaver, V. M. (2009). A tense situation: forcing tumour progression. *Nature Reviews Cancer*, 9(2), 108-122.

Butler, J. P., Tolic-Nørrelykke, I. M., Fabry, B., & Fredberg, J. J. (2002). Traction fields, moments, and strain energy that cells exert on their surroundings. *American Journal of Physiology-Cell Physiology*, 282(3), C595-C605.

Buttenschön, A., & Edelstein-Keshet, L. (2020). Bridging from single to collective cell migration: A review of models and links to experiments. *PLoS computational biology*, 16(12), e1008411.

C

Caballero, D., Comelles, J., Piel, M., Voituriez, R., & Riveline, D. (2015). Ratchetaxis: long-range directed cell migration by local cues. *Trends in cell biology*, 25(12), 815-827.

Caballero, D., Voituriez, R., & Riveline, D. (2014). Protrusion fluctuations direct cell motion. *Biophysical journal*, 107(1), 34-42.

Cagigas, M. L., Bryce, N. S., Ariotti, N., Brayford, S., Gunning, P. W., & Hardeman, E. C. (2022). Correlative cryo-ET identifies actin/tropomyosin filaments that mediate cell–substrate adhesion in cancer cells and mechanosensitivity of cell proliferation. *Nature materials*, 21(1), 120-128.

Cai, G., Nguyen, A., Bashirzadeh, Y., Lin, S. S., Bi, D., & Liu, A. P. (2022). Compressive stress drives adhesion-dependent unjamming transitions in breast cancer cell migration. *Frontiers in Cell and Developmental Biology*, *10*, 933042.

Calderwood, D. A., Campbell, I. D., & Critchley, D. R. (2013). Talins and kindlins: partners in integrin-mediated adhesion. *Nature reviews Molecular cell biology*, *14*(8), 503-517.

Campbell, S., Zitnay, R., Mendoza, M., & Bidone, T. C. (2021). Computational model of 3D cell migration based on the molecular clutch mechanism. *bioRxiv*, 2021-09.

Carter, S. B. (1965). Principles of cell motility: the direction of cell movement and cancer invasion.

Carter, S. B. (1967). Haptotaxis and the mechanism of cell motility. *Nature*, *213*(5073), 256-260.

Chan, C. E., & Odde, D. J. (2008). Traction dynamics of filopodia on compliant substrates. *Science*, 322(5908), 1687-1691.

Chang, J., & Chaudhuri, O. (2019). Beyond proteases: Basement membrane mechanics and cancer invasion. *Journal of Cell Biology*, *218*(8), 2456-2469.

Chang, Y. C., Nalbant, P., Birkenfeld, J., Chang, Z. F., & Bokoch, G. M. (2008). GEF-H1 couples nocodazole-induced microtubule disassembly to cell contractility via RhoA. *Molecular biology of the cell*, 19(5), 2147-2153.

Charras, G., & Paluch, E. (2008). Blebs lead the way: how to migrate without lamellipodia. *Nature reviews Molecular cell biology*, *9*(9), 730-736.

Chaudhary, A. R., Berger, F., Berger, C. L., & Hendricks, A. G. (2018). Tau directs intracellular trafficking by regulating the forces exerted by kinesin and dynein teams. *Traffic*, 19(2), 111-121.

Chaudhuri, O., Cooper-White, J., Janmey, P. A., Mooney, D. J., & Shenoy, V. B. (2020). Effects of extracellular matrix viscoelasticity on cellular behaviour. *Nature*, *584*(7822), 535-546.

Chen, L., Iijima, M., Tang, M., Landree, M. A., Huang, Y. E., Xiong, Y., ... & Devreotes, P. N. (2007). PLA2 and PI3K/PTEN pathways act in parallel to mediate chemotaxis. *Developmental cell*, 12(4), 603-614.

Chen, X., Zhu, H., Feng, X., Li, X., Lu, Y., Wang, Z., & Rezgui, Y. (2020). Predictive assembling model reveals the self-adaptive elastic properties of lamellipodial actin networks for cell migration. *Communications biology*, 3(1), 616.

Choi, C. K., Vicente-Manzanares, M., Zareno, J., Whitmore, L. A., Mogilner, A., & Horwitz, A. R. (2008). Actin and α-actinin orchestrate the assembly and maturation of nascent adhesions in a myosin II motor-independent manner. *Nature cell biology*, *10*(9), 1039-1050.

Choraghe, R. P., Kołodziej, T., Buser, A., Rajfur, Z., & Neumann, A. K. (2020). RHOA-mediated mechanical force generation through Dectin-1. *Journal of cell science*, 133(5), jcs236166.

Chrzanowska-Wodnicka, M., & Burridge, K. (1996). Rho-stimulated contractility drives the formation of stress fibers and focal adhesions. *The Journal of cell biology*, 133(6), 1403-1415.

Chung, C. Y., Funamoto, S., & Firtel, R. A. (2001). Signaling pathways controlling cell polarity and chemotaxis. *Trends in biochemical sciences*, 26(9), 557-566.

Ciobanasu, C., Faivre, B., & Le Clainche, C. (2013). Integrating actin dynamics, mechanotransduction and integrin activation: the multiple functions of actin binding proteins in focal adhesions. *European journal of cell biology*, 92(10-11), 339-348.

Cocciolone, A. J., Hawes, J. Z., Staiculescu, M. C., Johnson, E. O., Murshed, M., & Wagenseil, J. E. (2018). Elastin, arterial mechanics, and cardiovascular disease. *American Journal of Physiology-Heart and Circulatory Physiology*, *315*(2), H189-H205.

Colin, A., Orhant-Prioux, M., Guérin, C., Savinov, M., Cao, W., Vianay, B., ... & Blanchoin, L. (2023). Friction patterns guide actin network contraction. *Proceedings of the National Academy of Sciences*, 120(39), e2300416120.

Comelles, J., Fernández-Majada, V., Acevedo, V., Rebollo-Calderon, B., & Martínez, E. (2023). Soft topographical patterns trigger a stiffness-dependent cellular response to contact guidance. *Materials Today Bio*, *19*, 100593.

Comer, F. I., & Parent, C. A. (2002). PI 3-kinases and PTEN: how opposites chemoattract. *Cell*, 109(5), 541-544.

Condeelis, J., Jones, J., & Segall, J. E. (1992). Chemotaxis of metastatic tumor cells: clues to mechanisms from the Dictyostelium paradigm. *Cancer and Metastasis Reviews*, *11*, 55-68.

Corominas-Murtra, B., & Hannezo, E. (2023, December). Modelling the dynamics of mammalian gut homeostasis. *In Seminars in Cell & Developmental Biology* (Vol. 150, pp. 58-65). Academic Press.

Coste, B., Mathur, J., Schmidt, M., Earley, T. J., Ranade, S., Petrus, M. J., ... & Patapoutian, A. (2010). Piezo1 and Piezo2 are essential components of distinct mechanically activated cation channels. *Science*, *330*(6000), 55-60.

Craig, E. M., Gardel, M. L., & Mogilner, A. (2012). Modeling and Experimental Investigation of Actin-Myosin and Adhesion Dynamics at the Cell Leading Edge. *Biophysical Journal*, 102(3), 349a.

Czerwinski, T., Bischof, L., Böhringer, D., Kara, S., Wittmann, E., Winterl, A., ... & Mark, C. (2023). Immune cells employ traction forces to overcome steric hindrance in 3D biopolymer networks. *bioRxiv*, 2023-04.

D

Das, A., Fischer, R. S., Pan, D., & Waterman, C. M. (2016). YAP nuclear localization in the absence of cell-cell contact is mediated by a filamentous actin-dependent, myosin II-and phospho-YAP-independent pathway during extracellular matrix mechanosensing. *Journal of Biological Chemistry*, 291(12), 6096-6110.

De Boer, L. L., Vanes, L., Melgrati, S., Biggs O'May, J., Hayward, D., Driscoll, P. C., ... & Tybulewicz, V. L. (2023). T cell migration requires ion and water influx to regulate actin polymerization. *Nature Communications*, 14(1), 7844.

DeLong, S. A., Gobin, A. S., & West, J. L. (2005). Covalent immobilization of RGDS on hydrogel surfaces to direct cell alignment and migration. *Journal of Controlled Release*, *109*(1-3), 139-148.

DeMali, K. A., Barlow, C. A., & Burridge, K. (2002). Recruitment of the Arp2/3 complex to vinculin: coupling membrane protrusion to matrix adhesion. *The Journal of cell biology*, *159*(5), 881-891.

Dertinger, S. K., Jiang, X., Li, Z., Murthy, V. N., & Whitesides, G. M. (2002). Gradients of substrate-bound laminin orient axonal specification of neurons. *Proceedings of the National Academy of Sciences*, 99(20), 12542-12547.

DesMarais, V., Yamaguchi, H., Oser, M., Soon, L., Mouneimne, G., Sarmiento, C., ... & Condeelis, J. (2009). N-WASP and cortactin are involved in invadopodium-

dependent chemotaxis to EGF in breast tumor cells. *Cell motility and the cytoskeleton*, *66*(6), 303-316.

Devreotes, P. N., & Zigmond, S. H. (1988). Chemotaxis in eukaryotic cells: a focus on leukocytes and Dictyostelium. *Annual review of cell biology*, *4*(1), 649-686.

Dickinson, R. B. (2000). A generalized transport model for biased cell migration in an anisotropic environment. *Journal of mathematical biology*, 40, 97-135.

DiPersio, C. M. (2007). Double duty for Rac1 in epidermal wound healing. *Science's STKE*, 2007(391), pe33-pe33.

Diz-Muñoz, A., Fletcher, D. A., & Weiner, O. D. (2013). Use the force: membrane tension as an organizer of cell shape and motility. *Trends in cell biology*, *23*(2), 47-53.

Dominici, C., Moreno-Bravo, J. A., Puiggros, S. R., Rappeneau, Q., Rama, N., Vieugue, P., ... & Chédotal, A. (2017). Floor-plate-derived netrin-1 is dispensable for commissural axon guidance. *Nature*, *545*(7654), 350-354.

Dowdell, A., Paschke, P. I., Thomason, P. A., Tweedy, L., & Insall, R. H. (2023). Competition between chemoattractants causes unexpected complexity and can explain negative chemotaxis. *Current Biology*, 33(9), 1704-1715.

Driscoll, T. P., Cosgrove, B. D., Heo, S. J., Shurden, Z. E., & Mauck, R. L. (2015). Cytoskeletal to nuclear strain transfer regulates YAP signaling in mesenchymal stem cells. *Biophysical journal*, *108*(12), 2783-2793.

DuChez, B. J. (2017). *The Response of Cancer Cells to Local Changes in Extracellular Stiffness*. Georgetown University.

DuChez, B. J., Doyle, A. D., Dimitriadis, E. K., & Yamada, K. M. (2019). Durotaxis by human cancer cells. *Biophysical journal*, *116*(4), 670-683.

Duman, J. G., Mulherkar, S., Tu, Y. K., Cheng, J. X., & Tolias, K. F. (2015). Mechanisms for spatiotemporal regulation of Rho-GTPase signaling at synapses. *Neuroscience letters*, 601, 4-10.

Dzobo, K., & Dandara, C. (2023). The extracellular matrix: its composition, function, remodeling, and role in tumorigenesis. *Biomimetics*, *8*(2), 146.

d'Alessandro, J., Barbier--Chebbah, A., Cellerin, V., Benichou, O., Mège, R. M., Voituriez, R., & Ladoux, B. (2021). Cell migration guided by long-lived spatial memory. *Nature Communications*, 12(1), 4118.

de Beco, S., Vaidžiulytė, K., Manzi, J., Dalier, F., Di Federico, F., Cornilleau, G., ... & Coppey, M. (2018). Optogenetic dissection of Rac1 and Cdc42 gradient shaping. *Nature communications*, 9(1), 4816.

E

Eibauer, M., Weber, M. S., Kronenberg-Tenga, R., Beales, C. T., Boujemaa-Paterski, R., Turgay, Y., ... & Medalia, O. (2024). Vimentin filaments integrate low-complexity domains in a complex helical structure. *Nature Structural & Molecular Biology*, 1-11.

Elosegui-Artola, A., Andreu, I., Beedle, A. E., Lezamiz, A., Uroz, M., Kosmalska, A. J., ... & Roca-Cusachs, P. (2017). Force triggers YAP nuclear entry by regulating transport across nuclear pores. *Cell*, *171*(6), 1397-1410.

Elosegui-Artola, A., Bazellières, E., Allen, M. D., Andreu, I., Oria, R., Sunyer, R., ... & Roca-Cusachs, P. (2014). Rigidity sensing and adaptation through regulation of integrin types. *Nature materials*, 13(6), 631-637.

Elosegui-Artola, A., Oria, R., Chen, Y., Kosmalska, A., Pérez-González, C., Castro, N., ... & Roca-Cusachs, P. (2016). Mechanical regulation of a molecular clutch

defines force transmission and transduction in response to matrix rigidity. *Nature cell biology,* 18(5), 540-548.

Elosegui-Artola, A., Trepat, X., & Roca-Cusachs, P. (2018). Control of mechanotransduction by molecular clutch dynamics. *Trends in cell biology*, 28(5), 356-367.

Engelmann, T. W. (1881). Neue Methode zur Untersuchung der Sauerstoffausscheidung pflanzlicher und thierischer Organismen. *Archiv für die gesamte Physiologie des Menschen und der Tiere*, *25*(1), 285-292.

Espina, J. A., Marchant, C. L., & Barriga, E. H. (2022). Durotaxis: the mechanical control of directed cell migration. *The FEBS journal*, *289*(10), 2736-2754.

F

Fiorio Pla, A., Ong, H. L., Cheng, K. T., Brossa, A., Bussolati, B., Lockwich, T., ... & Ambudkar, I. S. (2012). TRPV4 mediates tumor-derived endothelial cell migration via arachidonic acid-activated actin remodeling. *Oncogene*, 31(2), 200-212.

Fischer, R. S., Sun, X., Baird, M. A., Hourwitz, M. J., Seo, B. R., Pasapera, A. M., ... & Waterman, C. M. (2021). Contractility, focal adhesion orientation, and stress fiber orientation drive cancer cell polarity and migration along wavy ECM substrates. *Proceedings of the National Academy of Sciences*, *118*(22), e2021135118.

Fletcher, D. A., & Mullins, R. D. (2010). Cell mechanics and the cytoskeleton. *Nature*, 463(7280), 485-492.

Fortunato, I. C., & Sunyer, R. (2022). The Forces behind Directed Cell Migration. *Biophysica*, *2*(4), 548-563.

Frantz, C., Stewart, K. M., & Weaver, V. M. (2010). The extracellular matrix at a glance*. Journal of cell science*, 123(24), 4195-4200.

Fratzl, P. (2008). Collagen: structure and mechanics, an introduction. In *Collagen: structure and mechanics* (pp. 1-13). Boston, MA: Springer US.

Fricke, R., Zentis, P. D., Rajappa, L. T., Hofmann, B., Banzet, M., Offenhäusser, A., & Meffert, S. H. (2011). Axon guidance of rat cortical neurons by microcontact printed gradients. *Biomaterials*, 32(8), 2070-2076.

Friedl, P., Entschladen, F., Conrad, C., Niggemann, B., & Zänker, K. S. (1998). CD4+ T lymphocytes migrating in three-dimensional collagen lattices lack focal adhesions and utilize β1 integrin-independent strategies for polarization, interaction with collagen fibers and locomotion. *European journal of immunology*, *28*(8), 2331-2343.

Friedl, P., Zänker, K. S., & Bröcker, E. B. (1998). Cell migration strategies in 3-D extracellular matrix: Differences in morphology, cell matrix interactions, and integrin function. *Microscopy research and technique*, *43*(5), 369-378.

Friedl, P., & Wolf, K. (2003). Tumour-cell invasion and migration: diversity and escape mechanisms. *Nature reviews cancer*, *3*(5), 362-374.

Fu, J., Liu, B., Zhang, H., Fu, F., Yang, X., Fan, L., ... & Zhang, S. (2022). The role of cell division control protein 42 in tumor and non-tumor diseases: a systematic review. *Journal of Cancer*, 13(3), 800.

Fujita, S., Ohshima, M., & Iwata, H. (2009). Time-lapse observation of cell alignment on nanogrooved patterns. *Journal of the Royal Society Interface*, *6*(suppl_3), S269-S277.

Fujiwara, I., Takeda, S., Oda, T., Honda, H., Narita, A., & Maéda, Y. (2018). Polymerization and depolymerization of actin with nucleotide states at filament ends. *Biophysical Reviews*, 10, 1513-1519.

Funamoto, S., Meili, R., Lee, S., Parry, L., & Firtel, R. A. (2002). Spatial and temporal regulation of 3-phosphoinositides by PI 3-kinase and PTEN mediates chemotaxis. *Cell*, 109(5), 611-623.

G

Gagné, D., Benoit, Y. D., Groulx, J. F., Vachon, P. H., & Beaulieu, J. F. (2020). ILK supports RhoA/ROCK-mediated contractility of human intestinal epithelial crypt cells by inducing the fibrillogenesis of endogenous soluble fibronectin during the spreading process. *BMC Molecular and Cell Biology*, 21, 1-19.

García-Arcos, J. M., Jha, A., Waterman, C.M., & Piel, M. (2024). Blebology: principles of bleb-based migration. *Trends in Cell Biology*.

Gardel, M. L., Sabass, B., Ji, L., Danuser, G., Schwarz, U. S., & Waterman, C. M. (2008). Traction stress in focal adhesions correlates biphasically with actin retrograde flow speed. *The Journal of cell biology*, 183(6), 999-1005.

Gattazzo, F., Urciuolo, A., & Bonaldo, P. (2014). Extracellular matrix: a dynamic microenvironment for stem cell niche. *Biochimica et Biophysica Acta (BBA)-General Subjects*, *1840*(8), 2506-2519.

Geiger, B., Spatz, J. P., & Bershadsky, A. D. (2009). Environmental sensing through focal adhesions. *Nature reviews Molecular cell biology*, 10(1), 21.

Gerisch, G., Hülser, D., Malchow, D., & Wick, U. (1975). Cell communication by periodic cyclic-AMP pulses. *Philosophical Transactions of the Royal Society of London. B, Biological Sciences*, 272(915), 181-192.

Giannone, G., Dubin-Thaler, B. J., Döbereiner, H. G., Kieffer, N., Bresnick, A. R., & Sheetz, M. P. (2004). Periodic lamellipodial contractions correlate with rearward actin waves. *Cell*, *116*(3), 431-443.

Gilles, C., Polette, M., Zahm, J. M., Tournier, J. M., Volders, L., Foidart, J. M., & Birembaut, P. (1999). Vimentin contributes to human mammary epithelial cell migration. *Journal of cell science*, *112*(24), 4615-4625.

González, M., Cambiazo, V., & Maccioni, R. B. (1998). The interaction of Mip-90 with microtubules and actin filaments in human fibroblasts. *Experimental cell research*, 239(2), 243-253.

Goode, B. L., Eskin, J., & Shekhar, S. (2023). Mechanisms of actin disassembly and turnover. *Journal of Cell Biology*, 222(12), e202309021.

Goulimari, P., Kitzing, T. M., Knieling, H., Brandt, D. T., Offermanns, S., & Grosse, R. (2005). Gα12/13 is essential for directed cell migration and localized Rho-Dia1 function. *Journal of Biological Chemistry*, 280(51), 42242-42251.

Grashoff, C., Hoffman, B. D., Brenner, M. D., Zhou, R., Parsons, M., Yang, M. T., ... & Schwartz, M. A. (2010). Measuring mechanical tension across vinculin reveals regulation of focal adhesion dynamics. *Nature*, *466*(7303), 263-266.

Gray, R. S., Roszko, I., & Solnica-Krezel, L. (2011). Planar cell polarity: coordinating morphogenetic cell behaviors with embryonic polarity. *Developmental cell*, 21(1), 120-133.

Grintsevich, E. E., Ahmed, G., Ginosyan, A. A., Wu, H., Rich, S. K., Reisler, E., & Terman, J. R. (2021). Profilin and Mical combine to impair F-actin assembly and promote disassembly and remodeling. *Nature communications*, 12(1), 5542.

Grobe, H., Wüstenhagen, A., Baarlink, C., Grosse, R., & Grikscheit, K. (2018). A Rac1-FMNL2 signaling module affects cell-cell contact formation independent of Cdc42 and membrane protrusions. *PLoS One*, 13(3), e0194716.

Gross, S. M., Dane, M. A., Smith, R. L., Devlin, K. L., McLean, I. C., Derrick, D. S., ... & Heiser, L. M. (2022). A multi-omic analysis of MCF10A cells provides a resource for integrative assessment of ligand-mediated molecular and phenotypic responses. *Communications biology*, *5*(1), 1066.

Gumbiner, B. M. (1996). Cell adhesion: the molecular basis of tissue architecture and morphogenesis. *Cell*, 84(3), 345-357.

Gupton, S. L., & Waterman-Storer, C. M. (2006). Spatiotemporal feedback between actomyosin and focal-adhesion systems optimizes rapid cell migration. *Cell*, *125*(7), 1361-1374.

H

Hadden, W. J., Young, J. L., Holle, A. W., McFetridge, M. L., Kim, D. Y., Wijesinghe, P., ... & Choi, Y. S. (2017). Stem cell migration and mechanotransduction on linear stiffness gradient hydrogels. *Proceedings of the National Academy of Sciences*, 114(22), 5647-5652.

Hakala, M., Wioland, H., Tolonen, M., Kotila, T., Jegou, A., Romet-Lemonne, G., & Lappalainen, P. (2021). Twinfilin uncaps filament barbed ends to promote turnover of lamellipodial actin networks. *Nature cell biology*, 23(2), 147-159.

Hakeem, R. M., Subramanian, B. C., Hockenberry, M. A., King, Z. T., Butler, M. T., Legant, W. R., & Bear, J. E. (2022). Zyxin and non-muscle myosin are required for single fibroblast durotaxis, but Rho-kinase activity and the Arp2/3 complex are dispensable. *bioRxiv*, 2022-06.

Hall, A. (2005). Rho GTPases and the control of cell behaviour. *Biochemical Society Transactions*, 33(5), 891-895.

Hamill, K. J., Kligys, K., Hopkinson, S. B., & Jones, J. C. (2009). Laminin deposition in the extracellular matrix: a complex picture emerges. *Journal of cell science*, *122*(24), 4409-4417.

Hamza, B., Wong, E., Patel, S., Cho, H., Martel, J., & Irimia, D. (2014). Retrotaxis of human neutrophils during mechanical confinement inside microfluidic channels. Integrative Biology, 6(2), 175-183.

Hapach, L. A., Mosier, J. A., Wang, W., & Reinhart-King, C. A. (2019). Engineered models to parse apart the metastatic cascade. *NPJ precision oncology*, *3*(1), 20.

Harrison, R. G. (1912). The cultivation of tissues in extraneous media as a method of morpho-genetic study[1]. *The Anatomical Record*, *6*, 181.

He, X., & Jiang, Y. (2018). A Multiscale Model of Cell Migration in Three-Dimensional Extracellular Matrix. *Cell Movement: Modeling and Applications*, 61-76.

Heit, B., Tavener, S., Raharjo, E., & Kubes, P. (2002). An intracellular signaling hierarchy determines direction of migration in opposing chemotactic gradients. *The Journal of cell biology*, 159(1), 91-102.

Hennig, K., Wang, I., Moreau, P., Valon, L., DeBeco, S., Coppey, M., ... & Balland, M. (2020). Stick-slip dynamics of cell adhesion triggers spontaneous symmetry breaking and directional migration of mesenchymal cells on one-dimensional lines. *Science Advances*, 6(1), eaau5670.

Herbert, C. B., McLernon, T. L., Hypolite, C. L., Adams, D. N., Pikus, L., Huang, C. C., ... & Hu, W. S. (1997). Micropatterning gradients and controlling surface densities of photoactivatable biomolecules on self-assembled monolayers of oligo (ethylene glycol) alkanethiolates. *Chemistry & biology*, 4(10), 731-737.

Heynen, S., Gough, D. A., & Price, J. H. (1997, May). Optically stabilized mercury short-arc lamp as UV light source for microscopy. *In Optical Diagnostics of Biological Fluids and Advanced Techniques in Analytical Cytology* (Vol. 2982, pp. 430-434). SPIE.

Higgins, G., Kim, J. E., Ferruzzi, J., Abdalrahman, T., Franz, T., & Zaman, M. H. (2021). Decreased cell stiffness facilitates detachment and migration of breast cancer cells in 3D collagen matrices: An exploratory study. *BioRxiv*, 2021-01.

Hotulainen, P., & Lappalainen, P. (2006). Stress fibers are generated by two distinct actin assembly mechanisms in motile cells. *The Journal of cell biology*, 173(3), 383-394.

Huang, C. H., & Iglesias, P. A. (2014). Cell memory and adaptation in chemotaxis. *Proceedings of the National Academy of Sciences*, 111(43), 15287-15288.

Huang, J., Zhang, L., Wan, D., Zhou, L., Zheng, S., Lin, S., & Qiao, Y. (2021). Extracellular matrix and its therapeutic potential for cancer treatment. *Signal Transduction and Targeted Therapy*, *6*(1), 153.

Huang, Y., Su, J., Liu, J., Yi, X., Zhou, F., Zhang, J., ... & Wu, C. (2022). YAP activation in promoting negative durotaxis and acral melanoma progression. *Cells*, *11*(22), 3543.

Humphries, J. D., Byron, A., & Humphries, M. J. (2006). Integrin ligands at a glance. *Journal of cell science*, *119*(19), 3901-3903.

Hynes, M. J., & Maurer, J. A. (2012). Photoinduced monolayer patterning for the creation of complex protein patterns. *Langmuir*, 28(47), 16237-16242.

Hynes, R. O., & Naba, A. (2012). Overview of the matrisome—an inventory of extracellular matrix constituents and functions. *Cold Spring Harbor perspectives in biology*, 4(1), a004903.

I

Ilina, O., Gritsenko, P. G., Syga, S., Lippoldt, J., La Porta, C. A., Chepizhko, O., ... & Friedl, P. (2020). Cell–cell adhesion and 3D matrix confinement determine jamming transitions in breast cancer invasion. *Nature cell biology*, 22(9), 1103-1115.

Inoue, Y., & Adachi, T. (2013). Role of the Actin–Myosin Catch Bond on Actomyosin Aggregate Formation. *Cellular and Molecular Bioengineering*, 6, 3-12.

Isomursu, A., Park, K. Y., Hou, J., Cheng, B., Mathieu, M., Shamsan, G., ... & Odde, D. J. (2022). Negative durotaxis: cell movement toward softer environments. *Nature materials*, *21*(9), 1081.

Isomursu, A. (2024). Biomechanics of cancer cell motility.

J

Janetopoulos, C., & Firtel, R. A. (2008). Directional sensing during chemotaxis. *FEBS letters*, *582*(14), 2075-2085.

Jennings, H. S. (1931). Behavior of the lower organisms. *Columbia University Press*.

Jensen, O. E., & Revell, C. K. (2023). Couple stresses and discrete potentials in the vertex model of cellular monolayers. *Biomechanics and modeling in mechanobiology*, 22(5), 1465-1486.

Jiang, X., Xu, Q., Dertinger, S. K., Stroock, A. D., Fu, T. M., & Whitesides, G. M. (2005). A general method for patterning gradients of biomolecules on surfaces using microfluidic networks. *Analytical chemistry*, 77(8), 2338-2347.

Jiu, Y., Lehtimäki, J., Tojkander, S., Cheng, F., Jäälinoja, H., Liu, X., ... & Lappalainen, P. (2015). Bidirectional interplay between vimentin intermediate filaments and contractile actin stress fibers. *Cell reports*, 11(10), 1511-1518.

Joo, E., & Olson, M. F. (2021). Regulation and functions of the RhoA regulatory guanine nucleotide exchange factor GEF-H1. *Small GTPases*, 12(5-6), 358-371.

K

Kalluri, R., & Zeisberg, M. (2006). Fibroblasts in cancer. *Nature reviews cancer*, *6*(5), 392-401.

Kalukula, Y., Luciano, M., Charras, G., Brueckner, D., & Gabriele, S. (2024). The actin cortex acts as a mechanical memory of morphology in confined migrating cells. *bioRxiv*, 2024-08.

Kardash, E., Reichman-Fried, M., Maître, J. L., Boldajipour, B., Papusheva, E., Messerschmidt, E. M., ... & Raz, E. (2010). A role for Rho GTPases and cell–cell adhesion in single-cell motility in vivo. *Nature cell biology*, 12(1), 47-53.

Karska, J., Kowalski, S., Saczko, J., Moisescu, M. G., & Kulbacka, J. (2023). Mechanosensitive ion channels and their role in cancer cells. *Membranes*, 13(2), 167.

Katoh, K., Hammar, K., Smith, P. J., & Oldenbourg, R. (1999). Arrangement of radial actin bundles in the growth cone of Aplysia bag cell neurons shows the immediate past history of filopodial behavior. *Proceedings of the National Academy of Sciences*, 96(14), 7928-7931.

Kaverina, I., Krylyshkina, O., & Small, J. V. (1999). Microtubule targeting of substrate contacts promotes their relaxation and dissociation. *The Journal of cell biology*, *146*(5), 1033-1044.

Kaverina, I., & Straube, A. (2011). Regulation of cell migration by dynamic microtubules. *In Seminars in cell & developmental biology* (Vol. 22, No. 9, pp. 968-974). Academic Press.

Kechagia, J. Z., Ivaska, J., & Roca-Cusachs, P. (2019). Integrins as biomechanical sensors of the microenvironment. *Nature reviews Molecular cell biology*, 20(8), 457-473.

Khataee, H., Czirok, A., & Neufeld, Z. (2020). Multiscale modelling of motility wave propagation in cell migration. *Scientific Reports*, 10(1), 8128.

King, S. J., Asokan, S. B., Haynes, E. M., Zimmerman, S. P., Rotty, J. D., Alb Jr, J. G., ... & Bear, J. E. (2016). Lamellipodia are crucial for haptotactic sensing and response. *Journal of cell science*, *129*(12), 2329-2342.

Ko, Y. G., Co, C. C., & Ho, C. C. (2013). Directing cell migration in continuous microchannels by topographical amplification of natural directional persistence. Biomaterials, 34(2), 353-360.

Koca, Y., Collu, G. M., & Mlodzik, M. (2022). Wnt-frizzled planar cell polarity signaling in the regulation of cell motility. *Current topics in developmental biology*, *150*, 255-297.

Koenderink, G. H., Silva, M. S., Depken, M., Stuhrmann, B., & MacKintosh, F. C. (2011). Active Patterning and Contractile Dynamics in Actin Networks Driven by Myosin Motors. *Biophysical Journal*, 100(3), 513a.

Kokate, S. B., Ciuba, K., Tran, V. D., Kumari, R., Tojkander, S., Engel, U., ... & Lappalainen, P. (2022). Caldesmon controls stress fiber force-balance through dynamic cross-linking of myosin II and actin-tropomyosin filaments. *Nature communications*, 13(1), 6032.

Kotila, T., Wioland, H., Enkavi, G., Kogan, K., Vattulainen, I., Jégou, A., ... & Lappalainen, P. (2019). Mechanism of synergistic actin filament pointed end depolymerization by cyclase-associated protein and cofilin. *Nature Communications*, 10(1), 5320.

Krawczyk, W. S. (1971). A pattern of epidermal cell migration during wound healing. *The Journal of cell biology*, *49*(2), 247-263.

Kraxner, J., Lorenz, C., Menzel, J., Parfentev, I., Silbern, I., Denz, M., ... & Köster, S. (2021). Post-translational modifications soften vimentin intermediate filaments. *Nanoscale*, 13(1), 380-387.

Krndija, D., El Marjou, F., Guirao, B., Richon, S., Leroy, O., Bellaiche, Y., ... & Matic Vignjevic, D. (2019). Active cell migration is critical for steady-state epithelial turnover in the gut. *Science*, *365*(6454), 705-710.

Kubow, K. E., Shuklis, V. D., Sales, D. J., & Horwitz, A. R. (2017). Contact guidance persists under myosin inhibition due to the local alignment of adhesions and individual protrusions. *Scientific reports*, *7*(1), 14380.

Kubow, K. E., Vukmirovic, R., Zhe, L., Klotzsch, E., Smith, M. L., Gourdon, D., ... & Vogel, V. (2015). Mechanical forces regulate the interactions of fibronectin and collagen I in extracellular matrix. *Nature communications*, *6*(1), 8026.

L

Labouesse, C., Vianay, B., & Meister, J. J. (2012). Dynamic of Stress Fibers in the Lamella of Spreading Fibroblasts. *Biophysical Journal*, 102(3), 376a.

Lachowski, D., Cortes, E., Pink, D., Chronopoulos, A., Karim, S. A., P. Morton, J., & del Río Hernández, A. E. (2017). Substrate rigidity controls activation and durotaxis in pancreatic stellate cells. *Scientific reports*, *7*(1), 2506.

Laly, A. C., Sliogeryte, K., Pundel, O. J., Ross, R., Keeling, M. C., Avisetti, D., ... & Connelly, J. T. (2021). The keratin network of intermediate filaments regulates keratinocyte rigidity sensing and nuclear mechanotransduction. *Science Advances*, 7(5), eabd6187.

Lamalice, L., Le Boeuf, F., & Huot, J. (2007). Endothelial cell migration during angiogenesis. *Circulation research*, *100*(6), 782-794.

Lambrechts, A., Van Troys, M., & Ampe, C. (2004). The actin cytoskeleton in normal and pathological cell motility. *The international journal of biochemistry & cell biology*, 36(10), 1890-1909.

Lämmermann, T., & Sixt, M. (2009). Mechanical modes of 'amoeboid'cell migration. *Current opinion in cell biology*, *21*(5), 636-644.

Lang, S., Von Philipsborn, A. C., Bernard, A., Bonhoeffer, F., & Bastmeyer, M. (2008). Growth cone response to ephrin gradients produced by microfluidic networks. *Analytical and bioanalytical chemistry*, 390, 809-816.

Latorre, E., Kale, S., Casares, L., Gómez-González, M., Uroz, M., Valon, L., ... & Trepat, X. (2018). Active superelasticity in three-dimensional epithelia of controlled shape. *Nature*, 563(7730), 203-208.

Laukaitis, C. M., Webb, D. J., Donais, K., & Horwitz, A. F. (2001). Differential dynamics of α5 integrin, paxillin, and α-actinin during formation and disassembly of adhesions in migrating cells. *The Journal of cell biology*, 153(7), 1427-1440.

Leal, J., Shaner, S., Jedrusik, N., Savelyeva, A., & Asplund, M. (2023). Electrotaxis evokes directional separation of co-cultured keratinocytes and fibroblasts. *Scientific Reports*, *13*(1), 11444.

Lee, G., Han, S. B., & Kim, D. H. (2021). Cell-ECM contact-guided intracellular polarization is mediated via lamin A/C dependent nucleus-cytoskeletal connection. *Biomaterials*, 268, 120548.

Lee, H. W., Shin, J. H., & Simons, M. (2022). Flow goes forward and cells step backward: endothelial migration. *Experimental & Molecular Medicine*, 54(6), 711-719.

Lee, H., Pelz, B., Ferrer, J. M., Nakamura, F., Kamm, R. D., & Lang, M. J. (2009). Measuring Molecular Interaction between Actin Filament and Actin Binding Protein Governing Mechanical Properties of Cross-Linked F-Actin Network. *Biophysical Journal*, 96(3), 124a.

Lee, J. (2018). Insights into cell motility provided by the iterative use of mathematical modeling and experimentation. *AIMS Biophysics*, 5(2), 97-124.

Lehmann, S., Te Boekhorst, V., Odenthal, J., Bianchi, R., van Helvert, S., Ikenberg, K., ... & Friedl, P. (2017). Hypoxia induces a HIF-1-dependent transition from collective-to-amoeboid dissemination in epithelial cancer cells. *Current Biology*, *27*(3), 392-400.

Lehne, F., Pokrant, T., Parbin, S., Salinas, G., Großhans, J., Rust, K., ... & Bogdan, S. (2022). Calcium bursts allow rapid reorganization of EFhD2/Swip-1 cross-linked actin networks in epithelial wound closure. *Nature Communications*, 13(1), 2492.

Lemańska-Perek, A., & Adamik, B. (2019). Fibronectin and its soluble EDA-FN isoform as biomarkers for inflammation and sepsis. *Adv Clin Exp Med*, *28*(11), 1561-1567.

Lemma, E. D., Jiang, Z., Klein, F., Landmann, T., Weißenbruch, K., Bertels, S., ... & Bastmeyer, M. (2022). Adaptation of cell spreading to varying fibronectin densities and topographies is facilitated by β1 integrins. *Frontiers in bioengineering and biotechnology*, 10.

Lennon-Duménil, A. M., & Moreau, H. D. (2021). Barotaxis: How cells live and move under pressure. *Current Opinion in Cell Biology*, *72*, 131-136.

Levental, I., Georges, P. C., & Janmey, P. A. (2007). Soft biological materials and their impact on cell function. *Soft Matter*, *3*(3), 299-306.

Levskaya, A., Weiner, O. D., Lim, W. A., & Voigt, C. A. (2009). Spatiotemporal control of cell signalling using a light-switchable protein interaction. *Nature*, 461(7266), 997-1001.

Li, G., Huang, S., Yang, S., Wang, J., Cao, J., Czajkowsky, D. M., ... & Zhu, X. (2018). abLIM1 constructs non-erythroid cortical actin networks to prevent mechanical tension-induced blebbing. *Cell Discovery*, 4(1), 42.

Li, J., Zou, Y., Li, Z., & Jiu, Y. (2019). Joining actions: crosstalk between intermediate filaments and actin orchestrates cellular physical dynamics and signaling. *Science China Life Sciences*, 62, 1368-1374.

Li, R., & Zheng, Y. (1997). Residues of the Rho family GTPases Rho and Cdc42 that specify sensitivity to Dbl-like guanine nucleotide exchange factors. *Journal of Biological Chemistry*, 272(8), 4671-4679.

Li, Y., Kučera, O., Cuvelier, D., Rutkowski, D. M., Deygas, M., Rai, D., ... & Théry, M. (2023). Compressive forces stabilize microtubules in living cells. *Nature Materials*, 22(7), 913-924.

Liu, A. P., Richmond, D. L., Maibaum, L., Pronk, S., Geissler, P. L., & Fletcher, D. A. (2008). Membrane-induced bundling of actin filaments. *Nature physics*, 4(10), 789-793.

Liu, C. S. C., Mandal, T., Biswas, P., Hoque, M. A., Bandopadhyay, P., Sinha, B. P., ... & Ganguly, D. (2024). Piezo1 mechanosensing regulates integrin-dependent chemotactic migration in human T cells. *Elife*, *12*, RP91903.

Liu, Y. J., Le Berre, M., Lautenschlaeger, F., Maiuri, P., Callan-Jones, A., Heuzé, M., ... & Piel, M. (2015). Confinement and low adhesion induce fast amoeboid migration of slow mesenchymal cells. *Cell*, *160*(4), 659-672.

Liu, Y. L., Chou, C. K., Kim, M., Vasisht, R., Kuo, Y. A., Ang, P., ... & Yeh, H. C. (2019). Assessing metastatic potential of breast cancer cells based on EGFR dynamics. *Scientific reports*, 9(1), 3395.

Lo, C. M., Wang, H. B., Dembo, M., & Wang, Y. L. (2000). Cell movement is guided by the rigidity of the substrate. *Biophysical journal*, *79*(1), 144-152.

Lu, J., Zhou, S., Siech, M., Habisch, H., Seufferlein, T., & Bachem, M. G. (2014). Pancreatic stellate cells promote hapto-migration of cancer cells through collagen I-mediated signalling pathway. *British journal of cancer*, 110(2), 409-420.

Luo, T., & Robinson, D. N. (2011). The role of the actin cytoskeleton in mechanosensation. *Mechanosensitivity and Mechanotransduction*, 25-65.

Luo, X., Seveau de Noray, V., Aoun, L., Biarnes-Pelicot, M., Strale, P. O., Studer, V., ... & Theodoly, O. (2020). Lymphocytes perform reverse adhesive haptotaxis mediated by LFA-1 integrins. *Journal of Cell Science*, *133*(16), jcs242883.

Lüchtefeld, I., Pivkin, I. V., Gardini, L., Zare-Eelanjegh, E., Gäbelein, C., Ihle, S. J., ... & Vassalli, M. (2024). Dissecting cell membrane tension dynamics and its effect on Piezo1-mediated cellular mechanosensitivity using force-controlled nanopipettes. *Nature Methods*, 1-11.

Lynch, M. D., & Watt, F. M. (2018). Fibroblast heterogeneity: implications for human disease. *The Journal of clinical investigation*, *128*(1), 26-35.

M

Machacek, M., Hodgson, L., Welch, C., Elliott, H., Pertz, O., Nalbant, P., ... & Danuser, G. (2009). Coordination of Rho GTPase activities during cell protrusion. *Nature*, 461(7260), 99-103.

Mack, N. A., & Georgiou, M. (2014). The interdependence of the Rho GTPases and apicobasal cell polarity. *Small GTPases*, 5(2), e973768.

Malik-Sheriff, R. S., Imtiaz, S., Grecco, H. E., & Zamir, E. (2018). Diverse patterns of molecular changes in the mechano-responsiveness of focal adhesions. *Scientific Reports*, 8(1), 2187.

Maninová, M., Klímová, Z., Parsons, J. T., Weber, M. J., Iwanicki, M. P., & Vomastek, T. (2013). The reorientation of cell nucleus promotes the establishment of front–rear polarity in migrating fibroblasts. *Journal of molecular biology*, 425(11), 2039-2055.

Mathieu, M., Isomursu, A., & Ivaska, J. (2024). Positive and negative durotaxis–mechanisms and emerging concepts. *Journal of Cell Science*, 137(8), jcs261919.

Matsuda, K., Kobayashi, T., Sugawa, M., Koiso, Y., Toyoshima, Y. Y., & Yajima, J. (2018). Myosin-driven fragmentation of actin filaments triggers contraction of a disordered actin network. *BioRxiv*, 332684.

Mayor, R., & Etienne-Manneville, S. (2016). The front and rear of collective cell migration. *Nature reviews Molecular cell biology*, *17*(2), 97-109.

McKenzie, A. J., Hicks, S. R., Svec, K. V., Naughton, H., Edmunds, Z. L., & Howe, A. K. (2018). The mechanical microenvironment regulates ovarian cancer cell morphology, migration, and spheroid disaggregation. *Scientific reports*, *8*(1), 7228.

Mehdi, M., & Goss, J. W. (2018). Utilizing an Optogenetic System for Manipulating Protein Localization in Fission Yeast. *The FASEB Journal*, 32, 533-103.

Melero, C., Kolmogorova, A., Atherton, P., Derby, B., Reid, A., Jansen, K., & Ballestrem, C. (2019). Light-induced molecular adsorption of proteins using the PRIMO system for micro-patterning to study cell responses to extracellular matrix proteins. *JoVE (Journal of Visualized Experiments)*, (152), e60092.

Ménager, M. M., & Littman, D. R. (2016). Actin dynamics regulates dendritic cell-mediated transfer of HIV-1 to T cells. *Cell*, 164(4), 695-709.

Miranda, I., Souza, A., Sousa, P., Ribeiro, J., Castanheira, E. M., Lima, R., & Minas, G. (2021). Properties and applications of PDMS for biomedical engineering: A review. *Journal of functional biomaterials*, 13(1), 2.

Mirvis, M., Stearns, T., & James Nelson, W. (2018). Cilium structure, assembly, and disassembly regulated by the cytoskeleton. *Biochemical Journal*, 475(14), 2329-2353.

Mitchison, T., & Kirschner, M. (1988). Cytoskeletal dynamics and nerve growth. *Neuron*, 1(9), 761-772.

Mohapatra, L., Goode, B. L., Jelenkovic, P., Phillips, R., & Kondev, J. (2016). Design principles of length control of cytoskeletal structures. *Annual review of biophysics*, 45, 85-116.

Mongera, A., Pochitaloff, M., Gustafson, H. J., Stooke-Vaughan, G. A., Rowghanian, P., Kim, S., & Campàs, O. (2023). Mechanics of the cellular microenvironment as probed by cells in vivo during zebrafish presomitic mesoderm differentiation. *Nature materials*, 22(1), 135-143.

Montcouquiol, M., Jones, J. M., & Sans, N. (2008). Detection of planar polarity proteins in mammalian cochlea. *Wnt Signaling: Pathway Methods and Mammalian Models*, 207-219.

Monteiro, P., Yeon, B., Wallis, S. S., & Godinho, S. A. (2023). Centrosome amplification fine tunes tubulin acetylation to differentially control intracellular organization. *The EMBO Journal*, 42(16), e112812.

Moreira, C. G., Jacinto, A., & Prag, S. (2013). Drosophila integrin adhesion complexes are essential for hemocyte migration in vivo. *Biology open*, 2(8), 795-801.

Moreno-Arotzena, O., Borau, C., Movilla, N., Vicente-Manzanares, M., & García-Aznar, J. M. (2015). Fibroblast migration in 3D is controlled by haptotaxis in a non-muscle myosin II-dependent manner. *Annals of Biomedical Engineering*, *43*, 3025-3039.

Mosier, J. A., Fabiano, E. D., Ludolph, C. M., White, A. E., & Reinhart-King, C. A. (2024). Confinement primes cells for faster migration by polarizing active mitochondria. *Nanoscale Advances*, 6(1), 209-220.

Mouw, J. K., Ou, G., & Weaver, V. M. (2014). Extracellular matrix assembly: a multiscale deconstruction. *Nature reviews Molecular cell biology*, *15*(12), 771-785.

Mysh, M., & Poulton, J. S. (2021). The basolateral polarity module promotes slit diaphragm formation in drosophila nephrocytes, a model of vertebrate podocytes. *Journal of the American Society of Nephrology*, *32*(6), 1409-1424.

N

Nalbant, P., Chang, Y. C., Birkenfeld, J., Chang, Z. F., & Bokoch, G. M. (2009). Guanine nucleotide exchange factor-H1 regulates cell migration via localized activation of RhoA at the leading edge. *Molecular biology of the cell*, 20(18), 4070-4082.

Nasrin, S. R., Ganser, C., Nishikawa, S., Kabir, A. M. R., Sada, K., Yamashita, T., ... & Kakugo, A. (2021). Deformation of microtubules regulates translocation dynamics of kinesin. *Science advances*, 7(42), eabf2211.

Natwick, D. E., & Collins, S. R. (2021). Optimized iLID membrane anchors for local optogenetic protein recruitment. *ACS synthetic biology*, 10(5), 1009-1023.

Ndiaye, A. B., Koenderink, G. H., & Shemesh, M. (2022). Intermediate filaments in cellular mechanoresponsiveness: mediating cytoskeletal crosstalk from membrane to nucleus and back. *Frontiers in cell and developmental biology*, 10, 882037.

Nelson, I., Stojkovic, T., Allamand, V., Leturcq, F., Bécane, H. M., Babuty, D., ... & Bonne, G. (2015). Laminin α2 deficiency-related muscular dystrophy mimicking Emery-Dreifuss and collagen VI related diseases. *Journal of neuromuscular diseases*, *2*(3), 229-240.

Nemethova, M., Auinger, S., & Small, J. V. (2008). Building the actin cytoskeleton: filopodia contribute to the construction of contractile bundles in the lamella. The *Journal of cell biology*, 180(6), 1233-1244.

Nia, H. T., Munn, L. L., & Jain, R. K. (2020). Physical traits of cancer. *Science*, 370(6516), eaaz0868.

Nikkhah, M., Strobl, J. S., Schmelz, E. M., Roberts, P. C., Zhou, H., & Agah, M. (2011). MCF10A and MDA-MB-231 human breast basal epithelial cell co-culture in silicon micro-arrays. *Biomaterials*, 32(30), 7625-7632.

Nobes, C. D., & Hall, A. (1995). Rho, rac, and cdc42 GTPases regulate the assembly of multimolecular focal complexes associated with actin stress fibers, lamellipodia, and filopodia. *Cell*, 81(1), 53-62.

O

Ohashi, K., Fujiwara, S., & Mizuno, K. (2017). Roles of the cytoskeleton, cell adhesion and rho signalling in mechanosensing and mechanotransduction. *The Journal of Biochemistry*, 161(3), 245-254.

Okimura, C., Taniguchi, A., Nonaka, S., & Iwadate, Y. (2018). Rotation of stress fibers as a single wheel in migrating fish keratocytes. *Scientific reports*, 8(1), 10615.

Ossipova, O., Mancini, P., & Sokol, S. Y. (2022). Imaging planar cell polarity proteins in Xenopus neuroectoderm. In *Cell Polarity Signaling: Methods and Protocols* (pp. 147-161). New York, NY: Springer US.

Oudin, M. J., Jonas, O., Kosciuk, T., Broye, L. C., Guido, B. C., Wyckoff, J., ... & Gertler, F. B. (2016). Tumor cell–driven extracellular matrix remodeling drives haptotaxis during metastatic progression. *Cancer discovery*, *6*(5), 516-531.

P

Palamidessi, A., Malinverno, C., Frittoli, E., Corallino, S., Barbieri, E., Sigismund, S., ... & Scita, G. (2019). Unjamming overcomes kinetic and proliferation arrest in terminally differentiated cells and promotes collective motility of carcinoma. *Nature materials*, *18*(11), 1252-1263.

Palecek, S. P., Loftus, J. C., Ginsberg, M. H., Lauffenburger, D. A., & Horwitz, A. F. (1997). Integrin-ligand binding properties govern cell migration speed through cell-substratum adhesiveness. *Nature*, 385(6616), 537-540.

Pallarès, M. E., Pi-Jaumà, I., Fortunato, I. C., Grazu, V., Gómez-González, M., Roca-Cusachs, P., ... & Trepat, X. (2023). Stiffness-dependent active wetting enables optimal collective cell durotaxis. *Nature Physics*, *19*(2), 279-289.

Panciera, T., Azzolin, L., Cordenonsi, M., & Piccolo, S. (2017). Mechanobiology of YAP and TAZ in physiology and disease. *Nature reviews Molecular cell biology*, 18(12), 758-770.

Parsons, J. T., Horwitz, A. R., & Schwartz, M. A. (2010). Cell adhesion: integrating cytoskeletal dynamics and cellular tension. *Nature reviews Molecular cell biology*, 11(9), 633-643.

Payne, L. B., Zhao, H., James, C. C., Darden, J., McGuire, D., Taylor, S., ... & Chappell, J. C. (2019). The pericyte microenvironment during vascular development. *Microcirculation*, *26*(8), e12554.

Pellegrin, S., & Mellor, H. (2005). The Rho family GTPase Rif induces filopodia through mDia2. *Current Biology*, 15(2), 129-133.

Pepper, I., & Galkin, V. E. (2022). Actomyosin Complex. *In Macromolecular Protein Complexes IV: Structure and Function* (pp. 421-470). Cham: Springer International Publishing.

Perez Ipiña, E., d'Alessandro, J., Ladoux, B., & Camley, B. A. (2024). Deposited footprints let cells switch between confined, oscillatory, and exploratory migration. *Proceedings of the National Academy of Sciences*, 121(22), e2318248121.

Petitjean, I. I., Tran, Q. D., Goutou, A., Kabir, Z., Wiche, G., Leduc, C., & Koenderink, G. H. (2024). Reconstitution of cytolinker-mediated crosstalk between actin and vimentin. *European Journal of Cell Biology*, 103(2), 151403.

Pfeffer, W. (1881). Locomotorische Richtungsbewegungen durch chemische Reize. Unters. aus dem Bot. Inst. *Tübingen, Bd. I*, *85*, 363.

Pieuchot, L., Marteau, J., Guignandon, A., Dos Santos, T., Brigaud, I., Chauvy, P. F., ... & Anselme, K. (2018). Curvotaxis directs cell migration through cell-scale curvature landscapes. *Nature communications*, *9*(1), 3995.

Piruska, A., Nikcevic, I., Lee, S. H., Ahn, C., Heineman, W. R., Limbach, P. A., & Seliskar, C. J. (2005). The autofluorescence of plastic materials and chips measured under laser irradiation. *Lab on a Chip*, 5(12), 1348-1354.

Pogoda, K., & Janmey, P. A. (2023). Transmit and protect: The mechanical functions of intermediate filaments. *Current Opinion in Cell Biology*, 85, 102281.

Porazinski, S., Wang, H., Asaoka, Y., Behrndt, M., Miyamoto, T., Morita, H., ... & Furutani-Seiki, M. (2015). YAP is essential for tissue tension to ensure vertebrate 3D body shape. *Nature*, *521*(7551), 217-221.

Prahl, L. S., & Odde, D. J. (2018). Modeling cell migration mechanics. *Biomechanics in Oncology*, 159-187.

Q

Qin, Z., Kreplak, L., & Buehler, M. J. (2009). Hierarchical structure controls nanomechanical properties of vimentin intermediate filaments. *PloS one*, 4(10), e7294.

Qiu, Z., Minegishi, T., Aoki, D., Abe, K., Baba, K., & Inagaki, N. (2024). Adhesion-clutch between DCC and netrin-1 mediates netrin-1–induced axonal haptotaxis. *Frontiers in Molecular Neuroscience*, *17*.

R

Raab, M., Swift, J., P. Dingal, P. D., Shah, P., Shin, J. W., & Discher, D. E. (2012). Crawling from soft to stiff matrix polarizes the cytoskeleton and phosphoregulates myosin-II heavy chain. *Journal of Cell Biology*, *199*(4), 669-683.

Ramirez-San Juan, G. R., Oakes, P. W., & Gardel, M. L. (2017). Contact guidance requires spatial control of leading-edge protrusion. *Molecular biology of the cell*, *28*(8), 1043-1053.

Rashid, S., Long, Z., Singh, S., Kohram, M., Vashistha, H., Navlakha, S., ... & Bar-Joseph, Z. (2019). Adjustment in tumbling rates improves bacterial chemotaxis on obstacle-laden terrains. *Proceedings of the National Academy of Sciences*, 116(24), 11770-11775.

Ren, K., Gao, J., & Han, D. (2021). AFM force relaxation curve reveals that the decrease of membrane tension is the essential reason for the softening of cancer cells. *Frontiers in Cell and Developmental Biology*, 9, 663021.

Richards, D., Swift, J., Wong, L. S., & Richardson, S. M. (2019). Photoresponsive Hydrogels with Photoswitchable Stiffness: Emerging Platforms to Study Temporal Aspects of Mesenchymal Stem Cell Responses to Extracellular Stiffness Regulation. *Cell Biology and Translational Medicine, Volume 5: Stem Cells: Translational Science to Therapy*, 53-69.

Ricoult, S. G., Kennedy, T. E., & Juncker, D. (2015). Substrate-bound protein gradients to study haptotaxis. *Frontiers in bioengineering and biotechnology*, 3, 40.

Riveline, D., Zamir, E., Balaban, N. Q., Schwarz, U. S., Ishizaki, T., Narumiya, S., ... & Bershadsky, A. D. (2001). Focal contacts as mechanosensors: externally applied local mechanical force induces growth of focal contacts by an mDia1-dependent and ROCK-independent mechanism. *The Journal of cell biology*, 153(6), 1175-1186.

Roca-Cusachs, P., Sunyer, R., & Trepat, X. (2013). Mechanical guidance of cell migration: lessons from chemotaxis. Current opinion in cell biology, 25(5), 543-549.

Roffay, C., García-Arcos, J. M., Chapuis, P., López-Andarias, J., Schneider, F., Colom, A., ... & Mercier, V. (2022). Technical insights into fluorescence lifetime microscopy of mechanosensitive Flipper probes. *bioRxiv*, 2022-09.

Rong, Y., Yang, W., Hao, H., Wang, W., Lin, S., Shi, P., ... & Wu, C. (2021). The Golgi microtubules regulate single cell durotaxis. *EMBO reports*, *22*(3), e51094.

Rother, J., Nöding, H., Mey, I., & Janshoff, A. (2014). Atomic force microscopy-based microrheology reveals significant differences in the viscoelastic response between malign and benign cell lines. *Open biology*, 4(5), 140046.

Rossetti, L., Grosser, S., Abenza, J. F., Valon, L., Roca-Cusachs, P., Alert, R., & Trepat, X. (2024). Optogenetic generation of leader cells reveals a force-velocity relation for collective cell migration. *bioRxiv*, 2024-01.

Roussos, E. T., Balsamo, M., Alford, S. K., Wyckoff, J. B., Gligorijevic, B., Wang, Y., ... & Condeelis, J. S. (2011a). Mena invasive (MenaINV) promotes multicellular streaming motility and transendothelial migration in a mouse model of breast cancer. *Journal of cell science*, *124*(13), 2120-2131.

Roussos, E. T., Condeelis, J. S., & Patsialou, A. (2011b). Chemotaxis in cancer. *Nature Reviews Cancer*, *11*(8), 573-587.

Ruprecht, V., Wieser, S., Callan-Jones, A., Smutny, M., Morita, H., Sako, K., ... & Heisenberg, C. P. (2015). Cortical contractility triggers a stochastic switch to fast amoeboid cell motility. *Cell*, *160*(4), 673-685.

S

Sadhu, R. K., Luciano, M., Xi, W., Martinez-Torres, C., Schröder, M., Blum, C., ... & Gov, N. S. (2024). A minimal physical model for curvotaxis driven by curved protein complexes at the cell's leading edge. *Proceedings of the National Academy of Sciences*, *121*(12), e2306818121.

Saidova, A. A., & Vorobjev, I. A. (2020). Lineage commitment, signaling pathways, and the cytoskeleton systems in mesenchymal stem cells. *Tissue Engineering Part B: Reviews*, 26(1), 13-25.

Sakamoto, Y., Boëda, B., & Etienne-Manneville, S. (2013). APC binds intermediate filaments and is required for their reorganization during cell migration. *Journal of Cell Biology*, 200(3), 249-258.

Santiago-Medina, M., & Yang, J. (2016). MENA promotes tumor-intrinsic metastasis through ECM remodeling and haptotaxis. *Cancer discovery*, *6*(5), 474-476.

Sarangi, B. R., Gupta, M., Doss, B. L., Tissot, N., Lam, F., Mège, R. M., ... & Ladoux, B. (2017). Coordination between intra-and extracellular forces regulates focal adhesion dynamics. *Nano letters*, 17(1), 399-406.

Saraswathibhatla, A., Indana, D., & Chaudhuri, O. (2023). Cell–extracellular matrix mechanotransduction in 3D. *Nature Reviews Molecular Cell Biology*, *24*(7), 495-516.

Sato, M., Schwartz, W. H., Selden, S. C., & Pollard, T. D. (1988). Mechanical properties of brain tubulin and microtubules. *The Journal of cell biology*, 106(4), 1205-1211.

Schaedel, L., Lorenz, C., Schepers, A. V., Klumpp, S., & Köster, S. (2021). Vimentin intermediate filaments stabilize dynamic microtubules by direct interactions. *Nature communications*, 12(1), 3799.

Schall, T. J., Bacon, K., Toy, K. J., & Goeddel, D. V. (1990). Selective attraction of monocytes and T lymphocytes of the memory phenotype by cytokine RANTES. *Nature*, 347(6294), 669-671.

Schmidt, A., & Hall, A. (2002). Guanine nucleotide exchange factors for Rho GTPases: turning on the switch. *Genes & development*, 16(13), 1587-1609.

Schreiber, C., Amiri, B., Heyn, J. C., Rädler, J. O., & Falcke, M. (2021). On the adhesion–velocity relation and length adaptation of motile cells on stepped fibronectin lanes. *Proceedings of the National Academy of Sciences*, 118(4), e2009959118.

Schroeder, A., Heller, D. A., Winslow, M. M., Dahlman, J. E., Pratt, G. W., Langer, R., ... & Anderson, D. G. (2012). Treating metastatic cancer with nanotechnology. *Nature Reviews Cancer*, 12(1), 39-50.

Seetharaman, S., Vianay, B., Roca, V., Farrugia, A. J., De Pascalis, C., Boëda, B., ... & Etienne-Manneville, S. (2022). Microtubules tune mechanosensitive cell responses. *Nature Materials*, 21(3), 366-377.

Serra-Picamal, X., Conte, V., Sunyer, R., Muñoz, J. J., & Trepat, X. (2015). Mapping forces and kinematics during collective cell migration. *In Methods in cell biology* (Vol. 125, pp. 309-330). Academic Press.

Shadwick, R. E. (1990). Elastic energy storage in tendons: mechanical differences related to function and age. *Journal of applied physiology*, *68*(3), 1033-1040.

Shams, H., Hoffman, B. D., & Mofrad, M. R. (2018). The "stressful" life of cell adhesion molecules: on the mechanosensitivity of integrin adhesome. *Journal of biomechanical engineering*, 140(2), 020807.

Shatkin, G., Yeoman, B., Birmingham, K., Katira, P., & Engler, A. J. (2020). Computational models of migration modes improve our understanding of metastasis. *APL bioengineering*, 4(4).

Shekhar, S., Hoeprich, G. J., Gelles, J., & Goode, B. L. (2020). Twinfilin bypasses assembly conditions and actin filament aging to drive barbed end depolymerization. *Journal of Cell Biology*, 220(1), e202006022.

Shellard, A., Weißenbruch, K., Hampshire, P. A., Stillman, N. R., Dix, C. L., Thorogate, R., ... & Mayor, R. (2023). Frictiotaxis underlies adhesion-independent durotaxis. *bioRxiv*, 2023-06.

Shellard, A., & Mayor, R. (2021). Collective durotaxis along a self-generated stiffness gradient in vivo. *Nature*, *600*(7890), 690-694.

Shim, G., Breinyn, I. B., Martínez-Calvo, A., Rao, S., & Cohen, D. J. (2024). Bioelectric stimulation controls tissue shape and size. *Nature Communications*, *15*(1), 2938.

Shin, M. E., He, Y., Li, D., Na, S., Chowdhury, F., Poh, Y. C., ... & Wang, F. (2010). Spatiotemporal organization, regulation, and functions of tractions during neutrophil chemotaxis. *Blood, The Journal of the American Society of Hematology,* 116(17), 3297-3310.

Shoulders, M. D., & Raines, R. T. (2009). Collagen structure and stability. *Annual review of biochemistry*, *78*, 929-958.

Simon, C., Caorsi, V., Campillo, C., & Sykes, C. (2018). Interplay between membrane tension and the actin cytoskeleton determines shape changes. *Physical biology*, 15(6), 065004.

Sitarska, E., & Diz-Muñoz, A. (2020). Pay attention to membrane tension: Mechanobiology of the cell surface. *Current opinion in cell biology*, 66, 11-18.

Siwik, D. A., Chang, D. L. F., & Colucci, W. S. (2000). Interleukin-1β and tumor necrosis factor-α decrease collagen synthesis and increase matrix metalloproteinase activity in cardiac fibroblasts in vitro. *Circulation research*, *86*(12), 1259-1265.

Skoge, M., Yue, H., Erickstad, M., Bae, A., Levine, H., Groisman, A., ... & Rappel, W. J. (2014). Cellular memory in eukaryotic chemotaxis. *Proceedings of the National Academy of Sciences*, 111(40), 14448-14453.

Smith, J. T., Elkin, J. T., & Reichert, W. M. (2006). Directed cell migration on fibronectin gradients: effect of gradient slope. Experimental cell research, 312(13), 2424-2432.

Squires, T. M., Messinger, R. J., & Manalis, S. R. (2008). Making it stick: convection, reaction and diffusion in surface-based biosensors. *Nature biotechnology*, 26(4), 417-426.

Steffen, A., Rottner, K., Ehinger, J., Innocenti, M., Scita, G., Wehland, J., & Stradal, T. E. (2004). Sra-1 and Nap1 link Rac to actin assembly driving lamellipodia formation. *The EMBO journal*, 23(4), 749-759.

Storm, C., Pastore, J. J., MacKintosh, F. C., Lubensky, T. C., & Janmey, P. A. (2005). Nonlinear elasticity in biological gels. *Nature*, *435*(7039), 191-194.

Straight, A. F., Cheung, A., Limouze, J., Chen, I., Westwood, N. J., Sellers, J. R., & Mitchison, T. J. (2003). Dissecting temporal and spatial control of cytokinesis with a myosin II Inhibitor. *Science*, 299(5613), 1743-1747.

Strale, P. O., Azioune, A., Bugnicourt, G., Lecomte, Y., Chahid, M., & Studer, V. (2016). Multiprotein printing by light-induced molecular adsorption. *Advanced Materials*, *28*(10), 2024-2029.

Sun, Z., Guo, S. S., & Fässler, R. (2016). Integrin-mediated mechanotransduction. *Journal of Cell Biology*, *215*(4), 445-456.

Sunyer, R., Conte, V., Escribano, J., Elosegui-Artola, A., Labernadie, A., Valon, L., ... & Trepat, X. (2016). Collective cell durotaxis emerges from long-range intercellular force transmission. *Science*, *353*(6304), 1157-1161.

Svensson, R. B., Hassenkam, T., Grant, C. A., & Magnusson, S. P. (2010). Tensile properties of human collagen fibrils and fascicles are insensitive to environmental salts. *Biophysical journal*, *99*(12), 4020-4027.

Swift, J., Ivanovska, I. L., Buxboim, A., Harada, T., Dingal, P. D. P., Pinter, J., ... & Discher, D. E. (2013). Nuclear lamin-A scales with tissue stiffness and enhances matrix-directed differentiation. *Science*, *341*(6149), 1240104.

Syeda, R., Florendo, M. N., Cox, C. D., Kefauver, J. M., Santos, J. S., Martinac, B., & Patapoutian, A. (2016). Piezo1 channels are inherently mechanosensitive. *Cell reports*, *17*(7), 1739-1746.

T

Tang, A. T., Campbell, W. B., & Nithipatikom, K. (2012). ROCK1 feedback regulation of the upstream small GTPase RhoA. *Cellular signalling*, 24(7), 1375-1380.

Tang, D. D., & Gerlach, B. D. (2017). The roles and regulation of the actin cytoskeleton, intermediate filaments and microtubules in smooth muscle cell migration. *Respiratory research*, 18, 1-12.

Tang, M. H. E., Blair, J. P., Bager, C. L., Bay-Jensen, A. C., Henriksen, K., Christiansen, C., & Karsdal, M. A. (2020). Matrix metalloproteinase-degraded type I collagen is associated with APOE/TOMM40 variants and preclinical dementia. *Neurology: Genetics*, *6*(5), e508.

Tantama, M., Martínez-François, J. R., Mongeon, R., & Yellen, G. (2013). Imaging energy status in live cells with a fluorescent biosensor of the intracellular ATP-to-ADP ratio. *Nature communications*, 4(1), 2550.

Ten Klooster, J. P., Evers, E. E., Janssen, L., Machesky, L. M., Michiels, F., Hordijk, P., & Collard, J. G. (2006). Interaction between Tiam1 and the Arp2/3 complex links activation of Rac to actin polymerization. *Biochemical journal*, 397(1), 39-45.

Tepass, U. (2012). The apical polarity protein network in Drosophila epithelial cells: regulation of polarity, junctions, morphogenesis, cell growth, and survival. *Annual review of cell and developmental biology*, *28*, 655-685.

Thapa, N., Wen, T., Cryns, V. L., & Anderson, R. A. (2023). Regulation of Cell Adhesion and Migration via Microtubule Cytoskeleton Organization, Cell Polarity, and Phosphoinositide Signaling. *Biomolecules*, 13(10), 1430.

Tharp, W. G., Yadav, R., Irimia, D., Upadhyaya, A., Samadani, A., Hurtado, O., ... & Poznansky, M. C. (2006). Neutrophil chemorepulsion in defined interleukin-8 gradients in vitro and in vivo. *Journal of leukocyte biology*, *79*(3), 539-554.

Théry, M., Racine, V., Piel, M., Pépin, A., Dimitrov, A., Chen, Y., ... & Bornens, M. (2006). Anisotropy of cell adhesive microenvironment governs cell internal organization and orientation of polarity. *Proceedings of the National Academy of Sciences*, 103(52), 19771-19776.

Théry, M., & Blanchoin, L. (2024). Reconstituting the dynamic steady states of actin networks in vitro. *Nature Cell Biology*, 1-4.

Thomson, J., Singh, M., Eckersley, A., Cain, S. A., Sherratt, M. J., & Baldock, C. (2019). Fibrillin microfibrils and elastic fibre proteins: Functional interactions and extracellular regulation of growth factors. In *Seminars in cell & developmental biology* (Vol. 89, pp. 109-117). Academic Press.

Tischer, D., & Weiner, O. D. (2014). Illuminating cell signalling with optogenetic tools. *Nature reviews Molecular cell biology*, 15(8), 551-558.

Toettcher, J. E., Voigt, C. A., Weiner, O. D., & Lim, W. A. (2011). The promise of optogenetics in cell biology: interrogating molecular circuits in space and time. *Nature methods*, 8(1), 35-38.

Toews, M. L., GoY, M. F., Springer, M. S., & Adler, J. (1979). Attractants and repellents control demethylation of methylated chemotaxis proteins in Escherichia coli. *Proceedings of the National Academy of Sciences*, *76*(11), 5544-5548.

Togo, T., Krasieva, T. B., & Steinhardt, R. A. (2000). A decrease in membrane tension precedes successful cell-membrane repair. *Molecular biology of the cell*, 11(12), 4339-4346.

Tomba, C., & Villard, C. (2015). Brain cells and neuronal networks: Encounters with controlled microenvironments. *Microelectronic Engineering*, *132*, 176-191.

Trepat, X., Wasserman, M. R., Angelini, T. E., Millet, E., Weitz, D. A., Butler, J. P., & Fredberg, J. J. (2009). Physical forces during collective cell migration. *Nature physics*, 5(6), 426-430.

Tse, J. R., & Engler, A. J. (2011). Stiffness gradients mimicking in vivo tissue variation regulate mesenchymal stem cell fate. *PloS one*, 6(1), e15978.

U

Ueda, N., Maekawa, M., Matsui, T. S., Deguchi, S., Takata, T., Katahira, J., ... & Hieda, M. (2022). Inner nuclear membrane protein, SUN1, is required for cytoskeletal force generation and focal adhesion maturation. *Frontiers in Cell and Developmental Biology*, 10, 885859.

Uehata, M., Ishizaki, T., Satoh, H., Ono, T., Kawahara, T., Morishita, T., ... & Narumiya, S. (1997). Calcium sensitization of smooth muscle mediated by a Rho-associated protein kinase in hypertension. *Nature*, 389(6654), 990-994.

V

Vaidžiulytė, K., Macé, A. S., Battistella, A., Beng, W., Schauer, K., & Coppey, M. (2022). Persistent cell migration emerges from a coupling between protrusion dynamics and polarized trafficking. *Elife*, 11, e69229.

Valon, L., Etoc, F., Remorino, A., Di Pietro, F., Morin, X., Dahan, M., & Coppey, M. (2015). Predictive spatiotemporal manipulation of signaling perturbations using optogenetics. *Biophysical journal*, 109(9), 1785-1797.

Valon, L., & de Beco, S. (2021). Control of Cell Migration Using Optogenetics. *The Epithelial-to Mesenchymal Transition: Methods and Protocols*, 415-425.

Van Bodegraven, E. J., & Etienne-Manneville, S. (2020). Intermediate filaments against actomyosin: the david and goliath of cell migration. *Current Opinion in Cell Biology*, 66, 79-88.

Van Der Rest, M., & Garrone, R. (1991). Collagen family of proteins. *The FASEB journal*, *5*(13), 2814-2823.

Van Helvert, S., Storm, C., & Friedl, P. (2018). Mechanoreciprocity in cell migration. *Nature cell biology*, 20(1), 8-20.

Vassilev, V., Platek, A., Hiver, S., Enomoto, H., & Takeichi, M. (2017). Catenins steer cell migration via stabilization of front-rear polarity. *Developmental cell*, 43(4), 463-479.

Vazquez, K., Saraswathibhatla, A., & Notbohm, J. (2022). Effect of substrate stiffness on friction in collective cell migration. *Scientific Reports*, 12(1), 2474.

Vercurysse, E., Brückner, D. B., Gómez-González, M., Remson, A., Luciano, M., Kalukula, Y., ... & Gabriele, S. (2022). Geometry-driven migration efficiency of autonomous epithelial cell clusters. *bioRxiv*, 2022-07.

Versaevel, M., Alaimo, L., Seveau, V., Luciano, M., Mohammed, D., Bruyère, C., ... & Gabriele, S. (2021). Collective migration during a gap closure in a two-dimensional haptotactic model. *Scientific Reports*, 11(1), 5811.

Vijayakumar, S., Dang, S., Marinkovich, M. P., Lazarova, Z., Yoder, B., Torres, V. E., & Wallace, D. P. (2014). Aberrant expression of laminin-332 promotes cell proliferation and cyst growth in ARPKD. *American Journal of Physiology-Renal Physiology*, *306*(6), F640-F654.

Vincent, L. G., Choi, Y. S., Alonso-Latorre, B., Del Álamo, J. C., & Engler, A. J. (2013). Mesenchymal stem cell durotaxis depends on substrate stiffness gradient strength. *Biotechnology journal*, *8*(4), 472-484.

Vlahos, C. J., Matter, W. F., Hui, K. Y., & Brown, R. F. (1994). A specific inhibitor of phosphatidylinositol 3-kinase, 2-(4-morpholinyl)-8-phenyl-4H-1-benzopyran-4-one (LY294002*). Journal of Biological Chemistry*, 269(7), 5241-5248.

Vogel, V. (2006). Mechanotransduction involving multimodular proteins: converting force into biochemical signals. *Annu. Rev. Biophys. Biomol. Struct.*, *35*, 459-488.

Voloshenyuk, T. G., Landesman, E. S., Khoutorova, E., Hart, A. D., & Gardner, J. D. (2011). Induction of cardiac fibroblast lysyl oxidase by TGF-β1 requires PI3K/Akt, Smad3, and MAPK signaling. *Cytokine*, *55*(1), 90-97.

W

Wang, H. B., Dembo, M., Hanks, S. K., & Wang, Y. L. (2001). Focal adhesion kinase is involved in mechanosensing during fibroblast migration. *Proceedings of the National Academy of Sciences*, *98*(20), 11295-11300.

Wang, J., Petefish, J. W., Hillier, A. C., & Schneider, I. C. (2015). Epitaxially grown collagen fibrils reveal diversity in contact guidance behavior among cancer cells. *Langmuir*, *31*(1), 307-314.

Wang, K., Meng, X., & Guo, Z. (2021). Elastin structure, synthesis, regulatory mechanism and relationship with cardiovascular diseases. *Frontiers in Cell and Developmental Biology*, *9*, 596702.

Watt, K. E. N., & Trainor, P. A. (2014). Neurocristopathies: the etiology and pathogenesis of disorders arising from defects in neural crest cell development. In *Neural Crest Cells* (pp. 361-394). Academic Press.

Webb, D. J., Parsons, J. T., & Horwitz, A. F. (2002). Adhesion assembly, disassembly and turnover in migrating cells–over and over and over again. *Nature cell biology*, *4*(4), E97-E100.

Weber, M., Hauschild, R., Schwarz, J., Moussion, C., De Vries, I., Legler, D. F., ... & Sixt, M. (2013). Interstitial dendritic cell guidance by haptotactic chemokine gradients. *Science*, 339(6117), 328-332.

Weimerskirch, H., Martin, J., Clerquin, Y., Alexandre, P., & Jiraskova, S. (2001). Energy saving in flight formation. *Nature*, *413*(6857), 697-698.

Weiss, P. (1934). In vitro experiments on the factors determining the course of the outgrowing nerve fiber. *Journal of Experimental Zoology*, *68*(3), 393-448.

Welf, E. S., Ahmed, S., Johnson, H. E., Melvin, A. T., & Haugh, J. M. (2012). Migrating fibroblasts reorient directionality by a metastable, PI3K-dependent mechanism. *Journal of Cell Biology*, 197(1), 105-114.

Wen, J. H., Choi, O., Taylor-Weiner, H., Fuhrmann, A., Karpiak, J. V., Almutairi, A., & Engler, A. J. (2015). Haptotaxis is cell type specific and limited by substrate adhesiveness. *Cellular and molecular bioengineering*, *8*, 530-542.

Wereszczak, A. A., & Anderson Jr, C. E. (2014). Borofloat and starphire float glasses: A comparison. *International Journal of Applied Glass Science*, *5*(4), 334-344.

Whitesides, G. M. (2006). The origins and the future of microfluidics. *nature*, 442(7101), 368-373.

Winograd-Katz, S. E., Fässler, R., Geiger, B., & Legate, K. R. (2014). The integrin adhesome: from genes and proteins to human disease. *Nature reviews Molecular cell biology*, *15*(4), 273-288.

Wolf, K. J., & Kumar, S. (2019). Hyaluronic acid: incorporating the bio into the material. *ACS biomaterials science & engineering*, *5*(8), 3753-3765.

Wolf, K., Mazo, I., Leung, H., Engelke, K., Von Andrian, U. H., Deryugina, E. I., ... & Friedl, P. (2003). Compensation mechanism in tumor cell migration: mesenchymal–amoeboid transition after blocking of pericellular proteolysis. *The Journal of cell biology*, 160(2), 267-277.

Wong, C. H., Heit, B., & Kubes, P. (2010). Molecular regulators of leucocyte chemotaxis during inflammation. *Cardiovascular research*, 86(2), 183-191.

Worbs, T., Hammerschmidt, S. I., & Förster, R. (2017). Dendritic cell migration in health and disease. *Nature Reviews Immunology*, 17(1), 30-48.

Wu, P. H., Giri, A., Sun, S. X., & Wirtz, D. (2014). Three-dimensional cell migration does not follow a random walk. *Proceedings of the National Academy of Sciences*, 111(11), 3949-3954.

Wu, P. H., Giri, A., & Wirtz, D. (2015). Statistical analysis of cell migration in 3D using the anisotropic persistent random walk model. *Nature protocols*, 10(3), 517-527.

Wyckoff, J. B., Pinner, S. E., Gschmeissner, S., Condeelis, J. S., & Sahai, E. (2006). ROCK-and myosin-dependent matrix deformation enables protease-independent tumor-cell invasion in vivo. *Current Biology*, *16*(15), 1515-1523.

Y

Yamada, K. M., Doyle, A. D., & Lu, J. (2022). Cell–3D matrix interactions: recent advances and opportunities. *Trends in cell biology*, 32(10), 883-895.

Yamashiro, S., & Watanabe, N. (2014). A new link between the retrograde actin flow and focal adhesions. *The journal of biochemistry*, 156(5), 239-248.

Yang, S., Tang, Y., Liu, Y., Brown, A. J., Schaks, M., Ding, B., ... & Chen, B. (2022). Arf GTPase activates the WAVE regulatory complex through a distinct binding site. *Science advances*, 8(50), eadd1412.

Yao, M., Goult, B. T., Chen, H., Cong, P., Sheetz, M. P., & Yan, J. (2014). Mechanical activation of vinculin binding to talin locks talin in an unfolded conformation. *Scientific reports*, 4(1), 4610.

Yao, M., Tijore, A., Cheng, D., Li, J. V., Hariharan, A., Martinac, B., ... & Sheetz, M. (2022). Force-and cell state–dependent recruitment of Piezo1 drives focal adhesion dynamics and calcium entry. *Science advances*, *8*(45), eabo1461.

Yeoman, B., Shatkin, G., Beri, P., Banisadr, A., Katira, P., & Engler, A. J. (2021). Adhesion strength and contractility enable metastatic cells to become adurotactic. *Cell reports*, *34*(10).

Yip, A. K., Zhang, S., Chong, L. H., Cheruba, E., Woon, J. Y. X., Chua, T. X., ... & Chiam, K. H. (2021). Zyxin is involved in fibroblast rigidity sensing and durotaxis. *Frontiers in cell and developmental biology*, *9*, 735298.

Yu, M., Le, S., Ammon, Y. C., Goult, B. T., Akhmanova, A., & Yan, J. (2019). Force-dependent regulation of talin–KANK1 complex at focal adhesions. *Nano letters*, 19(9), 5982-5990.

Yumura, S., Mori, H., & Fukui, Y. (1984). Localization of actin and myosin for the study of ameboid movement in Dictyostelium using improved immunofluorescence. *The Journal of cell biology*, *99*(3), 894-899.

Yurchenco, P. D. (2011). Basement membranes: cell scaffoldings and signaling platforms. *Cold Spring Harbor perspectives in biology*, *3*(2), a004911.

Z

Zaari, N., Rajagopalan, P., Kim, S. K., Engler, A. J., & Wong, J. Y. (2004). Photopolymerization in microfluidic gradient generators: microscale control of substrate compliance to manipulate cell response. *Advanced materials*, 16(23-24), 2133-2137.

Zanconato, F., Cordenonsi, M., & Piccolo, S. (2016). YAP/TAZ at the roots of cancer. *Cancer cell*, *29*(6), 783-803.

Zanotelli, M. R., Rahman-Zaman, A., VanderBurgh, J. A., Taufalele, P. V., Jain, A., Erickson, D., ... & Reinhart-King, C. A. (2019). Energetic costs regulated by cell mechanics and confinement are predictive of migration path during decision-making. *Nature communications*, 10(1), 4185.

Zanotelli, M. R., Zhang, J., & Reinhart-King, C. A. (2021). Mechanoresponsive metabolism in cancer cell migration and metastasis. *Cell metabolism*, 33(7), 1307-1321.

Zegers, M. M., & Friedl, P. (2014). Rho GTPases in collective cell migration. *Small GTPases*, 5(3), e983869.

Zhang, X., Jiang, G., Cai, Y., Monkley, S. J., Critchley, D. R., & Sheetz, M. P. (2008). Talin depletion reveals independence of initial cell spreading from integrin activation and traction. *Nature cell biology*, 10(9), 1062.

Zhao, B., Ye, X., Yu, J., Li, L., Li, W., Li, S., ... & Guan, K. L. (2008). TEAD mediates YAP-dependent gene induction and growth control. *Genes & development*, 22(14), 1962-1971.

Zimmermann, J., Brunner, C., Enculescu, M., Goegler, M., Ehrlicher, A., Käs, J., & Falcke, M. (2012). Actin filament elasticity and retrograde flow shape the force-velocity relation of motile cells. *Biophysical journal*, 102(2), 287-295.